Nonlinear Optical and Photovoltaic Studies of Specific Nonconjugated Conductive Polymers and Metallic Nanoparticles

by

Justin Van Cleave

A dissertation submitted to the Graduate Faculty of
Auburn University
In partial fulfillment of the
requirements for the Degree of
Doctor of Philosophy

Auburn, Alabama
August 3, 2024

Approved by

Mrinal Thakur, Chair, Professor of Mechanical Engineering
Robert Dean, McWane Endowed Professor of Electrical Engineering
Dan Marghitu, Professor of Mechanical Engineering
Nicholas Tsolas, Assistant Professor of Mechanical Engineering

Abstract

In this research, the nonlinear optical properties of specific nonconjugated conductive polymers and gold nanoparticles in transparent dielectric media have been investigated. Photovoltaic devices utilizing nonconjugated conductive polymers have also been studied.

Nonconjugated conductive polymers are polymers with at least one double bond in the repeat. 1,4-polyisoprene (cis and trans), styrene butadiene rubber, and poly(β-pinene) are readily available examples of nonconjugated conductive polymers that have been investigated. Nonconjugated conductive polymers exhibit increases of many orders of magnitude in electrical conductivity upon doping with electron acceptors such as iodine. This change in conductivity results from charge-transfer from isolated double bonds in the polymer to the dopant. Exceptionally large optical nonlinearities have been reported for nonconjugated conductive polymers since they form sub-nanometer size metallic domains (quantum dots) upon doping. Nonconjugated conductive polymers have been shown to have many potential applications in nonlinear optics, electro-optics, and photovoltaics. The quadratic electro-optic effect and electroabsorption have been investigated in several nonconjugated conductive polymers including cis-1,4-polyisoprene, trans-polyisoprene, styrene butadiene rubber, and polyethylene terephthalate. The effects of iodine doping on polyethylene terephthalate have also been investigated using spectroscopy.

Metallic nanoparticles in a dielectric medium have also been shown to have high magnitude nonlinear optical susceptibilities. Large nonlinear susceptibilities have been reported

near the surface plasmon resonance frequencies in the materials. These effects have been attributed to dielectric confinement of charges within the metal nanoparticles and were predicted theoretically to be related to the size of the related charge-system.

The nonlinear optical properties of gold nanoparticles in a dielectric medium (glass) and Iodine-doped nonconjugated conductive polymers have been investigated. These studies used the field-induced birefringence method to measure the Kerr effect in these materials. Measurements of Kerr coefficients for the materials investigated have been performed. The magnitudes of the Kerr coefficients for the gold nanoparticle samples have been compared and used to verify theoretical models on the relationship between particle diameter and third-order optical susceptibility. Nonlinear absorption (electroabsorption) has also been measured in these materials. These measurements were made using applied electric fields to change the absorption of the material. The results have been used to gain theoretical understanding of optical nonlinearities of metallic nanoparticles down to the sub-nanometer dimensions. The nonlinearity has been shown to increase as $\frac{1}{d^3}$ where d is the diameter of the nanoparticle (quantum dot). Newer nonconjugated conductive polymers such as polyethylene terephthalate have also been studied.

Photovoltaic devices utilizing Iodine doped nonconjugated conductive polymers have been constructed and evaluated. These devices were fabricated in a similar way to dye-sensitized solar cells with the polymer used as the absorbing layer. Incident light on the cell excites electrons in the nonconjugated polymer which are then transferred through an electrolyte to a thin layer of titanium dioxide. The created devices were exposed to light and

their open-circuit voltages and short-circuit currents were measured. These results have been compared for the various nonconjugated polymers. The stability of the devices has also been investigated. The cells typically show degradation in the photocurrent output over time. Attempts were made to determine the cause of the rapid reduction in output and to find a method of extending the lifetime of the fabricated cells. These studies showed that sealing cells in order to reduce the loss of the liquid electrolyte can extend the lifetime of the cells.

Acknowledgements

This dissertation is the culmination of work comprising a large portion of my early life. It would not have been possible without the help of many people, including some I never met who have laid the groundwork for the research I have completed. The contributions of those who have come before me have made this dissertation possible and I am sincerely grateful for their hard work and dedication. My personal journey would not have come to this point without the help of all the teachers and mentors I have had throughout my life, and I would like to thank all of them for providing the knowledge and support that allowed me to be where I am today.

I would like to thank Dr. Mrinal Thakur specifically for giving me the opportunity to work and study under his guidance. The work detailed within this dissertation would not have been possible without his expertise and his financial and institutional support. I would also like to thank all the members of my committee for their time and expertise in reviewing my work.

I would like to thank Dr. Jordan Roberts for his mentorship and support during my graduate studies. He was the best boss I have ever had, and it will be difficult for anyone to surpass him in that.

I would like to thank my family for their support and patience over the course of my studies and throughout my life. I would not be where I am without them. They were always there for me and provided constant encouragement as I pursued my education.

Last, but certainly not least, I would like to thank my partner, Moriah Kent. She has been a constant advocate for me and one of my biggest supporters. She has listened to my problems when I struggled with doubts and road bumps in my journey and always encouraged me. She never doubted that I could do this even when I wasn't sure. This would have been much more difficult without her.

There are many more people who have supported and helped me along the way, and I am sorry that I do not have the space to thank them all. Know that I am very grateful to everyone who has aided me in achieving this goal, and that I did not do it alone. Thank you all.

Table of Contents

Abstract 2

Acknowledgements 5

List of Tables 10

List of Figures 11

Chapter 1 Introduction 15

Chapter 2 Background 18

2.1 Introduction to Nonlinear Optics 18

2.2 History of Nonlinear Optics 19

2.3 Wave Propagation in Media 20

2.4 Polarization 21

2.5 Nonlinear Optical Processes 23

2.5.1 Third Order Nonlinear Optical Processes 24

2.6 Nonlinear Optics and Confinement 27

2.6.1 Quantum Confinement 28

2.6.2 Third Order Susceptibility and Quantum Confinement. 30

2.6.3 Dielectric Confinement 30

2.6.4 Third Order Susceptibility, Dielectric Confinement, and Local Plasmon Resonance 31

2.7 Third Order Susceptibility of a Small Metal Sphere 33

2.8 Phase-Space Filling Model 34

2.8.4 Oscillator Strength and Exciton Density 34

2.9 Third Order Materials 35

2.9.1 Nonlinear Optics in Metal Nanoparticles 38

2.9.2 Non-conjugated Conductive Polymers as Third Order Materials 41

2.10 Organic Polymeric Photovoltaics 43

2.10.1 Dye Sensitized Solar Cells 44

Chapter 3 Objectives 49

Chapter 4 Photovoltaic Cells Involving the Nonconjugated Conductive Polymer Iodine-Doped Styrene-Butadiene-Rubber (SBR) 51

4.1 Introduction 51

4.2 Fabrication and Experimental Procedure 52

4.3 Results and Discussion 55

4.4 Conclusions 58

Chapter 5 Photovoltaic Cells Involving the Nonconjugated Conductive Polymer, Iodine-Doped Cis-poly(isoprene) 60

5.1 Introduction 60

5.2 Fabrication and Experimental Procedure 60

5.3 Results and Discussion 63

5.4 Conclusions 66

Chapter 6 Lifetime Enhancement of Photovoltaic Cells Involving Nonconjugated Conductive Polymers 68

6.1 Introduction 68

6.2 Fabrication and Experiment Procedure 70

6.3 Results and Discussion 71

6.4 Conclusions 73

Chapter 7 Quadratic Electrooptic Effect in the Nonconjugated Conductive Polymer Polyethylene Terephthalate 75

7.1 Introduction 75

7.2 Experimental Equipment 76

7.3 Results and Discussion 77

7.5 Conclusions 84

Chapter 8 Quadratic Electro-Optic Effect in Metal Nanoparticles in a Transparent Dielectric Medium 86

8.1 Introduction 86

8.2 Experimental 88

8.3 Results and Discussion 90

8.4 Conclusions 97

Chapter 9 Electroabsorption in Metallic Nanoparticles within Transparent Dielectric Media 98

9.1 Introduction 98

9.2 Experimental 100

9.3 Results and Discussion 103

9.4 Conclusions 107

Chapter 10 Quadratic Electrooptic Effect in Other Nonconjugated Conductive Polymers 109

10.1 Introduction 109

10.2 Experimental 110

10.3 Determination of the Kerr Coefficient 113

10.4 Results and Discussion 114

10.5 Conclusions 117

Chapter 11 Conclusions 118

Chapter 12 References 125

List of Tables

Table 8.1: Calculated Kerr Coefficients for different sizes of gold nanoparticles. 91

List of Figures

Figure 2.1: Resonances in several nonlinear optical processes. (a) Third Harmonic Generation, (b) Coherent Anti-Stokes Raman Scattering, (c) Two-Photon Absorption 26

Figure 2.2: The structure and mechanism of a typical dye sensitized solar cell. 45

Figure 2.3: Working principle of a dye-sensitized solar cell. The maximum potential output of a cell (ΔV) is Ef – Ef`..... 48

Figure 4.1: Change in molecular structure of SBR due to doping with Iodine. 53

Figure 4.2: Changes in optical absorption spectra of SBR due to varying levels of doping with Iodine. 53

Figure 4.3: Cross sectional view of a completed solar cell. 54

Figure 4.4: Experimental setup for photovoltaic measurements. Insert shows spectral output of the light source used..... 55

Figure 4.5: A schematic of the mechanism involved in the photovoltaic effect in these cells. ... 56

Figure 4.6: Measured photovoltage for varying light intensities for a solar cell utilizing SBR. 57

Figure 4.7: Measured photocurrent for varying light intensities for a solar cell utilizing SBR. 58

Figure 5.1: Chemical structure of cis-1,4-poly(isoprene) (CPI) before and after doping. 61

Figure 5.2: Optical absorption spectra of cis-1,4-poly(isoprene) (CPI) for different amounts of iodine doping. 62

Figure 5.3: Experimental set-up for photovoltaic measurements. The insert shows the emission spectrum of the light source used in the experiment. 63

Figure 5.4: Measured photovoltage for varying light intensities for a solar cell utilizing CPI. 64

Figure 5.5: Measured photocurrent for varying light intensities for a solar cell utilizing CPI. The insert shows the J-V characteristics of the cell in dark conditions. 65
Figure 5.6: A schematic of the mechanism involved in the photovoltaic effect in cells utilizing the iodine-doped nonconjugated conductive polymer cis-1,4-poly(isoprene) (CPI). 66
Figure 6.1: Solar cell involving an Iodine-doped nonconjugated conductive polymer. 68
Figure 6.2: The mechanism for the photovoltaic effect in a cell involving a nonconjugated conductive polymer. 69
Figure 6.3: A fabricated photovoltaic cell sealed between two glass slides using a rubber O-ring. 71
Figure 6.4: Experimental set-up for photovoltaic measurements. The insert shows the emission spectrum of the light source used in the experiment. 71
Figure 6.5: Changes in photovoltage over time for sealed and not sealed SBR devices. 72
Figure 6.6: Changes in photocurrent over time for sealed and not sealed SBR devices. 72
Figure 6.7: Pictures of a sealed photovoltaic cell under 100x magnification after (a) 1 day, (b) 7 days, and (c) 14 days. 73
Figure 7.1: Experimental set-up for the measurement of the quadratic electro-optic effect/Kerr coefficient. 77
Figure 7.2: UV/Vis spectra for 50 micron films of polyethylene terephthalate with varying levels of Iodine doping. The molar concentrations of iodine are: light doping ~ 0.16, medium doping ~ 0.28, heavy doping ~ 0.83. 79
Figure 7.3: FTIR spectra for undoped and lightly doped polyethylene terephthalate. 81

Figure 7.4: Schematic of the effect of Iodine doping on the molecular structure of polyethylene terephthalate. 82
Figure 7.5: Quadratic electro-optic effect measurements for medium doping (molar concentration ~ 0.28) polyethylene terephthalate at 633 nm. 83
Figure 7.6: Quadratic electro-optic effect measurements for heavily doped (molar concentration ~ 0.83) polyethylene terephthalate at 633 nm. 84
Figure 8.1: Experimental set-up for the measurement of the quadratic electro-optic effect/Kerr coefficient. 89
Figure 8.2: Surface plasmon resonance spectrum of gold nanoparticles in glass (sample 1). Peak at 534 nm with a particle diameter of about 50 nm. 91
Figure 8.3: Surface plasmon resonance spectrum of gold nanoparticles in glass (sample 3). Peak at 520 nm with a particle diameter of about 15 nm. 91
Figure 8.4: Quadratic electro-optic effect measurements at 633 nm for gold nanoparticles with a diameter of about 50 nm. 93
Figure 8.5: Quadratic electro-optic effect measurements at 633 nm for gold nanoparticles with a diameter of about 25 nm. 94
Figure 8.6: Quadratic electro-optic effect measurements at 633 nm for gold nanoparticles with a diameter of about 15 nm. 94
Figure 8.7: Kerr coefficient correlated with the diameter of a metallic nanoparticle. 95
Figure 9.1: Experimental set-up for measurement of electroabsorption. 102
Figure 9.2: Surface plasmon resonance spectrum of gold nanoparticles in glass. Peak at 520 nm with a particle diameter of about 15 nm. 102

Figure 9.3: Electroabsorption modulation in gold nanoparticles within glass for different applied electric fileds. Particle diameter about 15 nm. Interaction length about 3 cm. 104

Figure 9.4: Electroabsorption modulation in a nonconjugated conductive polymer (iodine-doped polyisoprene) for different applied electric fields. Film thickness about 1 μm. 105

Figure 10.1: Experimental set-up for the measurement of the quadratic electro-optic effect. 112

Figure 10.2: Profilometer measurement for a nonconjugated polymer film on a glass slide. This sample has a thickness of about 2 microns in the center of the sample. 113

Figure 10.3: Quadratic electro-optic effect measurements for cis-1,4-polyisoprene at 633 nm. 115

Figure 10.4: Quadratic electro-optic effect measurements for trans-1,4-polyisoprene at 633nm. 116

Figure 10.5: Quadratic electro-optic effect measurements for styrene-butadiene rubber at 633 nm. 116

Chapter 1

Introduction

As optically based sensing and communication technologies have become increasingly common, the field of photonics has become increasingly important. Photonics combines the study of electronics and optics and enables the development of devices that are capable of handling large amounts of data quickly. In the field of photonics nonlinear optical materials have been of particular importance. Specifically, organic nonlinear optical materials have attracted research attention due to their ease of fabrication, their ability to be engineered at a molecular level, and the high speeds possible due to their low dielectric constants and fast response times. Organic nonlinear optical materials show exciting potential for the development of devices to be used in a variety of critical fields including telecommunication, optical sensors, and data storage and manipulation.

Issues surrounding climate change and the environmental effects of energy production have led to the need for renewable and sustainable methods of energy production. The abundance and availability of solar radiation makes solar power conversion an attractive solution for both large-scale power generation and remote power needs. Traditional silicon based photovoltaic devices have dominated these markets, but they suffer from large energy requirements in production and harmful environmental effects at end of life. Organic materials provide a promising alternative on these fronts as they typically do not require the same high temperature processes in production and are more easily disposed of at the end of their

operational life. Despite these advantages, low power conversion efficiencies have hampered the widespread adoption of organic photovoltaics. The study and understanding of how organic materials operate in photovoltaic applications is important to producing devices with commercially viable efficiencies.

This research focusses on studying materials with nonlinear optical and photovoltaic applications. This includes the nonconjugated conductive polymers cis-1,4-polyisoprene, trans-1,4-polyisoprene, poly-β-pinene, styrene butadiene rubber, and polyethylene terephthalate, as well as gold nanoparticles. The nonlinear optical properties of the conjugated polymers and varying sizes of metal nanoparticles have been investigated. Also, photovoltaic devices utilizing nonconjugated conductive polymers have been fabricated and evaluated.

This research is organized into several chapters. This chapter serves as an introduction to the topics that will be covered and the organization of the dissertation. Chapter 2 provides a summary of the background work related to the topics covered. This includes the history of nonlinear optics, electromagnetic wave propagation, polarization of light, third order nonlinear optical processes, and the basic function of photovoltaic devices. Chapter 3 outlines the specific objectives of the research that was performed. Chapter 4 covers photovoltaic cells utilizing the nonconjugated conductive polymer styrene-butadiene-rubber. Chapter 5 covers photovoltaic cells utilizing the nonconjugated conductive polymer cis-1,4-polyisoprene. Chapter 6 covers research on improving the performance lifetime of photovoltaic cells involving nonconjugated conductive polymers. Chapter 7 shows research on the effects of Iodine-doping and the quadratic electro-optic effect in the nonconjugated polymer polyethylene terephthalate. Chapters 8 and 9 cover the quadratic electro-optic and electroabsorption effects respectively

for metal nanoparticles in a dielectric medium. Chapter 10 shows quadratic electro-optic effect results for several nonconjugated conductive polymers. Chapter 11 contains the conclusions and summarizes the work presented in this report.

Chapter 2

Background

2.1 Introduction to Nonlinear Optics

In classical terms, light is viewed as electromagnetic radiation. Electromagnetic waves consist of oscillating electric and magnetic fields. Electromagnetic waves are oriented such that the electric field, magnetic field, and propagation occur in mutually perpendicular directions. In optics, four vector quantities representing electromagnetic fields are important; the electric field strength **E**; the electric flux density **D**; the magnetic field strength **H**; and the magnetic flux density **B**. The theory of electromagnetic propagation of waves was developed by Maxwell and confirmed by Hertz. The fundamental theory of electromagnetic waves is governed by the following four equations collectively termed Maxwell's equations [1].

$$\boldsymbol{\nabla} \cdot \boldsymbol{D} = \rho \tag{2.1}$$

$$\boldsymbol{\nabla} \cdot \boldsymbol{B} = 0 \tag{2.2}$$

$$\boldsymbol{\nabla} \times \boldsymbol{E} = -\frac{\partial \boldsymbol{B}}{\partial t} \tag{2.3}$$

$$\boldsymbol{\nabla} \times \boldsymbol{H} = \boldsymbol{J} + \frac{\partial \boldsymbol{D}}{\partial t} \tag{2.4}$$

Where **ρ** is the charge density and **J** is the current density. Gauss' law for electric fields in equation (2.1) shows the relationship between contained charge and the electric flux through a surface. Gauss' law for magnetism, equation (2.2), shows that the net flux through a closed

surface is zero, and therefore magnetic monopoles cannot exist. Faraday's law, equation (2.3), shows that an electric field is created by a changing magnetic field. Ampere's law, equation (2.4), shows that a magnetic field is created by either a steady current or a changing electric field.

2.2 History of Nonlinear Optics

In the field of optics, the response of atoms and molecules to applied electromagnetic fields is of particular concern. The interaction of light and matter is governed by the Schrödinger equation. In this the wave function is linear, but the response of the wave function to perturbations is nonlinear. Although this was widely understood, early optical studies generally proceeded under the assumption that the response of optical materials to an applied electric field was linear. This linear assumption worked for early scientists because the electric fields they were able to apply were much weaker than the fields inside of atoms and molecules. As a result of this the perturbations were very small and linear approximations were generally appropriate. It was not until the 1870's that it was demonstrated that the refractive index of a number of materials could be changed by the application of a strong DC field. This phenomenon was the first nonlinear optical effect to be observed and is now known as the DC Kerr effect. In the 1890's a related process, now known as the Pockels effect was discovered. While the Kerr effect is related to the square of the electric field, the Pockels effect is directly proportional [2].

After the invention of the laser in the 1960's, many more nonlinear optical processes were discovered. This is due to the fact that typically only laser light has a large enough intensity to modify the optical properties of a material. The beginning of the field of nonlinear

optics is often taken to be the discovery of second-harmonic generation by Fraken *et al.* in 1961 [3]. Second-harmonic generation is a quadratic effect where the intensity of generated light varies by the square of the intensity of the applied light [4].

2.3 Wave Propagation in Media

Optical media are either isotropic or anisotropic. In an isotropic media polarization does not depend on the direction of the electric field. If the material is far from the source of the electromagnetic wave both **ρ** and **J** are zero and two equations can be developed to describe of the effect of the electromagnetic field on the media.

$$\boldsymbol{D} = \varepsilon \boldsymbol{E} = \varepsilon_0 \boldsymbol{E} + \boldsymbol{P} \tag{2.5}$$

$$\boldsymbol{B} = \mu \boldsymbol{H} = \mu_0 \boldsymbol{H} + \boldsymbol{M} \tag{2.6}$$

Where ε and μ are the permittivity and permeability respectively, ε_0 and μ_0 are the vacuum permittivity and permeability respectively, and **P** and **M** are the electric and magnetic polarization respectively. The permittivity is related to the electric susceptibility, χ, of the media as shown in equation (2.7).

$$\varepsilon = (1 + \chi)\varepsilon_0 \tag{2.7}$$

Using Maxwell's equations, the optical wave equation for an isotropic, nonmagnetic media can be derived as shown in equation (2.9).

$$\nabla^2 \boldsymbol{E} = -\mu \frac{\partial \boldsymbol{J}}{\partial t} + \frac{1}{\varepsilon} \nabla \rho \tag{2.8}$$

If **J** and ρ are zero, equation (2.9) reduces to the homogeneous wave equation.

$$\nabla^2 \boldsymbol{E} = \mu\varepsilon \frac{\partial^2 \boldsymbol{E}}{\partial t^2} \tag{2.9}$$

A similar equation can be developed for the magnetic field **H**.

$$\nabla^2 \boldsymbol{H} = \mu\varepsilon \frac{\partial^2 \boldsymbol{H}}{\partial t^2} \tag{2.10}$$

2.4 Polarization

The polarization of an electromagnetic wave describes its time-varying behavior at given point in space [4]. In a linear isotropic medium the polarization is always parallel to the applied field and is related to the magnitude of the electric field and the susceptibility as shown in equation (2.8).

$$\boldsymbol{P} = \varepsilon_0 \chi \boldsymbol{E} \tag{2.11}$$

In a nonlinear anisotropic medium, polarization is no longer necessarily parallel to the applied electric field and the susceptibility becomes a tensor. This results in a more complicated polarization equation.

$$\mathbf{P}_1 = \varepsilon_0(\chi_{11}\boldsymbol{E_1} + \chi_{12}\boldsymbol{E}_2 + \chi_{13}\boldsymbol{E}_3) \tag{2.12}$$

$$\mathbf{P}_2 = \varepsilon_0(\chi_{21}\boldsymbol{E_1} + \chi_{22}\boldsymbol{E}_2 + \chi_{23}\boldsymbol{E}_3) \tag{2.13}$$

$$\mathbf{P}_3 = \varepsilon_0(\chi_{31}\boldsymbol{E_1} + \chi_{32}\boldsymbol{E}_2 + \chi_{33}\boldsymbol{E}_3) \tag{2.14}$$

The total polarization is typically split between the linear and nonlinear parts, or between the relationships to the applied fields.

$$\boldsymbol{P} = \boldsymbol{P_L} + \boldsymbol{P_{NL}} = \boldsymbol{P}^{(1)}(\boldsymbol{E}) + \boldsymbol{P}^{(2)}(\boldsymbol{E}) + \boldsymbol{P}^{(3)}(\boldsymbol{E}) \ldots \tag{2.15}$$

Where $\boldsymbol{P}$ is the total polarization, $\boldsymbol{P_L}$ is the linear portion of the polarization, and $\boldsymbol{P_{NL}}$ is the nonlinear portion of the polarization caused by the electric field $\boldsymbol{E}$. This can also be written generally in the following form:

$$\boldsymbol{P_L} = \varepsilon_0 \chi^{(1)} \boldsymbol{E} \tag{2.16}$$

$$\boldsymbol{P_{NL}} = \varepsilon_0 \chi^{(2)} \boldsymbol{E}^2 + \varepsilon_0 \chi^{(3)} \boldsymbol{E}^3 \ldots \tag{2.17}$$

These equations assume an instantaneous response from the medium, which implies that the medium must be lossless and dispersionless. In general, nonlinear susceptibilities are also dependent on the frequency of the applied field. The electric displacement vector also changes due to its relation to the direction dependent susceptibility and permittivity.

$$\boldsymbol{D_i} = \varepsilon_0 \left(1 + \chi_{ij}\right) \boldsymbol{E}_j = \varepsilon_{ij} \boldsymbol{E}_j \tag{2.18}$$

If the coordinate system is chosen such that the axes fall along the principal dielectric axes of the medium, this equation can be re-written in a simplified form.

$$\begin{pmatrix} \boldsymbol{D_x} \\ \boldsymbol{D_y} \\ \boldsymbol{D_z} \end{pmatrix} = \begin{pmatrix} \varepsilon_x & 0 & 0 \\ 0 & \varepsilon_y & 0 \\ 0 & 0 & \varepsilon_z \end{pmatrix} \times \begin{pmatrix} \boldsymbol{E_x} \\ \boldsymbol{E_y} \\ \boldsymbol{E_z} \end{pmatrix} \tag{2.19}$$

This coordinate system is called the principal axis system since the dielectric tensor can be written as a diagonal matrix. The energy density due to the electric field is given by equation (2.15), and, if the material is nonmagnetic, the stored electric field is shown in equation (2.16).

$$\boldsymbol{U} = \frac{1}{2} \boldsymbol{E} \cdot \boldsymbol{D} \tag{2.20}$$

$$2\boldsymbol{U_e} = \left(\frac{\boldsymbol{D_x}^2}{\varepsilon_x} + \frac{\boldsymbol{D_y}^2}{\varepsilon_y} + \frac{\boldsymbol{D_z}^2}{\varepsilon_z} \right) \tag{2.21}$$

The electrical displacement vectors corresponding to this stored electrical energy describe and ellipsoid. If the principal indices of refraction are defined as n_x, n_y, and n_z, the following equation can be developed.

$$\frac{x^2}{{n_x}^2} + \frac{y^2}{{n_y}^2} + \frac{z^2}{{n_z}^2} = 1 \tag{2.22}$$

Equation (2.17) is in the general form of an ellipsoid and is commonly referred to as the indicatrix or index ellipsoid. The index ellipsoid relates the refractive index to the direction of polarization for a monochromatic light wave propagating through a nonlinear anisotropic media.

2.5 Nonlinear Optical Processes

Nonlinear optical materials can be classified in two groups, centrosymmetric or non-centrosymmetric. Materials for which the polarization is an odd function of the electric field are referred to as centrosymmetric. For a centrosymmetric material:

$$\boldsymbol{P}(-\boldsymbol{E}) = -\boldsymbol{P}(\boldsymbol{E}) \tag{2.23}$$

$$\chi^{(2)}\boldsymbol{E}^2 = -\chi^{(2)}\boldsymbol{E}^2 \tag{2.24}$$

This can only be true for the case that the second order susceptibility ($\chi^{(2)}$) is zero. Similarly, all even orders of the susceptibility for a centrosymmetric material must also be zero. For a non-centrosymmetric material, polarization is an even function of the applied electric field.

$$\boldsymbol{P}(-\boldsymbol{E}) = \boldsymbol{P}(\boldsymbol{E}) \tag{2.25}$$

In non-centrosymmetric materials all orders of susceptibility, even and odd, can be nonzero. Therefore, it can be clearly shown that in order for a material to exhibit second order nonlinearities, it must be non-centrosymmetric. Although many higher order optical nonlinearities can exist, the magnitude of the susceptibilities reduces exponentially at higher orders.

2.5.1 Third Order Nonlinear Optical Processes

Unlike second order processes, third order process can also happen in centrosymmetric materials. These processes rely on the third order susceptibility $\chi^{(3)}$. Some commonly investigated third order processes are, third harmonic generation, the DC and optical Kerr effects, intensity dependent refractive index, two photon absorption, and electro absorption.

The equation for the electric field strength of a laser beam is shown in equation (2.26)

$$\widetilde{\boldsymbol{E}}(t) = \boldsymbol{E}e^{-i\omega t} + c.c. \tag{2.26}$$

If a DC component, with magnitude A_0, is added to the electric field of a laser beam, equation (2.26), equation (2.27) can be developed.

$$\widetilde{\boldsymbol{E}}(t) = \boldsymbol{A_0} + \boldsymbol{E_1}e^{-i\omega t} + c.c. \tag{2.27}$$

Third order processes can be investigated by first writing out the polarization equation with the terms for first, second, and third order susceptibilities included. This is shown in equation (2.28).

$$\boldsymbol{P} = \varepsilon_0\left(\chi^{(1)}\boldsymbol{E} + \chi^{(2)}\boldsymbol{E}^2 + \chi^{(3)}\boldsymbol{E}^3\right) \tag{2.28}$$

If equation (2.27) is inserted into equation (2.28), several new polarization components are developed. These new terms are shown in equation (2.29).

$$\boldsymbol{P} = \varepsilon_0 \begin{pmatrix} \ldots + 3\chi^{(3)}\left({A_0}^2 + \frac{1}{4}\boldsymbol{E}_1^2\right)\boldsymbol{E}_1 e^{-i\omega t} \\ + \frac{3}{2}\chi^{(3)} A_0 \boldsymbol{E}_1^2 e^{-i2\omega t} + \frac{1}{4}\chi^{(3)}\boldsymbol{E}_1^3 e^{-i3\omega t} + \cdots \end{pmatrix} \quad (2.29)$$

Here the first term is similar to Pockels effect in that it represents a change in the refractive index. The A_0 term represents the DC Kerr effect and is a change in the refractive index based on the square of the applied DC electric field. The DC Kerr effect is often written in terms of the change in the refractive index as shown in equation (2.30).

$$\Delta n = K\lambda E^2 \quad (2.30)$$

Where K is the Kerr coefficient, λ is the wavelength of the optical wave, and E is the magnitude of the applied DC field. The $\boldsymbol{E}_1$ term in equation (2.29) is the electric field of the optical wave, and it represents the optical frequency Kerr effect, also sometimes referred to as the AC Kerr effect. The optical Kerr effect is the origin of the intensity dependent refractive index. This is a process by which a beam of light changes its own refractive index [2]. This term is directly related to the intensity (I) of the optical field through equation (2.31).

$$\boldsymbol{E}_1^2 = \frac{2I}{c\varepsilon_0 n} \quad (2.31)$$

Therefore, the intensity of the laser beam is directly proportional to the change in refractive index as shown in equation (2.32).

$$\Delta n = n_2 I \quad (2.32)$$

The n_2 term can be related to the third order susceptibility $\chi^{(3)}$ through equation (2.33).

$$n_2 = \frac{3\chi^{(3)}}{4c\varepsilon_0 n^2} \tag{2.33}$$

The final two terms in equation (2.29) represent the DC induced second harmonic generation and third harmonic generation, respectively. The application of a DC electric field to a centrosymmetric system removes the symmetry and allows the previously forbidden process of second harmonic generation to occur. Third harmonic generation is very similar to second harmonic generation but is the third order version and thus possible in centrosymmetric and non-centrosymmetric systems. In this process three photons of frequency ω are destroyed and one photon at frequency 3ω is created. The energy band diagram for third harmonic generation is shown in figure 2.1 (a).

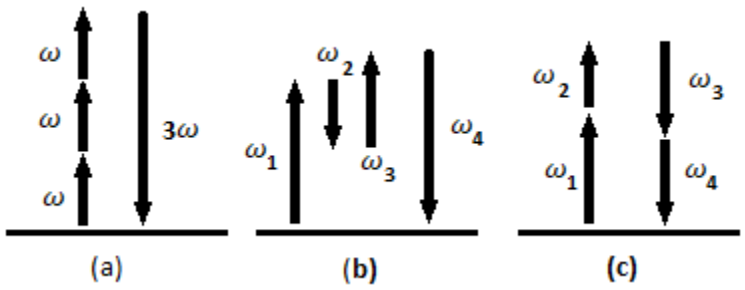

Figure 0.1: Resonances in several nonlinear optical processes. (a) Third Harmonic Generation, (b) Coherent Anti-Stokes Raman Scattering, (c) Two-Photon Absorption

Electroabsorption refers to a nonlinear change in the absorption coefficient of a material due to an applied electric field and is related to the DC Kerr effect. Electroabsorption is based on the imaginary portion of the Kerr coefficient and is therefore related to the

absorption coefficient of the material. Electroabsorption can be written in terms of the change in a materials absorption coefficient as shown in equation (2.34).

$$\Delta\alpha = 4\pi K' E^2 \tag{2.34}$$

Where K' is the imaginary portion of the Kerr coefficient, E is the magnitude of the applied DC field, and $\Delta\alpha$ is the change in the absorption coefficient. This effect is related to two-photon absorption which is given by equation (2.35).

$$\Delta\alpha = \alpha_2 I \tag{2.35}$$

Where $\Delta\alpha$ is the change in the absorption coefficient, $\alpha_2$is the two-photon absorption coefficient, and I is the optical intensity. The magnitude of K' is related to saturation of absorption and the two-photon absorption coefficient. The magnitude of the two-photon absorption coefficient is proportional to the imaginary portion of the third-order susceptibility $\chi^{(3)}$.

2.6 Nonlinear Optics and Confinement

Charge confinement occurs when the valence electrons in a material are restricted to regions smaller than the delocalization length. This results in optical resonances that are determined by the extent of the confinement. Charge confinement has been widely demonstrated to affect the optical nonlinearities of a material. These effects have been demonstrated in a variety of materials, including metals, semiconductors, and polymers, and is typically achieved through quantum effects or with the use of dielectric materials.

2.6.1 Quantum Confinement

Quantum confinement occurs when an exciton is confined to a region whose size approaches or is smaller than the exciton Bohr radius. This effect was first seen by Ekimov et al in spectroscopic studies of CuCl crystals, and later observed by the same group in other semiconductor microcrystals [5, 6]. The exciton Bohr radius in a bulk semiconductor is the radius associated with a Wannier exciton and is given by the equation (2.36).

$$r_n = \left(\frac{m_0 \varepsilon_r \alpha_H}{\mu}\right) n^2 \tag{2.36}$$

Where m_0 is the mass of the electron, ε_r is the relative permittivity, μ is the reduced mass of the electron and hole, and α_H is the Bohr radius. The De Broglie wavelength of an electron, shown in equation (2.37), is also important to quantum confinement.

$$\lambda_d = \frac{h}{p} \tag{2.37}$$

Where h is the Planck constant, and p is the momentum. The free electrons in a bulk material are able to move in any direction, and their linear momentum can be related to their thermal kinetic energy (E_T) by equation (2.38)

$$E_T = \frac{{p_i}^2}{2m_e{}^*} \approx \frac{1}{2} K_B T \tag{2.38}$$

Where p_i is the linear momentum, $m_e{}^*$ is the effective mass of the electron, K_B is Boltzmann's constant, and T is the temperature. Equations (2.37) and (2.38) can be combined to find a relationship between the temperature and the De Broglie wavelength given by equation (2.39)

$$\lambda_d = \frac{h}{\sqrt{K_B T m_e{}^*}} \tag{2.39}$$

In bulk materials the crystal dimensions are generally much larger than either the De Broglie wavelength or the exciton Bohr radius. Quantum confinement in these materials occurs when the crystal dimensions are reduced in any direction to a size that approaches these values. This results in the energy level becoming quantized in that direction. Quantum confinement is generally split into three categories based on the number of constrained dimensions. One dimensional confinement happens when the electrons and holes are constrained in one direction. This can be seen in semiconductors when a thin layer of a lower-bandgap material is placed between two higher band gap materials. This constrains the electrons and holes in the lower band gap material and is comparable to a quantum well. Two-dimensional confinement happens when electrons and holes are allowed to move in only one direction. This occurs in quantum wires and results in energy levels that are quantized in the two directions perpendicular to the direction of the wire. Three-dimensional confinement occurs when the electrons and holes are bound in all three directions. This is referred to as a quantum dot and results in energy levels that are quantized in all three directions. The energy level of a simple quantum dot is given by equation (2.40).

$$E_n = \frac{\hbar^2 \pi}{2m_e}\left[\left(\frac{n_x}{l_x}\right)^2 + \left(\frac{n_y}{l_y}\right)^2 + \left(\frac{n_z}{l_z}\right)^2\right] \tag{2.40}$$

Where h is Plank's constant, m_e is the mass of the electron, and n and l are the quantum numbers and lengths for the corresponding directions.

2.6.2 Third Order Susceptibility and Quantum Confinement.

In the transparent regions of compounds, the third order susceptibility is related to the optical delocalization parameter (N_d) and the critical regions in the density of states. These are both related to quantum confinement with the density of states varying based on quantum confinement. For a system confined in one dimension, with a critical point E_0, $\chi^{(3)}$ can be expressed as shown in equation (2.41) [7].

$$\chi^{(3)} = \chi_\sigma{}^{(3)} \left(\frac{E_f}{E_0}\right)^6 \tag{2.41}$$

Where $\chi_\sigma{}^{(3)}$ is the third order susceptibility of the non-confined structure, E_f is the Fermi level, and the ratio E_f/E_0 is related to N_d and the confinement length.

For an electron that is confined in all three directions, with a critical surface E_2 the third order susceptibility is given by equation (2.42) [8].

$$\chi^{(3)} \approx \frac{P_{cv}{}^2}{E_2{}^{9/2}} \tag{2.42}$$

Where P_{cv} is the interband transition dipole moment, which is related to the amount of confinement. In both of these cases, the increased confinement results in larger third order susceptibilities.

2.6.3 Dielectric Confinement

When confined systems are in a material with a non-uniform charge density distribution, the local field strengths can vary from the external field. This difference in field

strength occurs at the interface between the confined systems and the surrounding material and arises due to the additional effect of the surface polarization along these interfaces. Large differences in the dielectric constant between the confined region and the surrounding areas can be observed. Incident light on these systems can see an enhancement of the nonlinear optical properties due to this increase in local field strength [9].

2.6.4 Third Order Susceptibility, Dielectric Confinement, and Local Plasmon Resonance

When spherical quantum dots of sufficiently small radii (r<λ) are dispersed in a medium with a dielectric constant ε_0, the field inside each particle (E_i) is given by equation (2.43) [10].

$$E_i = \frac{3\varepsilon_0}{\varepsilon+2\varepsilon_0} E \approx E f_1 \tag{2.43}$$

Where E is the applied electric field, and f_1 is an approximation of the ratio between the internal and external electric fields. The effective dipole moment of this composite material ($\tilde{\varepsilon}$) can be related to the volume fraction of quantum dots inside the material (μ) by equation (2.44), which was developed by Maxwell Garnett through theoretical studies of small metal particles in glass. [11].

$$\tilde{\varepsilon} = \varepsilon_0 + 3\mu\varepsilon_0 \frac{\varepsilon-\varepsilon_0}{\varepsilon+2\varepsilon_0} \tag{2.44}$$

For a specific frequency ω_{spr} such that

$$\varepsilon'(\omega_{spr}) + 2\varepsilon_0 = 0 \tag{2.45}$$

Where ε' is the real part of the bulk dielectric constant. This relationship is also shown in equations Mie developed for an analytical solution to the scattering and absorption of light by spherical particles using Maxwell's equations [12]. Their equation for the scattering cross-section is shown in equation (2.46).

$$\sigma_{sca} = \frac{32\pi^4 {\varepsilon_m}^2 V^2}{\lambda^4} \frac{(\varepsilon_1 - \epsilon_m)^2 + (\varepsilon_2)^2}{(\varepsilon_1 + 2\epsilon_m)^2 + (\varepsilon_2)^2} \tag{2.46}$$

Where V is the particle volume, λ is the wavelength of light, ϵ_m is the dielectric constant for the medium, and ϵ_1 and ϵ_2 are the real and imaginary portions of the particle's dielectric constant. Here it can be seen that the denominator is minimized when $\epsilon_1 = -2\epsilon_m$. This relationship as well as equation (2.45) shows the dependence of the surface plasmon resonance on the surrounding dielectric medium. The peak frequency for the surface plasmon resonance can be found using the Drude model. The frequency dependent form of $\epsilon_1$using this model is given by equation (2.47).

$$\epsilon_1 = 1 - \frac{{\omega_p}^2}{\omega^2 + \gamma^2} \tag{2.47}$$

Where ω_p is the plasma frequency and γ is the damping parameter for the bulk metal. For visible and near infrared frequencies, $\gamma \ll \omega_p$. This means that equation (2.47) can be simplified as:

$$\epsilon_1 = 1 - \frac{{\omega_p}^2}{\omega^2} \tag{2.48}$$

Using equation (2.48) and the $\epsilon_1 = -2\epsilon_m$ relationship, an equation for the peak surface plasmon resonance frequency based on the plasma frequency and the dielectric constant of the surrounding medium can be developed as shown in equation (2.49).

$$\omega_{spr} = \frac{\omega_p}{\sqrt{2\varepsilon_m + 1}} \tag{2.49}$$

At frequencies near ω_{spr}, there is a significant increase in the local field strength. This phenomenon is known as the surface plasmon resonance (SPR). The surface plasmon resonance has a large effect on the nonlinear optical properties of a material. This is especially true for the Kerr effect. The optically induced change in dielectric constant is given by equation (2.50).

$$\delta\tilde{\varepsilon} = 12\pi\chi^{(3)}|E(\omega)|^2 \tag{2.50}$$

Utilizing equations (2.43) through (2.46), an expression for the third order susceptibility of the composite ($\tilde{\chi}^{(3)}$) can be developed as shown by equation (2.51).

$$\tilde{\chi}^{(3)} = p|f_1|^2 {f_1}^2 \chi^{(3)} \tag{2.51}$$

For quantum dots in a dielectric medium, when the Kerr effect is measured at frequencies near the surface plasmon resonance frequency, a large increase in $\tilde{\chi}^{(3)}$ can be seen. This enhancement is larger than that seen in the bulk material, due to the combination of the effects of the dielectric and quantum confinements.

2.7 Third Order Susceptibility of a Small Metal Sphere

Metal particles within a dielectric medium exhibit large third order susceptibilities that are not found in the bulk forms of the same materials. These systems were first modeled by

Hache et al in 1986 to determine the relationship between the size of the particle and the third order susceptibility $\chi^{(3)}$)[13].

$$\chi^{(3)}_{xxxx} = -i\frac{0.45}{\pi}T_1T_2\frac{1}{a^3}\frac{e^4}{m^2\hbar^5\omega^7}{E_f}^4 g_1(\nu)\left(1-\frac{a}{a_0}\right) \quad (2.52)$$

From Equation (2.52), when a is much smaller than a_0, the main size dependence of $\chi^{(3)}$is a^{-3}. Therefore, the third-order susceptibility of a small metal sphere is, according to the model developed by Hache et al, proportional to inverse cube of the sphere's diameter.

2.8 Phase-Space Filling Model

The phase-space filling model is an experiment based theoretical model that explains transient optical absorption processes [14-18]. Initially this was developed for semiconductor quantum wells. Subsequently it was experimentally verified for organic nonlinear optical systems involving single-crystal polydiacetylene (r-d system). Prior models suggested that screening governed the nonlinear optical effects near the band gap of semi-conductors and that charged plasmas were much more effective at screening the Coulomb reaction than excitons [19]. Experimental observations showed that the effects of excitons on the absorption spectra are larger than that of free carriers [20], consistent with the phase-space filling model.

2.8.4 Oscillator Strength and Exciton Density

The phase-space filling model provides a simple relationship between the oscillator strength and exciton density as shown in equation (2.53) [14].

$$\frac{\delta f}{f} = -\frac{N}{N_S} \quad (2.53)$$

Where f is the oscillator strength, N is the exciton density per unit length, and N_s is the saturation density.

The change in oscillator strength, as described here, is related to two processes, the blocking mechanism due to the exclusion principle, and the changes in the exciton orbital wave function due to the modification of the electron-hole interaction due to the presence of other electron hole pairs. The exclusion principle limits transitions because only transitions into unoccupied final states are allowed.

Since the oscillator strength is related to the transition probability, as shown in the previous section, a greater change in absorption or emission is expected as the ratio of excited electrons to the total number of electrons available is increased.

2.9 Third Order Materials

Third order nonlinear optical processes are not limited by material symmetry. For this reason, a larger variety of materials can be investigated than in second order nonlinear optics. Several third order processes are commonly used to evaluate these materials including third harmonic generation, the DC and optical Kerr effects, degenerate four wave mixing, self-focusing techniques, and the intensity dependent refractive index. Due to the variety of methods used, and differences in experimental conditions, direct comparisons of third order susceptibility are difficult to make.

One of the most common methods for measuring the third order susceptibility of a material is known as the z scan method. This measures the third order nonlinear optical properties of a material through the process of nonlinear absorption. The measurements are

performed by varying the intensity of incident light on a sample by moving it in the direction of laser propagation and measuring the transmitted light using a detector. One drawback of this technique is that the high laser intensities required to perform the measurement makes thermal effects difficult to isolate. This is important because in most materials thermal effects have a much greater magnitude than the third order optical effects [4].

Early research suggested that the magnitude of the third order susceptibility of a material was dependent on its conjugation length. In 1966 Schafer and Schmidt developed a geometrical relationship between the two-photon absorption of an organic dye and dimension of the π-electron cloud referred to as the Schafer-Schmidt relation [21]. In the 1970's several different research groups attempted to develop an empirical relationship for this dependence. Foucault, Hermann, and Ducuing reported on the relationship between delocalization length and number of electrons in a material [22-24]. Their experimental results contradicted the Schafner-Schmidt relation, suggesting a more complicated relationship [25]. Rustugi developed a relationship between delocalization length and microscopic polarizability in one dimension using a free electron gas model [26]. Agarwal reported a dependence on the magnitude of third order susceptibility on the sixth power of π electron delocalization length in one dimensional π conjugated polymers [7]. Their research also suggested that the third order susceptibility of a material was related to donor-acceptor functionalities, the orientation of the polymer chain, the packing density, and inversely related to the sixth power of the energy gap.

Materials that have been developed or studied for third order nonlinear optics can be broadly classified as: inorganic materials, organic liquids, organic molecular solids, organic charge transfer complexes, organic π conjugated polymers, organometallic compounds, liquid

crystals, organic composites, nano-metallics, semiconductor nano-composites, dye grafted polymers, and non-conjugated conductive polymers. Among these, organic π conjugated polymers, semiconductor nano-composites, and metallic nanoparticles, have been researched heavily in the recent past.

Organic π conjugated polymers have been shown to have exceptionally larger third order properties. Sauteret reported on the third order nonlinear properties of polydiacetylene *p*-toluene sulfonate (PDA-PTS) [27]. Their team measured a $\chi^{(3)}$ value of 8.5×10^{-10} esu at 1.89 μm. The large optical nonlinearity and fast response times are attributed to the delocalization of the π electrons along the conjugated chain or quantum wire and the small average distance between the C-C bonds. These results proved to be a turning point in the study of third order nonlinear optics in organic π conjugated polymers. Some of the other organic π conjugated polymers that were investigated included: poly (*p*-phenylenevinylene) (PPV), polyacetylenes, and polythiophenes [28-33]. The first time-resolved measurement of optical nonlinearity using polydiacetylene single-crystal film was reported by Carter et al. in 1985 [34]. The largest third order susceptibility resonant for a polydiacetylene, 2×10^{-5} esu, was measured in p-toluene sulfonate polydiacetylene by Greene et al. [15]. The mechanism of third-order optical nonlinearity was evaluated using polydiacetylene (PTS) single-crystal film [17].

In semiconductor nanoclusters, small particle sizes are required to achieve large third order nonlinear optical properties. In these materials, small particles sizes increase the inter-particle spacing which confines the valence electrons into smaller dimensions. This confinement changes the electron quantum states and affects the way they interact with applied optical

fields. This is known as the quantum confinement effect [35]. Materials that exhibit quantum confinement effects are sometimes referred to as quantum dots. A variety of semiconductor materials have been shown to have large third order optical nonlinearities due to the quantum confinement effect including: cadmium sulfide (CdS), cadmium selenide (CdSe), zinc sulfide (ZnS), and zinc selenide (ZnSe) [36-40].

2.9.1 Nonlinear Optics in Metal Nanoparticles

Metallic nanoparticles and semiconductor nanoclusters have also been extensively investigated for third order optical nonlinearities. Third order susceptibilities in these materials are related to the size of the related charge system [13]. By keeping the containment distance of the valence electrons very small, typically within a few nanometers, high third order optical nonlinearities can be obtained. These confinements are typically categorized as quantum confinement or dielectric confinement [35].

When investigating metallic nanoparticles for their third order nonlinear optical properties, they are typically contained within a dielectric medium such as glass. When metallic nanoparticles are confined in a dielectric medium, the difference in the dielectric properties of the metal and the surrounding medium leads to dielectric confinement. In these materials third order nonlinearities are related to the surface plasmon resonance effect. Near the peak frequency of the surface plasmon resonance, high third order optical nonlinearities are seen due to changes in the field distribution within the material [41].

Ricard et al were the first to report experimental studies on the nonlinear optical properties of small metallic particles [42]. In 1986 Hache et al published reports observing the

temporal behavior of optical phase conjugation in gold nanoparticles [13]. They determined that the optical nonlinearity in these materials was produced from the electrons within the metal and developed a model calculation of the electric-dipole third-order susceptibility of conduction electrons in a metal sphere. This model predicted that the third-order susceptibility of small metallic particles should be roughly related to the inverse of the third power of the radius of the metallic particle.

In addition to size and concentration, the shape of the embedded metallic particles has also been shown to have an effect on their nonlinear optical properties. In 1999, Link and El-Sayed compared the optical properties of nanodots and nanorods [43]. They found that the shape of the particle had a drastic effect on the surface plasmon resonance, and therefore the location of the absorption peaks of the particles. They found that for nanorods the plasmon absorption splits into two bands corresponding to the oscillation of free electrons in either the transverse or the longitudinal axis of the rods. The transverse resonance was coincident with spherical particles of the same diameter, while the longitudinal resonance was found to be red-shifted with a strong dependence on the aspect ratio of the nanorod (the ratio of the length divided by the width).

Composite materials containing copper, silver, and gold have been produced by a variety of research groups through ion implantation, sputtering and melt-quenching techniques. Ion implantation and sputtering can be used on a variety of dielectric matrices, with zinc oxide (ZnO) and silicon dioxide (SiO_2) being the most used materials [44]. In 1993, Magruder et al used ion implantation into fused silica to synthesize gold clusters with diameters between 5 and 30 nm [45]. They reported a third-order nonlinear optical response of less than

35 picoseconds and an effective susceptibility of 200 times those of similarly sized clusters in melt glass. In 1994, Tanahashi et al used a multitarget sputtering method to prepare SiO2 samples containing embedded silver particles [46]. They reported a third-order susceptibility of 1.6×10^{-8} esu using degenerated four-wave mixing. Also in 1994, Uchida et al reported on glasses doped with silver or copper nanoparticles [47]. They used degenerative four-wave mixing and focused on the dependence of the third-order nonlinearities on particle size. They found a maximum value on the order of 10^{-7} esu for the third order susceptibility. In 1998, Inouye et al used a sputtering method to embed gold nanoparticles into SiO2 [48]. They reported a third-order susceptibility of 2.0×10^{-8} esu using a femtosecond optical Kerr shutter experiment. In 2002, Pinçon-Roetzinger et al reported on thin films of gold particles with varying concentrations embedded into SiO2 substrates using sputtering techniques [49]. They reported third order susceptibilities of 0.5×10^{-7} to 63.8×10^{-7} for different mean particle diameters and concentrations using the z-scan technique. In 2007, Ghosh et al used the z scan technique to measure the nonlinear optical properties of copper nanoclusters embedded in glass using ion implantation [50]. They found relatively small values of third order nonlinear optical properties which they attributed to higher magnitude thermal effects masking the electronic contributions. In 2009, Garcia et al reported on the nonlinear optical properties of silver-copper and silver-gold nanocomposites in glass [51]. They compared the third-order response for different volume fractions of the metals in the nanoclusters and found a maximum third-order susceptibility of 1.2×10^{-8} esu for 0.09 copper/0.03 silver sample. In 2010, Wang et al reported on copper nanoclusters imbedded in glass through ion implantation [52]. They

measured the third-order susceptibility using the z-scan technique and found a magnitude of 2.1×10^{-7} esu.

2.9.2 Non-conjugated Conductive Polymers as Third Order Materials

Historically, polymers are known to be insulators. In 1977 Shirakawa demonstrated that iodine doping could drastically increase the conductivity of the conjugated polymer polyacetylene [53]. Building on this data, the conductivity of a variety of doped conjugated polymers was reported. In 1988 Thakur published research that dramatically changed the prevailing thought on conductive polymers [54]. This research demonstrated that polymers with isolated double bonds could be made conductive upon doping with electron donors or acceptors. This proved that a polymer did not need to be conjugated to be conductive as was previously thought. These materials formed a new classification and became known as nonconjugated conductive polymers. The first nonconjugated conductive polymer reported by Thakur was cis-1,4-polyisoprene (CPI) [54]. Thakur demonstrated that the conductivity of CPI could be increased by about ten orders of magnitude when doped with iodine. Following this research, several other nonconjugated conductive polymers were reported on by Thakur and others. These included styrene butadiene rubber (SBR), poly-β-pinene (PBP), poly(ethylenepyrrolediyl) (PEP), polyalloocimene, polyaniline furfural, polynorbornene, and trans-1,4-polyisoprene (TPI) [54-60].

In nonconjugated conductive polymers, doping agents interact with the isolated double bonds within the material. Charge transfer occurs from the isolated double bond to the dopant creating a radical cation. The number of double bonds affected, and thus the conductivity,

increases proportionally with the amount of dopant added. This charge transfer creates a highly confined metallic domain or quantum dot. The size of the charge system has been theoretically shown to be related to the magnitude of the third order optical nonlinearity as a function of $\frac{1}{d^3}$, where d is the diameter of the charge system [13]. The size of this charge system is sub-nanometer and results in exceptionally large third order optical nonlinearities. This is the sole source of optical nonlinearities in nonconjugated conductive polymers as, unlike conjugated polymers, they do not have extended delocalization.

Thakur went on to report on the nonlinear optical properties of several nonconjugated conductive polymers. The first nonconjugated conductive polymer that Thakur reported on was CPI. Their research showed that doped CPI demonstrated a 4×10^{-4} change in the refractive index for and applied voltage of $2\frac{V}{\mu m}$ at 633nm [61]. This corresponded to a reported Kerr coefficient of $1.6 \times 10^{-10} \frac{m}{V^2}$. This was around 67 times larger than what had been reported for nitrobenzene at 589nm. In 2006, a modulation depth of 0.12% was reported for iodine doped PBP also at 633nm [57]. This corresponded to a Kerr coefficient $1.2 \times 10^{-10} \frac{m}{V^2}$ and a $\chi^{(3)}$ of 0.65×10^{-8}esu. Thakur also performed two-photon absorption measurements on iodine doped PBP using a 150fs Ti-Sapphire laser. This research reported a two-photon absorption coefficient of $2.6 \frac{cm}{MW}$ at 810nm [62]. Iodine doped PEP was also investigated and a Kerr coefficient of $1.2 \times 10^{-10} \frac{m}{V^2}$ at 633nm was reported [58]. Thakur also investigated the quadratic electrooptic affect in trans-1,4-polyisoprene. These results were published in 2011, and showed a Kerr coefficient of $3.5 \times 10^{-10} \frac{m}{V^2}$ at 633 nm and $2.5 \times 10^{-10} \frac{m}{V^2}$ at 1550 nm [63] In 2012, Thakur and Telang published research on the quadratic electrooptic effect in styrene-

butadiene-rubber at both 633 nm and 1550 nm. These results showed Kerr coefficients of $3.1 \times 10^{-10} \frac{m}{V^2}$ and $1.2 \times 10^{-10} \frac{m}{V^2}$ at 633 nm and 1550 nm respectively [60].

2.10 Organic Polymeric Photovoltaics

Solar power conversion technology has been a popular field of study for many years due to the vast amounts of solar energy available on the earth's surface as well as in space. Devices that are capable of harnessing this energy have become increasingly important as the need for energy production without the emission of carbon has become more and more apparent. Although the amount of solar radiation varies based on location, time of year, and atmospheric conditions, the raw energy input for solar power generation systems is free and available long term. This provides benefits over traditional power generation systems where the raw input costs can be a significant portion of the operational costs, and price fluctuations can greatly impact ROI calculations, or in situations where remote power generation is needed.

Solar power devices rely on the photovoltaic effect, where incident light on a material produces both a voltage and a current. For the photovoltaic effect to occur, a junction must be present with an electrical bias in one direction. When photons are absorbed by the materials that form this junction charge carriers, electrons and holes, can be created. The junction then separates these charge carriers so they can be collected in electrical terminals. One method of creating this junction is to use a Schottky barrier, which uses the interface between a metal and a semiconductor. More commonly, especially in modern solar cells, a junction is created between p and n type doped semiconductors. These are referred to as p-n junction solar cells.

2.10.1 Dye Sensitized Solar Cells

Although p-n junction solar cells have traditionally dominated the commercial and research aspects of solar power conversion, dye sensitized solar cells have emerged as a viable alternative. Dye sensitized solar cells are thin film devices that are typically composed of two electrodes, a light absorbing molecule, titanium dioxide, and a liquid electrolyte. These devices are cheaper and easier to produce than traditional solar panels. They do not require the same high temperature processes, expensive materials, or advanced clean room environments for their fabrication. They can also be fabricated on flexible substrates which allows them to be used in applications where traditional cells would not be viable. Although the power conversion efficiency of these devices is less than other thin film solar technologies, the price to performance potential of these cells allows them to be potentially commercially viable.

Dye sensitized solar cells were developed following studies into how chlorophyll functioned during photosynthesis. In 1968 Gerischer et al published experimental data and models showing how organic dyes can produce photocurrents at semiconductor electrodes when exposed to light illumination [64]. In 1971 Tributsch and Calvin showed that chlorophyll, when excited by light, could be used to pump electrons into semiconductor electrodes [65]. Then in 1972, Tributsch published research showing the first device that used organic dyes to convert light into electrochemical energy [66]. These devices used a zinc-oxide electrode, and the power conversion efficiencies were about 1%. In 1991 Grätzel used titanium dioxide and a monolayer of dye to produce the first dye sensitized solar cells with a usable power conversion efficiency of around 7-8% [67]. For this reason, dye sensitized cells are often now referred to as

Grätzel cells and the majority of modern devices follow the same basic architecture as these cells. Later, in 1997, they were able to produce devices with efficiencies of up to 10% [68].

Traditional dye sensitized solar cells are typically fabricated beginning with a transparent electrode. A thin layer of titanium dioxide is then added to the back side of this electrode. The titanium dioxide forms a porous structure with a very high surface area. An organic dye is then added which bonds to the surface of the titanium dioxide layer. Then a counter electrode is added, and an electrolyte solution introduced. This structure is shown in figure 2.2.

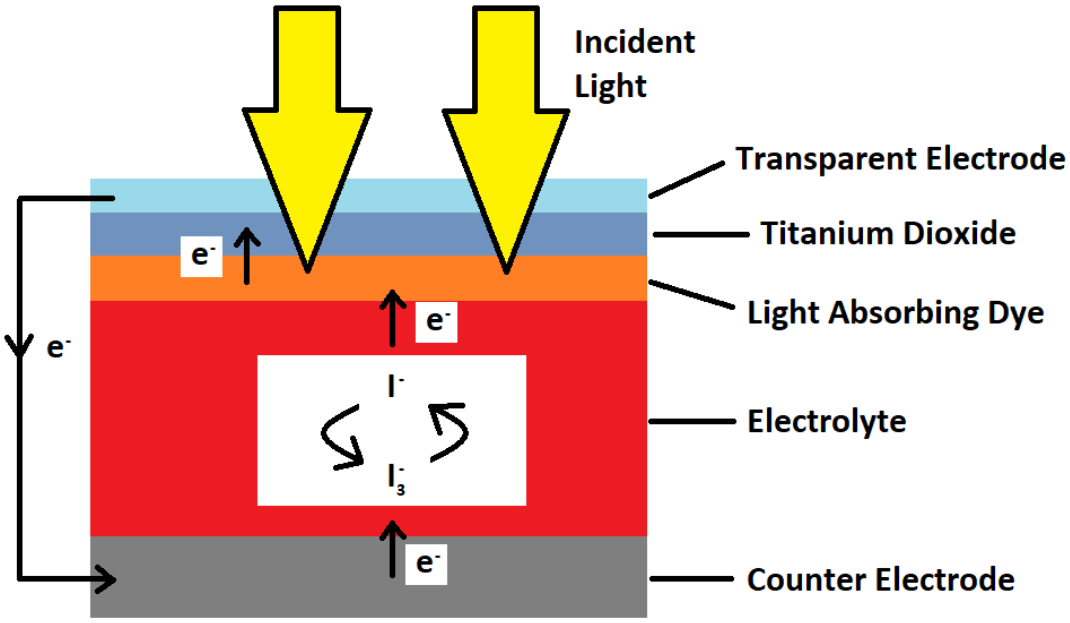

Figure 0.2: The structure and mechanism of a typical dye sensitized solar cell.

Dye sensitized solar cells operate similarly to traditional photovoltaic devices, but the mechanisms performed by the semiconductor, light absorption and charge carrier transport, are instead split between the different components of the dye sensitized cell. In these devices, current is produced when an absorbed photon leads to electron injection into the

semiconductor (typically TiO_2). For the circuit to be completed, an electron needs to be returned to the light absorbing material via electron transfer from a redox species in solution which is then reduced at the counter electrode. The monochromatic current yield as a ratio of electric current to the incident photon flux is given by equation (2.54) [67].

$$\eta_i(\lambda) = LHE(\lambda) \times \varphi_{inj} \times \eta_e \tag{2.54}$$

Where LHE (light harvesting efficiency) is the fraction of the incident photons that are absorbed, φ_{inj} is the quantum yield for charge injection, and η_e is the efficiency of collecting the injected charge at the back contact. The overall efficiency of the cell is also related to the difference in the excited and ground states for the dye [69, 70].

A diagram of the energy states involved in a dye sensitized solar cell is shown in figure 2.3. First, an incident photon is absorbed in the absorption layer. This results in an electron in the material being promoted from the ground state (S) to the excited state (S^*) of the material as shown in equation (2.55).

$$S + h\nu \rightarrow S^* \tag{2.55}$$

These electrons are then injected into the conduction band of the TiO_2 as shown in equation (2.56), which must be below the excited state of the absorbing material. This causes the absorbing material to be oxidized.

$$S^* \rightarrow S^+ + e^- (TiO_2) \tag{2.56}$$

The injected electrons are then transferred between the TiO_2 particles toward the transparent electrode. They then travel through an external circuit to the counter electrode. At the counter electrode the electrons then reduce I^-_3 to I^- in the electrolyte as shown in equation (2.57).

$$I^-_3 + 2e^- \rightarrow 3I^- \tag{2.57}$$

The maximum voltage attainable by a dye-sensitized solar cell is therefore the difference between the redox potential and the potential of the injected electrons as they reach the transparent electrode. Under standard illumination this value is 0.7 V [71, 72]. The regeneration of the absorbing material to the ground state can then take place through the acceptance of electrons from the I^- ion redox mediator as shown in equation (2.58). This then oxidizes I^- to I^-_3 completing the redox cycle.

$$S^+ + e^- \rightarrow S \tag{2.58}$$

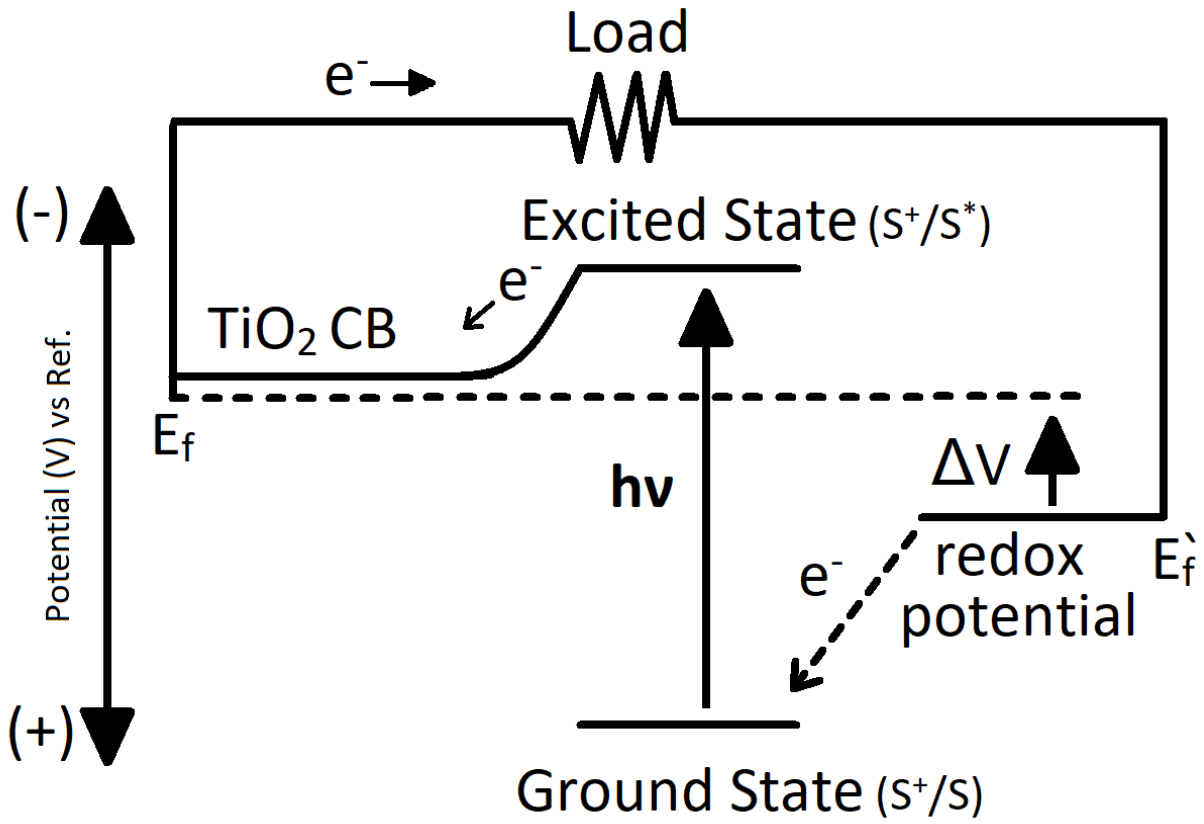

Figure 0.3: Working principle of a dye-sensitized solar cell. The maximum potential output of a cell (ΔV) is Ef – Ef`.

Chapter 3

Objectives

The objective of the performed research was to study the nonlinear optical properties and photovoltaic properties of selected organic polymeric and nano-optical materials. Third order nonlinear optical studies have been performed on a number of nonconjugated conductive polymers in comparison with metallic nanoparticles in a transparent dielectric medium. In particular, cis-1,4-polyisoprene, trans-1,4-polyisoprene, styrene butadiene rubber, poly-β-pinene, and polyethylene terephthalate have been investigated. The Third order nonlinear optical properties of metal nanoparticles, specifically of gold, have been studied. Theoretical understanding of the nonlinear optical characteristics dependance on particle diameter has been developed. The photovoltaic properties of these nonconjugated polymers, as well as ways to improve the lifetime of photovoltaic cells created from these materials, have been investigated.

The specific objectives of this research were:

1. To prepare samples of varying thickness of cis-1,4-polyisoprene, trans-1,4-polyisoprene, styrene butadiene rubber, and polyethylene terephthalate and doping them with iodine to be used in electro-optic measurements.
2. To investigate the effects of Iodine doping on polyethylene terephthalate using UV/Vis and IR spectroscopy.

3. To determine the Kerr coefficients for cis-1,4-polyisoprene, trans-1,4-polyisoprene, styrene butadiene rubber, and polyethylene terephthalate at 633nm using the field-induced birefringence method.
4. To determine Kerr coefficients and electroabsorption characteristics of gold nanoparticles in glass by studying nanoparticles of varying diameters.
5. To compare the measured Kerr coefficients and nonlinear absorption characteristics between the nonconjugated polymers and metal nanoparticles; to determine the relationship between particle size and the third order nonlinear optical properties of these materials.
6. To prepare thin film samples of cis-1,4-polyisoprene and styrene butadiene rubber and doping them with iodine in order to study these materials potential in photovoltaic applications.
7. To produce photovoltaic devices utilizing cis-1,4-polyisoprene and styrene butadiene rubber and to study potential methods of extending the lifetime of created cells.

Chapter 4

Photovoltaic Cells Involving the Nonconjugated Conductive Polymer Iodine-Doped Styrene-Butadiene-Rubber (SBR)

4.1 Introduction

Photovoltaic cells of various structures and mechanisms based on organic molecules and polymers have been widely studied and reported [73-75]. Organic materials enjoy ease of processing and a variety of molecular structures making them an attractive area of study. This also provides them the opportunity of being potentially lower cost alternatives to inorganic materials in photovoltaic applications [73-79]. For these reasons, a wide range of organic molecules and polymers have been investigated and increased efficiencies in solar energy conversion have been reported. Conjugated polymers specifically have been extensively studied for photovoltaic effects. More recently, the photovoltaic effect in specific nonconjugated conductive polymers have been reported [80-82]. The photovoltaic effect involving charge transfer between and undoped nonconjugated polymer and fullerene was reported but showed very limited photocurrents [81]. In a different cell structure than was used in this report, iodine-doped nonconjugated conductive polymer poly(β-pinene) was shown to have significantly higher photocurrents that previous reports [82]. In this report, photovoltaic cells have been constructed involving iodine doped styrene butadiene rubber (SBR). The fabricated cells have been constructed on indium-tin-oxide (ITO) coated polyethylene terephthalate (PET) substrates with layers of titanium dioxide, the nonconjugated conductive polymer, and a carbon electrode.

These cells have produced substantially higher conversion efficiencies than previous reports involving nonconjugated conductive polymers.

4.2 Fabrication and Experimental Procedure

PET substrates were used with transparent ITO coatings to act as an electrode on the light incident side of the cell. The dark side of the cell also used a PET substrate with a thin layer of carbon as the electrode. A solution of styrene-butadiene-rubber and toluene was created, and this solution was used to apply a film of nonconjugated polymer on top of the carbon electrode. This layer acts as the light absorber and acts similarly to the dye molecules in a dye-sensitized solar cell. This film was then doped with iodine to around 0.8 molar through exposure to iodine vapor for several hours in a room temperature environment. Isolated double bonds in the nonconjugated polymer are affected by the iodine creating quantum dots. This results in large increases in conductivity as well as changes to the optical absorption spectra of the nonconjugated polymer. Changes to the molecular structure and optical absorption of SBR due to doping with iodine are shown in figure 4.1 and figure 4.2 respectively.

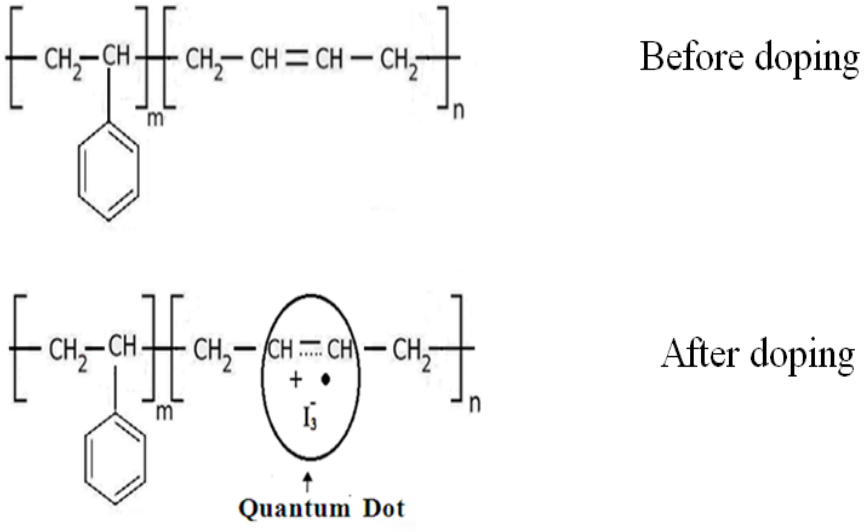

Figure 0.1: Change in molecular structure of SBR due to doping with Iodine.

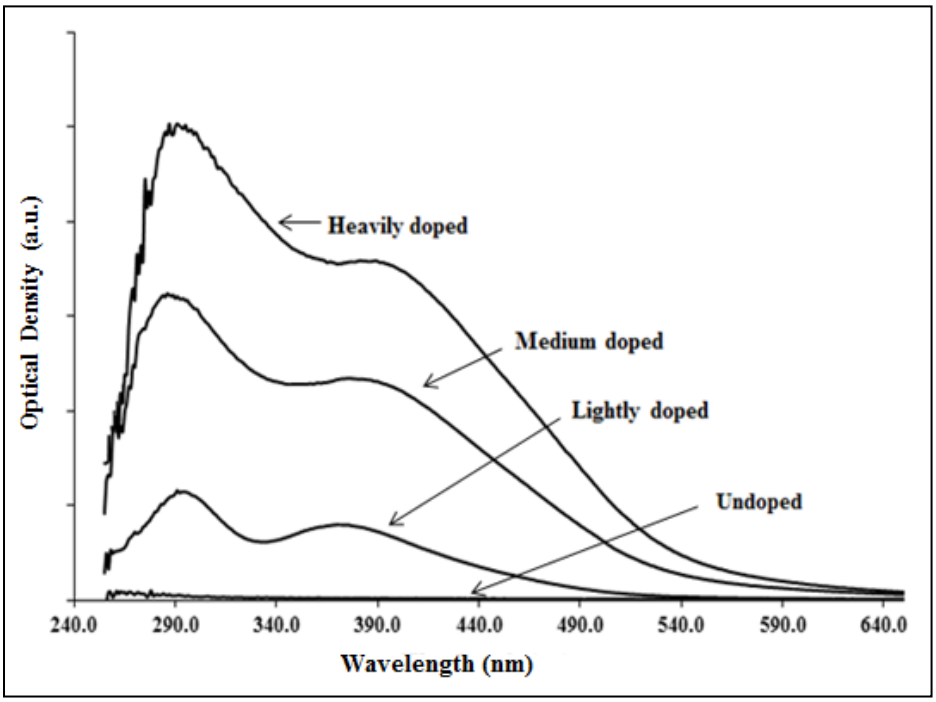

Figure 0.2: Changes in optical absorption spectra of SBR due to varying levels of doping with Iodine.

Nanocrystalline titanium dioxide, procured from Sigma-Aldrich, was ground, and then mixed with small amounts of a dilute acetic acid solution and triton X-100 surfactant. This

produced a viscous fluid that could then be applied to the transparent ITO electrode. This titanium dioxide coated substrate was then heated and slowly cooled to dry the layer and prepare it for use in the cell.

The two previously prepared substrates, one with a carbon electrode and the iodine doped SBR, and the other with the ITO electrode and the titanium dioxide layer, were then brought into contact with each other to create the cell. These were then fixed to a glass slide in order to ensure that the two halves of the cell remained in good contact and copper leads attached to allow for connections to a digital multimeter for measuring output voltages and currents. An electrolyte solution of 1-methyl-3-propylimidazolium iodide and ethylene glycol in a 1 to 4 ratio was produced. This electrolyte solution was introduced to the side of the assembled cell using a pipette, and the cell was left for 4-5 hours to allow the electrolyte to spread evenly and for residual charges in the cell to dissipate. Completed devices had a typical active area of around 4 square centimeters. A cross-sectional view of the completed cell is shown in figure 4.3.

Figure 0.3: Cross sectional view of a completed solar cell.

A light source with a broad emission spectrum of around 300-700 nm was used to provide incident light to the completed cell. Intensity measurements were made using a Newport model 1916-R optical power meter at varying distances from the light source. The

completed photovoltaic cell was then connected to a Keithley 617 programmable electrometer, and the cell exposed to differing light intensities. The electrometer was used to measure the open circuit voltages and short circuit currents produced by the photovoltaic cell. This experimental setup, along with an insert showing the spectral output of the light source, is shown in figure 4.4.

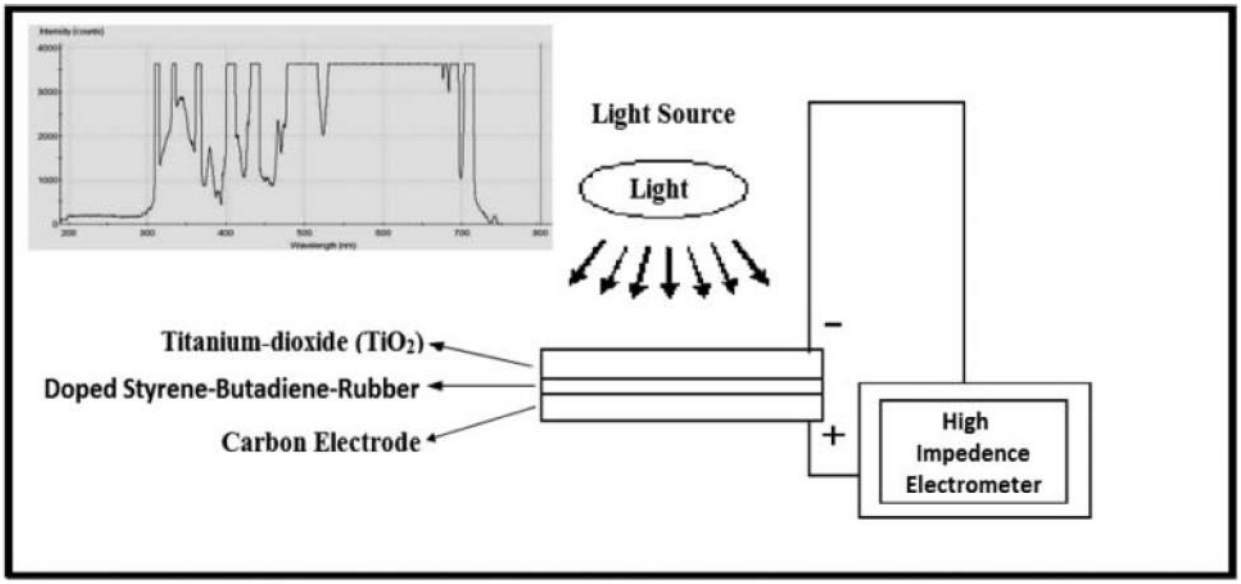

Figure 0.4: Experimental setup for photovoltaic measurements. Insert shows spectral output of the light source used.

4.3 Results and Discussion

The recorded photovoltage and photocurrent from these cells was plotted as a function of incident light intensity. A linear increase with incident light intensity was seen in both the photocurrent density and the photovoltage. Although the range of incident light intensities is not broad, this relationship allows for the performance of the devices to be characterized.

The mechanism for the photovoltaic effect in these devices, shown in figure 4.5, is similar to that of a dye-sensitized solar cell. Light absorption by the doped nonconjugated

polymer results in some of the electrons within the polymer being moved to an excited state. These electrons are then transferred to the TiO_2 electrode and transported through the leads to the carbon electrode. These electrons then interact with the I^-/I_3^- redox couple in the electrolyte to return the polymer-molecular system to the original state. Therefore, the doped polymer acts like the dye molecules in a Grätzel cell [83]. Iodine-doped SBR does not show any measurable photoluminescence. This implies the photon-excited electrons may efficiently transfer to the TiO_2 from the doped polymer facilitating the photovoltaic process.

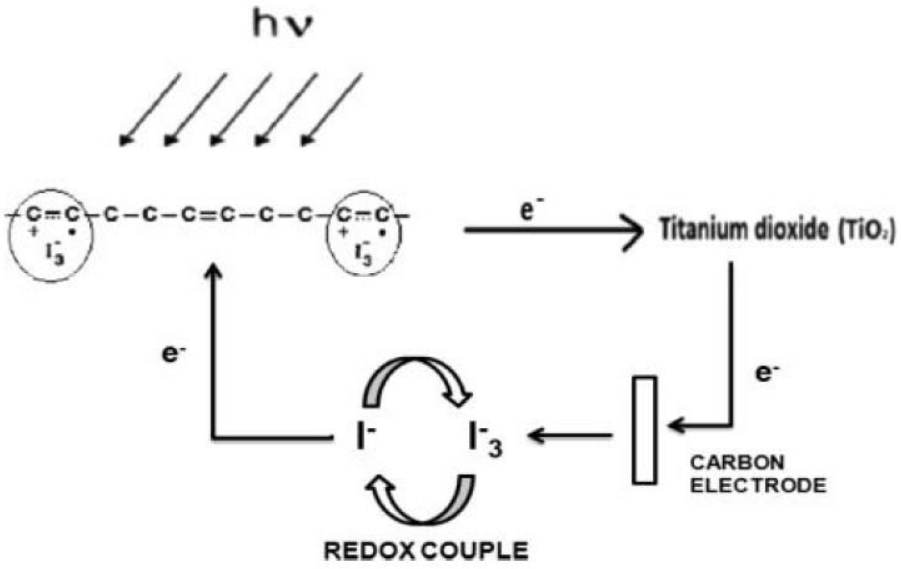

Figure 0.5: A schematic of the mechanism involved in the photovoltaic effect in these cells.

The recorded photovoltages and photocurrent densities for cells utilizing SBR are shown in figures 4.6 and 4.7, respectively. A photocurrent density of around 0.25 mA/cm^2 and photovoltage of about 0.74 V were observed at a light intensity of around 4 mW/cm^2 [84]. A conversion efficiency of around 2% has been estimated which is a significant improvement over previous reports [82]. The photocurrent is significantly higher than previous reports utilizing an undoped nonconjugated conductive polymer [81]. The photocurrent is also higher than that

previously reported for another doped nonconjugated conductive polymer [82]. There is room for enhancement of these devices as they are still in the preliminary stages of development. These cells may provide a less expensive alternative to other reported cells since SBR is inexpensive and stable in air.

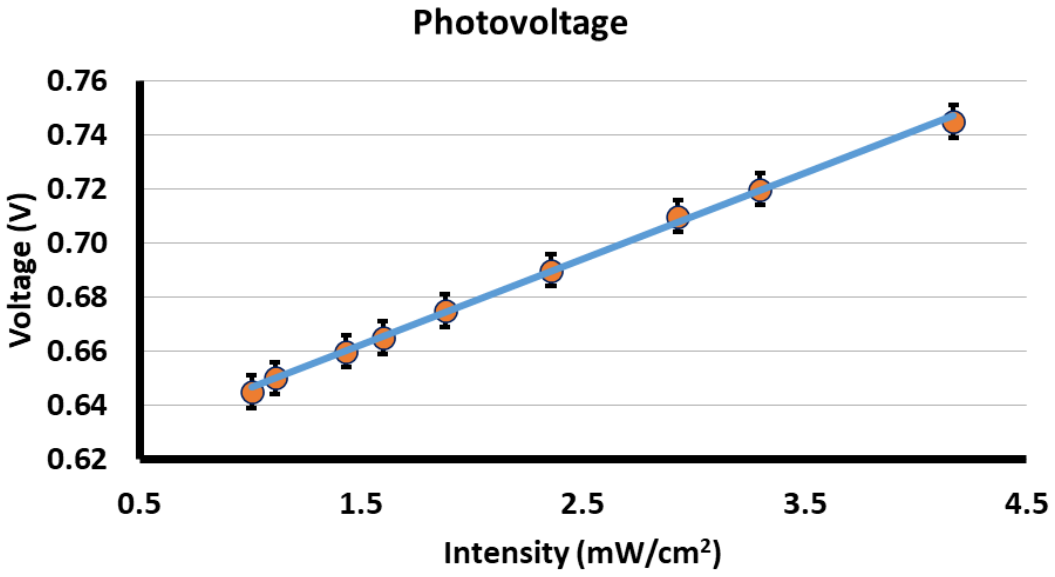

Figure 0.6: Measured photovoltage for varying light intensities for a solar cell utilizing SBR.

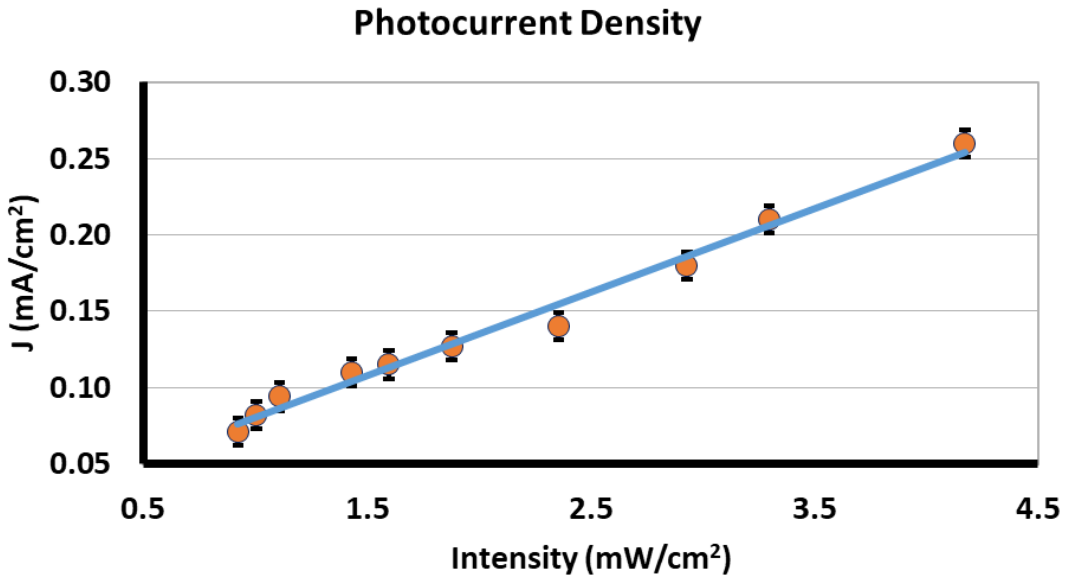

Figure 0.7: Measured photocurrent for varying light intensities for a solar cell utilizing SBR.

4.4 Conclusions

Photovoltaic cells involving the nonconjugated conductive polymer, iodine-doped styrene-butadiene-rubber between TiO_2 and carbon electrodes have been fabricated. The observed photovoltage and photocurrent-density for these cells was 0.74 V and 0.24 mA/cm^2 respectively with an incident light intensity of about 4 mW/cm^2. The fabricated cells are Grätzel type photovoltaic devices and the operational mechanism is as follows: i) absorption of incident light by the iodine-doped nonconjugated conductive polymer leads to excited-state transition of the electrons, ii) these electrons are transferred to TiO_2, and they subsequently complete the cycle involving an I^-/I_3^- redox couple which returns the polymer molecular system to the original state through charge-transfer. This mechanism produces the photovoltaic effect seen in the fabricated cells. This is the first report of a photovoltaic cell involving a nonconjugated conductive polymer that has shown a significant conversion efficiency. These cells, after further

study and improvement, may provide a lower cost alternative to other reported photovoltaic cells.

Chapter 5

Photovoltaic Cells Involving the Nonconjugated Conductive Polymer, Iodine-Doped Cis-poly(isoprene)

5.1 Introduction

Photovoltaic cells based on organic molecules have been widely studied and reported [73-75]. Organic materials provide the potential for lower cost alternatives to inorganic materials in photovoltaic applications due to their ease of processing and widely varying molecular structures [73-79]. Several reports on the photovoltaic effect in nonconjugated conductive polymers have been published [80-82, 84]. Early reports on these materials showed very limited photocurrents [81]. More recent reports on poly(β-pinene) in a different cell structure and styrene-butadiene-rubber in a similar cell structure to that used in this report have shown significantly increased photocurrents [82, 84]. In this report, photovoltaic cells have been constructed involving the nonconjugated conductive polymer iodine doped cis-1,4-poly(isoprene) (CPI). The fabricated cells have been constructed on indium-tin-oxide (ITO) coated polyethylene terephthalate (PET) substrates with layers of titanium dioxide, the nonconjugated conductive polymer, and a carbon electrode. These cells have produced significantly high conversion efficiencies.

5.2 Fabrication and Experimental Procedure

PET substrates were used with transparent ITO coatings to act as an electrode on the light incident side of the cell. The dark side of the cell also used a PET substrate with a thin layer

of carbon as the electrode. A solution of cis-1,4-poly(isoprene) and toluene was created, and this solution was used to apply a film of the nonconjugated polymer on top of the carbon electrode. The resulting films were about 0.5 microns thick. This layer acts as the light absorber and acts similarly to the dye molecules in a dye-sensitized solar cell. This film was then doped with iodine to around 0.8 molar through exposure to iodine vapor for several hours in a room temperature environment. Isolated double bonds in the nonconjugated polymer are affected by the iodine creating quantum dots. This results in large increases in conductivity as well as changes to the optical absorption spectra of the nonconjugated polymer. Changes to the molecular structure and optical absorption of SBR due to doping with iodine are shown in figure 5.1 and figure 5.2 respectively.

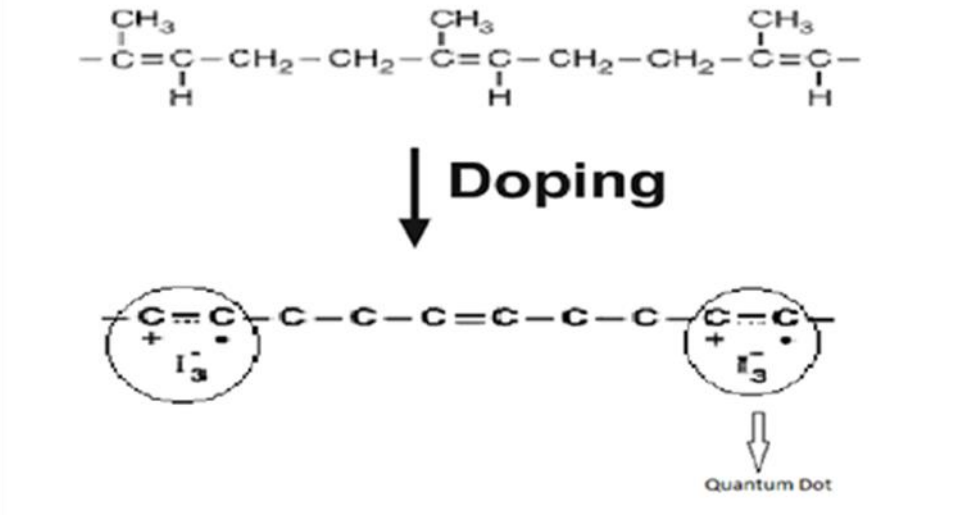

Figure 0.1: Chemical structure of cis-1,4-poly(isoprene) (CPI) before and after doping.

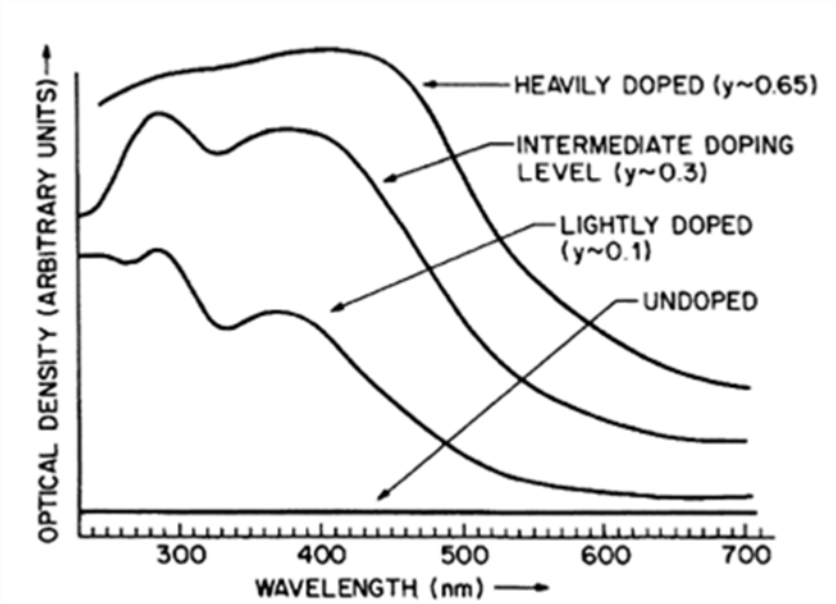

Figure 0.2: Optical absorption spectra of cis-1,4-poly(isoprene) (CPI) for different amounts of iodine doping.

Nanocrystalline titanium dioxide, procured from Sigma-Aldrich, was ground, and then mixed with small amounts of a dilute acetic acid solution and triton X-100 surfactant. This produced a viscous fluid that could then be applied to the transparent ITO electrode. This titanium dioxide coated substrate was then heated and slowly cooled to dry the layer and prepare it for use in the cell.

The two previously prepared substrates, one with a carbon electrode and the iodine doped CPI, and the other with the ITO electrode and the titanium dioxide layer, were then brought into contact with each other to create the cell. These were then fixed to a glass slide in order to ensure that the two halves of the cell remained in good contact and copper leads attached to allow for connections to a digital multimeter for measuring output voltages and currents. An electrolyte solution of 1-methyl-3-propylimidazolium iodide and ethylene glycol in a 1 to 4 ratio was produced. This electrolyte solution was introduced to the side of the

assembled cell using a pipette, and the cell was left for 4-5 hours to allow the electrolyte to spread evenly and for residual charges in the cell to dissipate. Completed devices had a typical active area of around 4 square centimeters. The completed cell structure and experimental setup are shown in figure 5.3 with an insert showing the emission spectrum of the light source used in the experiment.

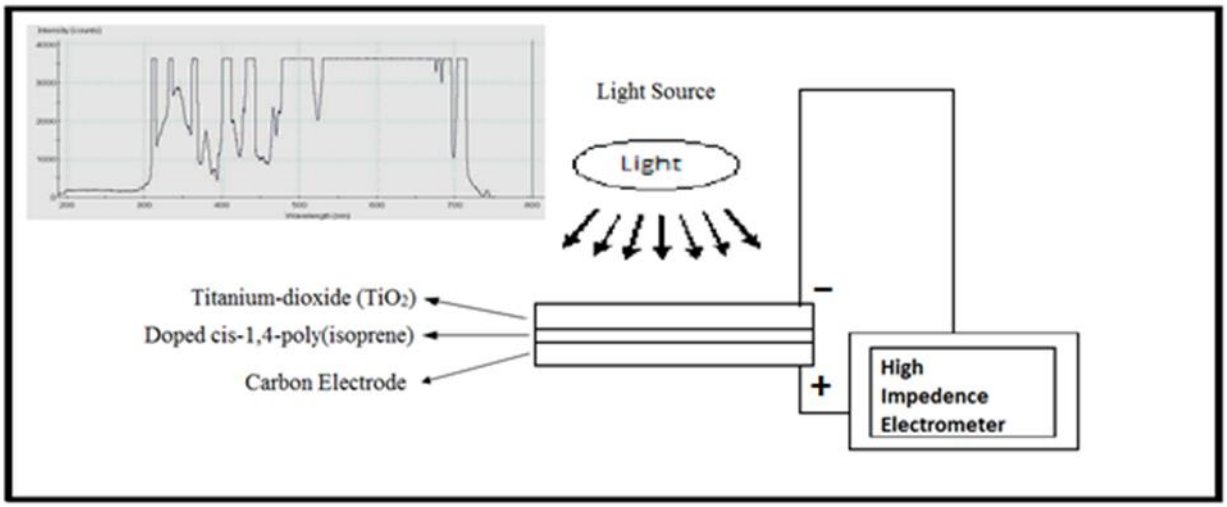

Figure 0.3: Experimental set-up for photovoltaic measurements. The insert shows the emission spectrum of the light source used in the experiment.

5.3 Results and Discussion

The recorded photovoltages and photocurrent densities for cells utilizing CPI are shown in figures 5.4 and 5.5, respectively. A photocurrent density of around 0.27 mA/cm^2 and photovoltage of about 0.73 V were observed at a light intensity of around 4 mW/cm^2. The inset in figure 5.5 shows the J-V characteristics in dark conditions for the fabricated cells. Due to the limited maximum available intensity in the experiment, significant changes in the J-V characteristics were not expected with the light on. Although a broad range of light intensity was not used in the experiment, a linear relationship between the observed photocurrent and

the incident light intensity was obtained. This allowed the desired device characteristics to be determined. A conversion efficiency of around 2.5% has been estimated assuming a fill factor of about 0.5 [85]. This is a significant improvement compared to previous reports involving different cell structures [81, 82].

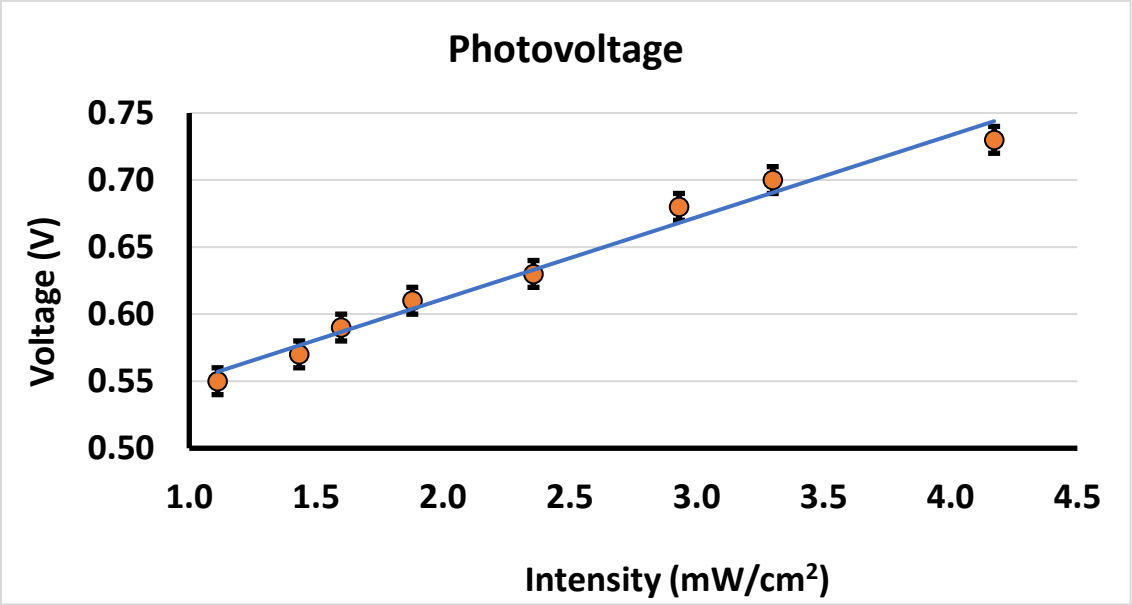

Figure 0.4: Measured photovoltage for varying light intensities for a solar cell utilizing CPI.

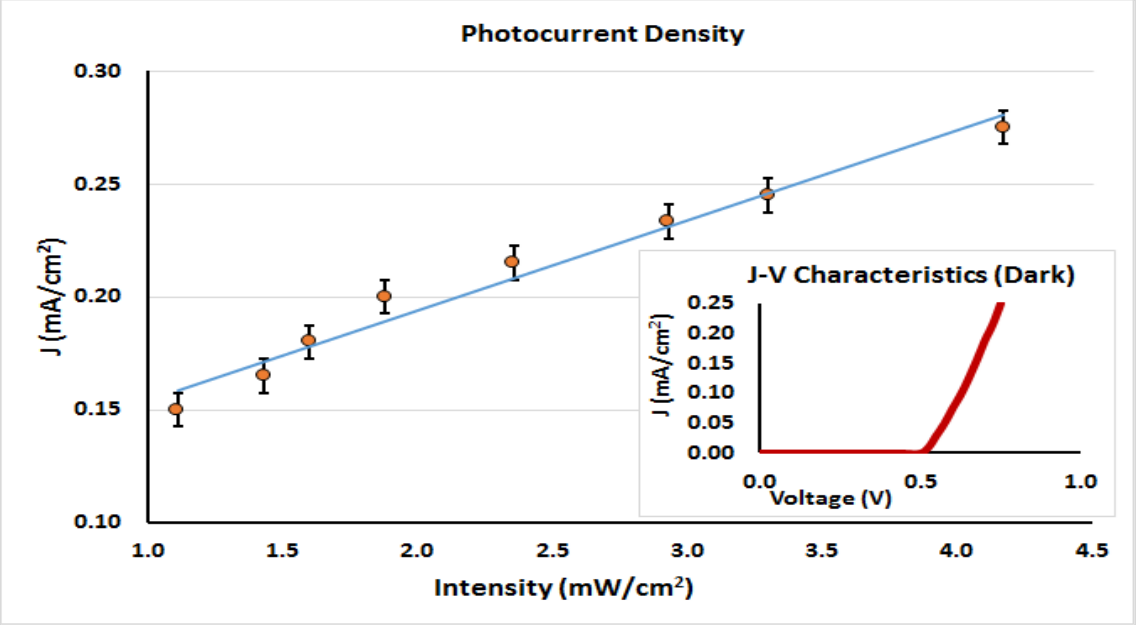

Figure 0.5: Measured photocurrent for varying light intensities for a solar cell utilizing CPI. The insert shows the J-V characteristics of the cell in dark conditions.

The mechanism of the photovoltaic effect seen in these devices is shown in figure 5.6. Resulting from the absorbance of incident light, some of the electrons in the doped polymer move to the excited state. These electrons are transferred to the TiO_2 electrode and transported through the leads to the carbon electrode. These electrons then interact with the I^-/I_3^- redox couple in the electrolyte solution to return the polymer molecular system to the original state and thus completing the cycle. The iodine-doped nonconjugated conductive polymer in the cell acts like the dye molecule in a Grätzel cell [83]. Iodine-doped CPI does not show any measurable photoluminescence. This implies that the photo-excited electrons in the polymer may efficiently transfer to the TiO_2 which facilitates the photovoltaic process. The photocurrent observed in these cells is significantly higher compared to previous reports involving photovoltaic cells involving an undoped nonconjugated conductive polymer [81]. The photocurrent is also higher than that recently reported for another iodine-doped

nonconjugated conductive polymer using a different cell structure [82]. The measured photovoltages and photocurrents were similar to those previously reported for the iodine-doped nonconjugated conductive polymer styrene-butadiene-rubber in the same cell structure [84]. There is room for enhancement of the photocurrent and photovoltage since the devices that have been developed are early generations of its kind using a nonconjugated conductive polymer. These cells may provide significantly less expensive and more versatile alternatives to other reported cells since polymers such as CPI are inexpensive and stable in air.

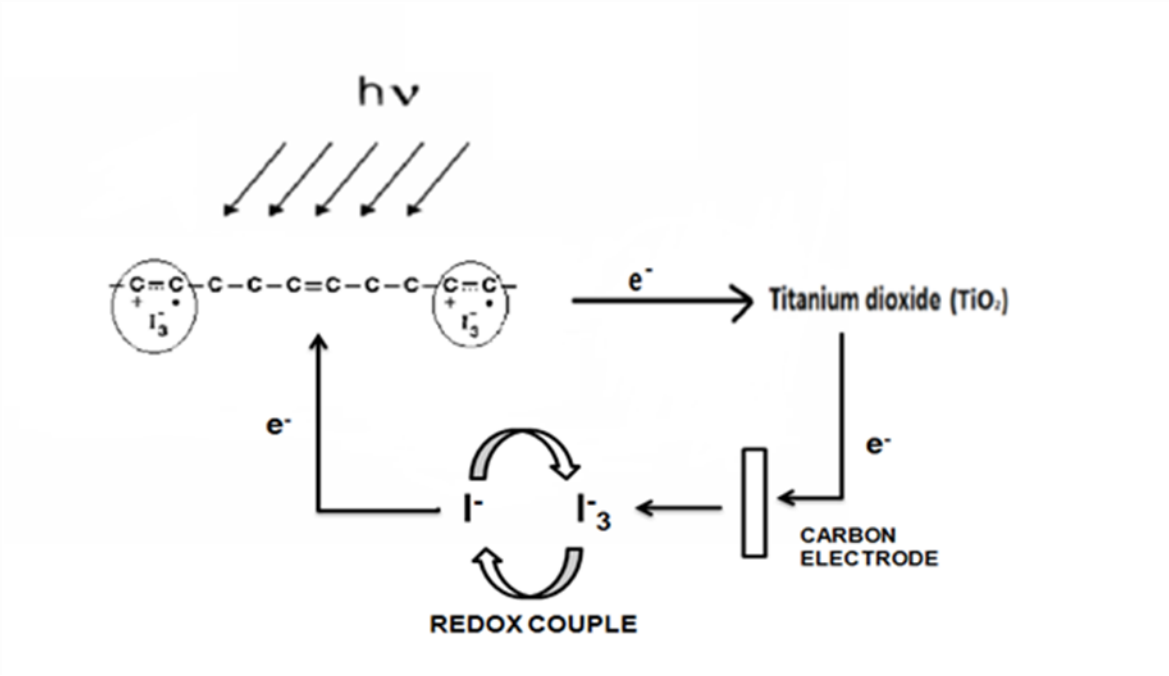

Figure 0.6: A schematic of the mechanism involved in the photovoltaic effect in cells utilizing the iodine-doped nonconjugated conductive polymer cis-1,4-poly(isoprene) (CPI).

5.4 Conclusions

Photovoltaic cells involving the nonconjugated conductive polymer, iodine-doped cis-1,4-poly(isoprene) (CPI) between TiO_2 and carbon electrodes have been fabricated. The photocurrent density and photovoltage for the fabricated cells was about 0.27 mA/cm^2 and

0.73 V respectively with an incident light intensity of about 4 mW/cm^2. These are Grätzel type cells with an operational mechanism as follows: i) absorption of incident light by the iodine-doped nonconjugated conductive polymer leads to excited-state transition of the electrons, ii) these electrons are transferred from the polymer to the TiO_2 electrode and then subsequently complete the cycle involving the I^-/I_3^- redox couple which returns the polymer molecular system to the original state through charge-transfer. This mechanism results in the photovoltaic effect seen in the fabricated cells. The reported results are similar to other iodine-doped nonconjugated conductive polymers using the same device structure. The estimated conversion efficiency of the fabricated cells was about 2.5% which is significant. Further improvement on cells utilizing nonconjugated conductive polymers may provide significantly less expensive and more versatile alternatives to other reported photovoltaic cells.

Chapter 6

Lifetime Enhancement of Photovoltaic Cells Involving Nonconjugated Conductive Polymers

6.1 Introduction

Photovoltaic cells based on organic molecules have been widely studied and reported [73-75]. Organic materials provide the potential for lower cost alternatives to inorganic materials in photovoltaic applications due to their ease of processing and widely varying molecular structures [73-79]. Several reports on the photovoltaic effect in nonconjugated conductive polymers have been published [80-82]. Early reports on these materials showed very limited photocurrents [81]. More recent reports involving styrene butadiene rubber and cis-1,4-polyisoprene have shown significantly increased photocurrents and conversion efficiencies [84, 85]. Although these cells, shown in figure 6.1, have exhibited significant performance increases, as fabricated, they have a limited usable lifetime with greatly reduced performance within a week of fabrication. This is a major issue limiting the commercial viability of the devices. One hypothesis for the cause of the limited lifetime is loss of the liquid electrolyte due to evaporation.

Figure 0.1: Solar cell involving an Iodine-doped nonconjugated conductive polymer.

The mechanism for the photovoltaic effect in these cells is shown in figure 6.2. Incident light on the Iodine-doped nonconjugated polymer is absorbed causing some electrons within the polymer to move to the excited state. These electrons are then transferred to the titanium dioxide layer and through the leads to the carbon electrode. These electrons then interact with the I^-/I_3^- redox couple in the electrolyte solution to return the polymer molecular system to the original state and thus completing the cycle. The iodine-doped nonconjugated conductive polymer in the cell acts like the dye molecule in a Grätzel cell [83].

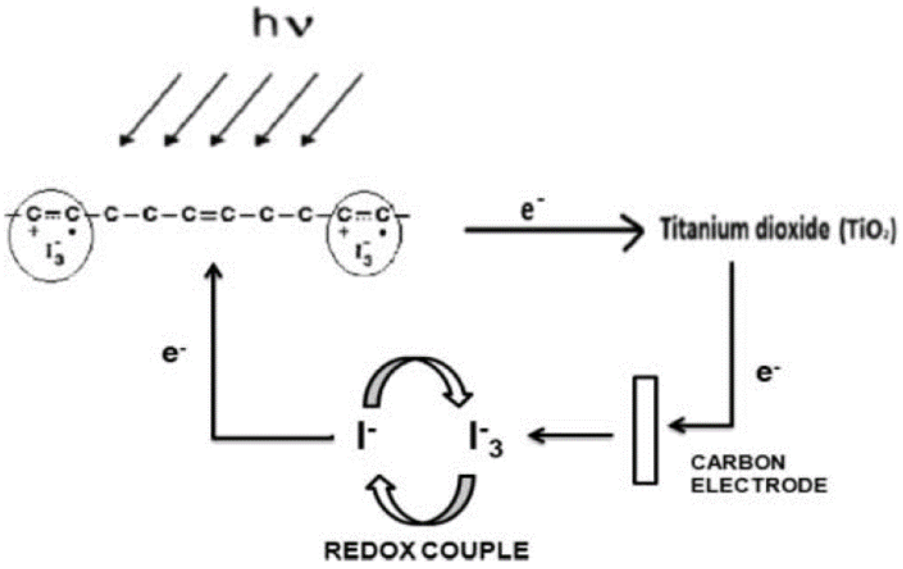

Figure 0.2: The mechanism for the photovoltaic effect in a cell involving a nonconjugated conductive polymer.

Although there may be other causes for the reduction in the performance of the fabricated cells over time, degraded cells have been able to show a return to previous performance by adding new electrolyte to the cell. This suggests that the immediate reduction in performance is most likely caused by the loss of the liquid electrolyte. In this report, an experiment was developed to reduce the loss of the electrolyte from the cell and monitor the

photovoltage and photocurrent over time. The results of this experiment showed that the photovoltage and photocurrent showed significantly less reduction in cells that suffered less loss of electrolyte.

6.2 Fabrication and Experiment Procedure

Cells were fabricated and a method was created to attempt to seal the cell to outside air to limit electrolyte loss. The fabricated cell was attached to a glass slide with copper electrodes leading from the cell. A rubber O-ring with a diameter larger than the completed cell was placed over it and another glass slide placed on top. The two glass slides were clamped together, crushing the O-ring, and providing a sealed environment for the cell. A picture of one of the completed samples is shown in figure 6.3. The sealed cell was compared to a cell fabricated at the same time and left open to the air. The fabricated cells were evaluated periodically over two weeks to see how the maximum measured photovoltage and photocurrent changed over time. These experiments were performed by exposing the cells to varying levels of incident light and measuring the photovoltage and photocurrents using a high impedance electrometer as shown in figure 6.4. The sealed cells were also viewed and photographed under a microscope to monitor the loss of electrolyte.

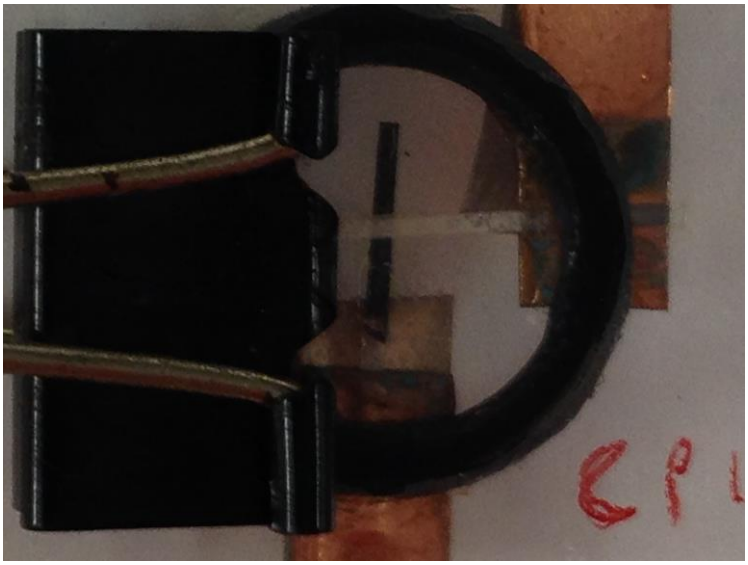

Figure 0.3: A fabricated photovoltaic cell sealed between two glass slides using a rubber O-ring.

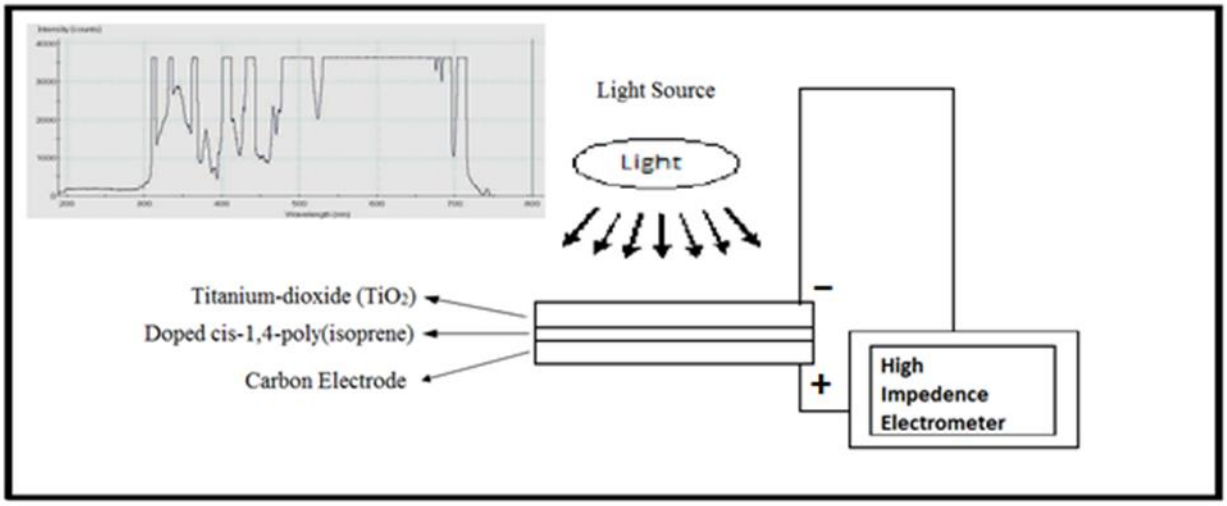

Figure 0.4: Experimental set-up for photovoltaic measurements. The insert shows the emission spectrum of the light source used in the experiment.

6.3 Results and Discussion

The sealed cells maintained their performance longer than those that were not sealed. This can be clearly seen in the plots of maximum voltage and maximum current over time as shown in figures 6.5 and 6.6. The cells that were not sealed showed almost immediate degradation with a significant performance loss after three days and almost no output after a

week. This reduction was seen in both the photovoltages and photocurrents. The sealed cells in comparison showed almost no loss of performance after a week, with the difference being especially apparent in the photocurrent results.

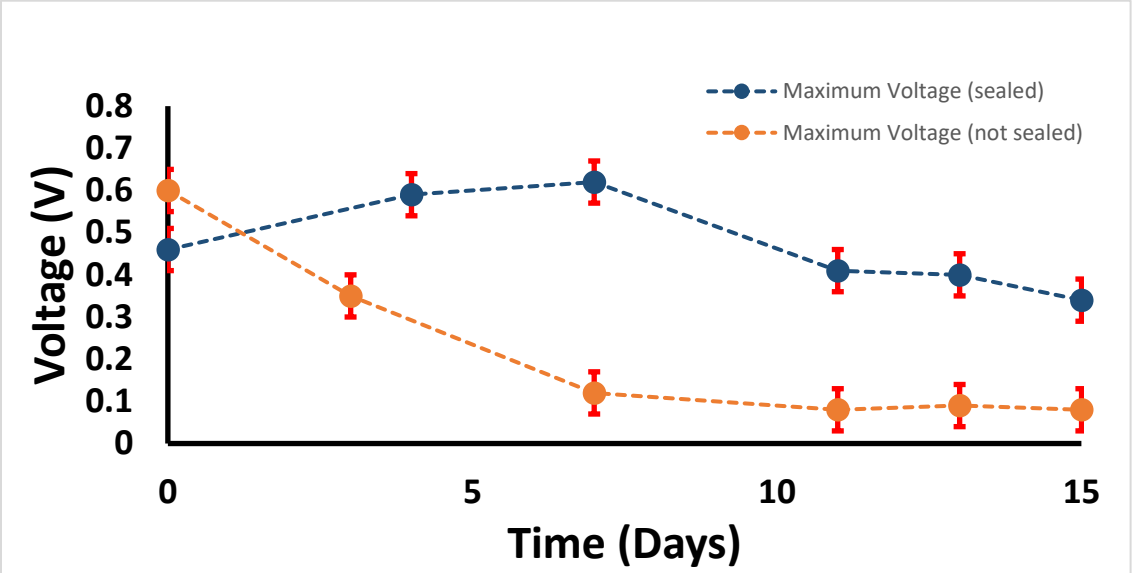

Figure 0.5: Changes in photovoltage over time for sealed and not sealed SBR devices.

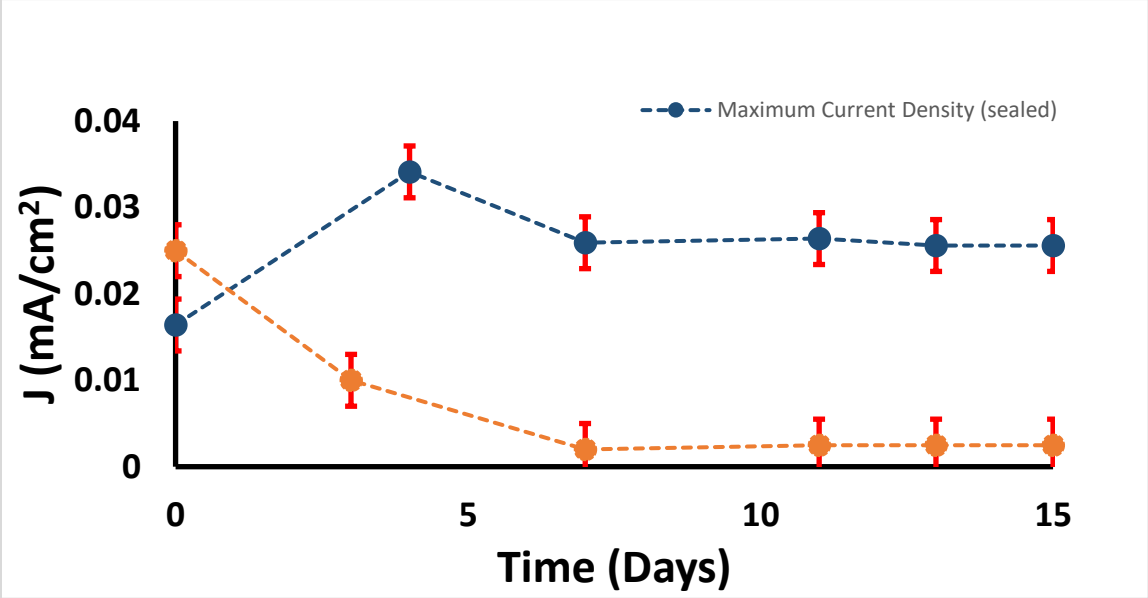

Figure 0.6: Changes in photocurrent over time for sealed and not sealed SBR devices.

The loss of electrolyte in the sealed cells was monitored through a microscope as shown in figure 6.7. These results match up with the changes in photovoltages and photocurrents. Liquid electrolyte was still present in the sample after two weeks. These results do show that the electrolyte was still leaving the cell and the slight reduction in performance seen in the sealed cell over time can be attributed to this. A large spot of liquid electrolyte is seen in figure 6.7a. This spot is still slightly visible after a week as seen in figure 6.7b but is completely evaporated after 2 weeks as seen in figure 6.7c.

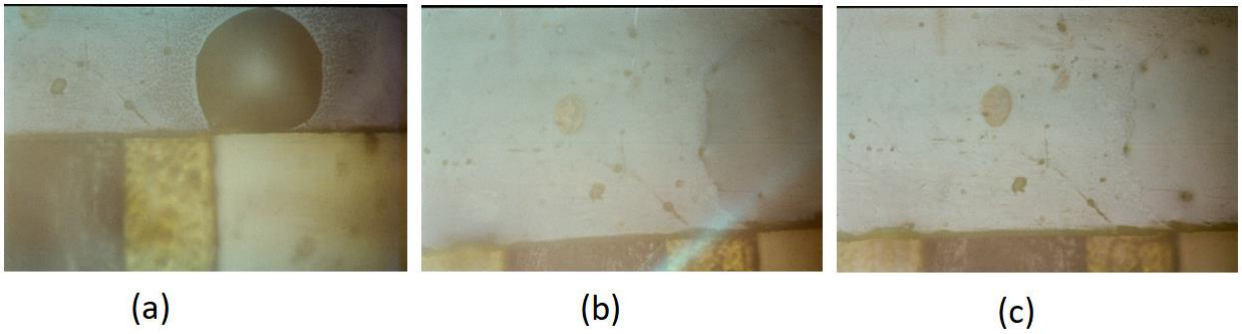

Figure 0.7: Pictures of a sealed photovoltaic cell under 100x magnification after (a) 1 day, (b) 7 days, and (c) 14 days.

6.4 Conclusions

Photovoltaic cells involving nonconjugated conductive polymers have been fabricated and the changes in their performance characteristics over time have been compared between sealed cells and ones left open to the air. The cells that were sealed showed significantly reduced degradation in photovoltage and photocurrent compared to cells that were left open to the air. Open air cells showed almost no photocurrent and heavily reduced photovoltage after about 3 days. Sealed cells showed almost no reduction in photovoltage and photocurrent after about 14 days.

The sealed cells were photographed under 100x magnification in order to determine if the liquid electrolyte was being maintained within the cell. These pictures showed that the electrolyte was still being lost to the environment, but at a reduced rate. These results show that the rapid degradation in the performance characteristics of the cells is due to the loss of the electrolyte.

Further experiments on the long-term performance of these cells will be required to determine if there are other factors that affect the output of the cells. The method used to seal the cells in this report was able to slow the loss of the electrolyte, but not stop it completely. Better methods for sealing the cells are under investigation and will provide an opportunity to see if the cells performance can be maintained if the electrolyte is captured within the cell.

Chapter 7

Quadratic Electrooptic Effect in the Nonconjugated Conductive Polymer Polyethylene Terephthalate

7.1 Introduction

Nonlinear optical properties of materials, specifically nanoparticles and quantum dots have been extensively studied [18, 44, 52, 58, 60, 62, 63, 86-99]. The field of nonlinear optics is important to the future of communications, optical sensing, and photonics. As more optical methods are used in commercial applications, faster optical switching and modulation become more important to the advancement of a variety of industries. Organic materials, specifically nonconjugated conductive polymers, have been widely investigated due to their low cost, ease of manufacture, and exceptionally large nonlinear optical properties [18, 54, 56-63, 80, 82, 86, 88, 90, 93, 100-102]. The effects of Iodine doping on polyethylene terephthalate have been investigated. Several nonconjugated polymers have been shown to have significantly increased conductivities and third-order optical susceptibilities upon doping with electron acceptors such as Iodine [17, 54, 56, 86, 100, 102, 103]. The large susceptibilities are a result of charge confinement within a subnanometer charge domain. Samples of polyethylene terephthalate have been doped with Iodine and studied using UV/Vis and IR spectroscopy to determine the effect of Iodine doping on the material. The nonlinear optical properties of Iodine doped polyethylene terephthalate were then investigated using the field-induced birefringence method to measure the quadratic electro-optic effect[104]. Quadratic electro-optic effects have

applications in ultrafast electro-optic modulation, switching, Kerr cells, Kerr gates for mode-locking, Q-switching, and other applications in optoelectronics.

7.2 Experimental Equipment

Sample films of polyethylene terephthalate were obtained with a thickness of 50 microns. These samples were doped with Iodine in the vapor phase using the standard procedure. The effect of doping was studied using FTIR and UV/Vis spectroscopy. UV/Vis measurements were performed using a CRAIC microspectrophotometer. IR measurements were performed using a Shimadzu IRPrestige-21 Fourier Transform Infrared Spectrophotometer. The results for samples of varying doping levels were compared to determine how the Iodine was interacting with the polyethylene terephthalate films.

The Iodine-doped polyethylene terephthalate samples were fitted with copper electrodes. An ac field at 4 kHz was applied to the samples through the electrodes using a variable power supply. The quadratic electro-optic effect was measured using the field-induced birefringence method shown in figure 7.1. A Uniphase 1508-1 helium-neon laser with a wavelength of 633 nm was used in these experiments. The laser beam was passed through a polarizer oriented 45 degrees relative to the direction of the applied electric field. The beam then passed through the sample and then through an analyzer that was cross-polarized with respect to the polarizer. The beam was then detected by a photodiode. A Stanford Research Systems SR530 lock-in amplifier, using 2f synchronization, and a Hewlett Packard 5416B oscilloscope were used to measure the modulation signals. The modulation signal was recorded for varying strengths of applied electric field and was found to depend quadratically on the

applied electric field strength. The Kerr coefficients were then determined from the observed modulation signals, applied electric field strength, and interaction path length within the sample, for a given wavelength.

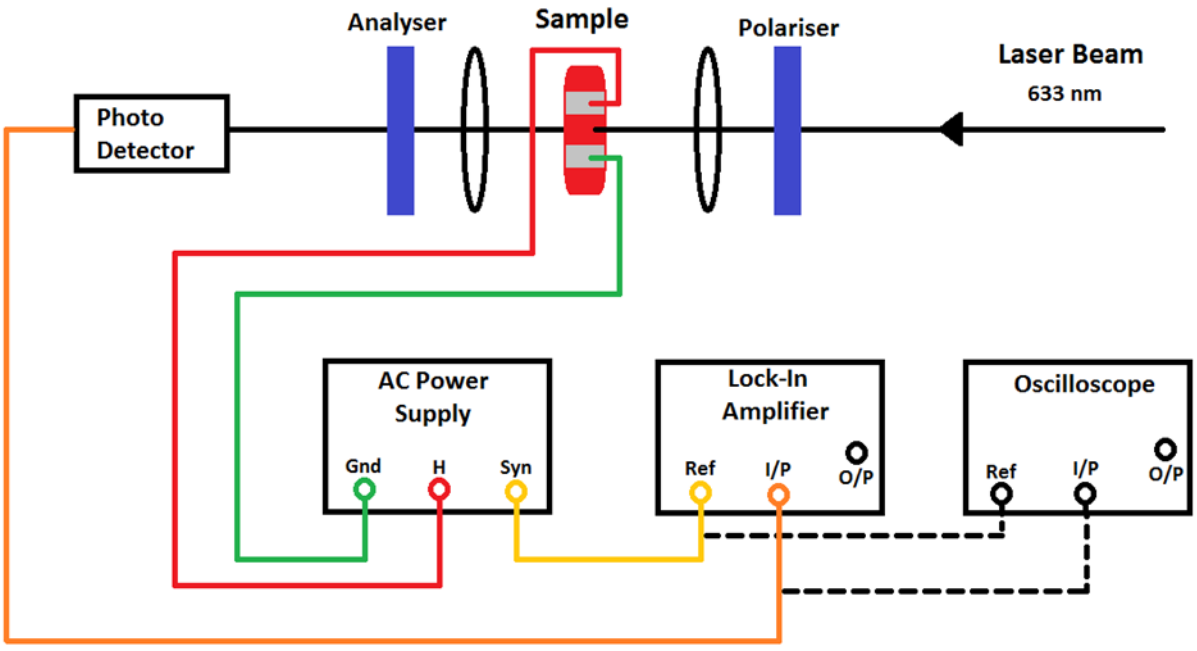

Figure 0.1: Experimental set-up for the measurement of the quadratic electro-optic effect/Kerr coefficient.

7.3 Results and Discussion

Samples of polyethylene terephthalate were obtained as films with a thickness of 50 microns. These films were doped with Iodine in the vapor phase using the standard procedure. Doping of polyethylene terephthalate films took significantly longer (days rather than minutes or hours) compared to other nonconjugated conductive polymers. After doping with Iodine, the films were observed to change from transparent to dark based on the doping time and concentration. This effect can be clearly seen on the UV/Vis spectroscopy with the absorption increasing and an additional absorption peak appearing and growing in magnitude as shown in

figure 7.2. The peak at about 300 nm in the UV/Vis absorption is due to the terephthalic ring in the polymer. This is the only peak present in the undoped polyethylene terephthalate sample. After doping with Iodine, a peak at about 312 nm and a broad absorption with a peak at about 375 nm appeared. These peaks were seen to increase with additional doping. The 312 nm (~ 3.97 eV) peak in the doped polyethylene terephthalate is due to a radical cation and the broad absorption at 375 nm is due to charge-transfer or the surface plasmon resonance. The surface plasmon resonance in this system occurs at a much shorter wavelength compared to the peak seen in metal nanoparticles [43]. This is due to the subnanometer particle size found in doped polyethylene terephthalate and other nonconjugated conductive polymers. The radical cation peak at about 310 nm was also observed in another nonconjugated conductive polymer, iodine-doped poly(ethylene pyrrolidinyl) derivative, which has a similar double-bond containing group in the polymer backbone [58]. The electrical conductivity of polyethylene terephthalate increased by many orders of magnitude after doping with Iodine. The conductivity reached a maximum of about 10^{-3} S/cm at a molar concentration of about 0.8. This magnitude is lower than that seen in other Iodine doped nonconjugated conductive polymers. This is due to the lower double-bond number fraction in the repeat of polyethylene terephthalate [61, 86, 105].

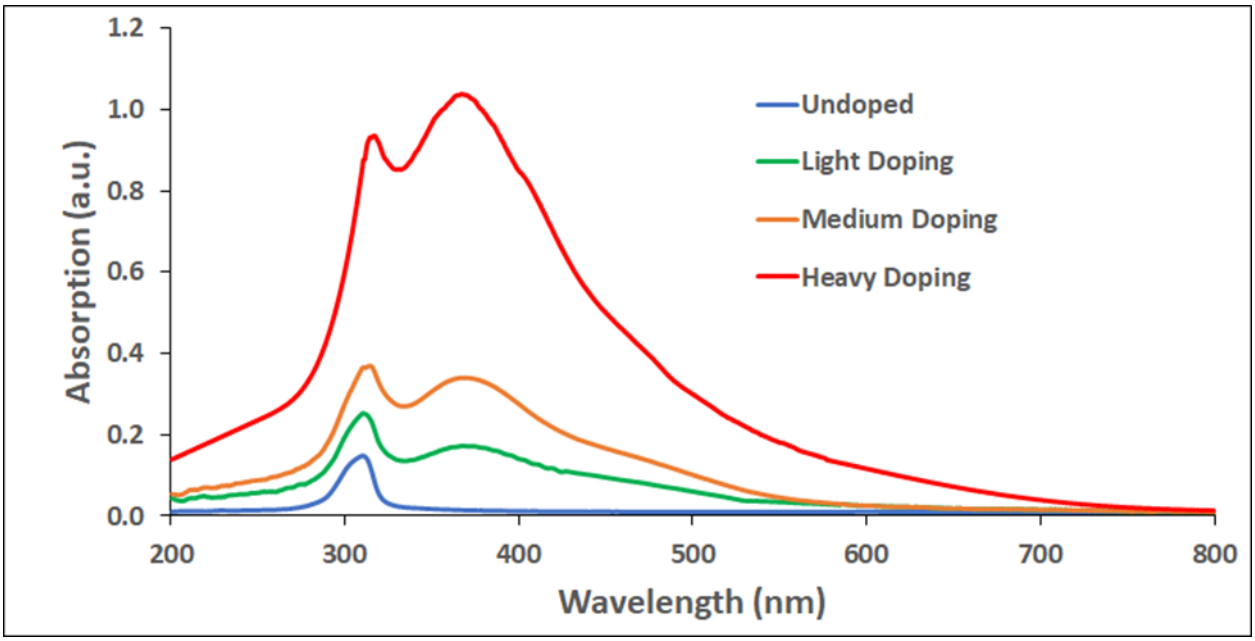

Figure 0.2: UV/Vis spectra for 50 micron films of polyethylene terephthalate with varying levels of Iodine doping. The molar concentrations of iodine are: light doping ~ 0.16, medium doping ~ 0.28, heavy doping ~ 0.83.

No shift was seen in the peak at about 375 nm. This is a unique feature of iodine-doped polyethylene terephthalate compared to other nonconjugated conductive polymers which see a shift to higher wavelengths with increased doping levels[104]. This result for polyethylene terephthalate may be because the charge-transfer is occurring between the terephthalic ring and the dopant. This would limit the quantum size to near the size of the ring plus the dopant counterion. Therefore, the size of the quantum dot would remain the same regardless of the dopant concentration.

FTIR measurements for doped and undoped polyethylene terephthalate are shown in figure 7.3. After doping with Iodine, a reduction in the 1505 wavenumber peak was seen. The 1505 wavenumber peak is associated with the Carbon-Carbon bonds in the polymer ring. This matches the effect seen in other nonconjugated conductive polymers where the Iodine doping

is only affecting isolated Carbon bonds. An electron is transferred from the Carbon bond to the Iodine which forms a hole or positive charge at the bond site. The molecular structure of polyethylene terephthalate and the effect of Iodine doping is shown in figure 7.4. The charge transfer from the ring to Iodine is also responsible for the changes seen in the UV/Vis absorption spectra. The hole present at the bond site leads to a significant increase in the conductivity of the material due to interstitial hoping. This hole is loosely bound to the dopant counterion. An applied electric field may affect the movement of the hole without dissociating it from the counterion. The confinement of the charges within these subnanometer sized systems causes the material to have the characteristics of a metallic quantum dot.

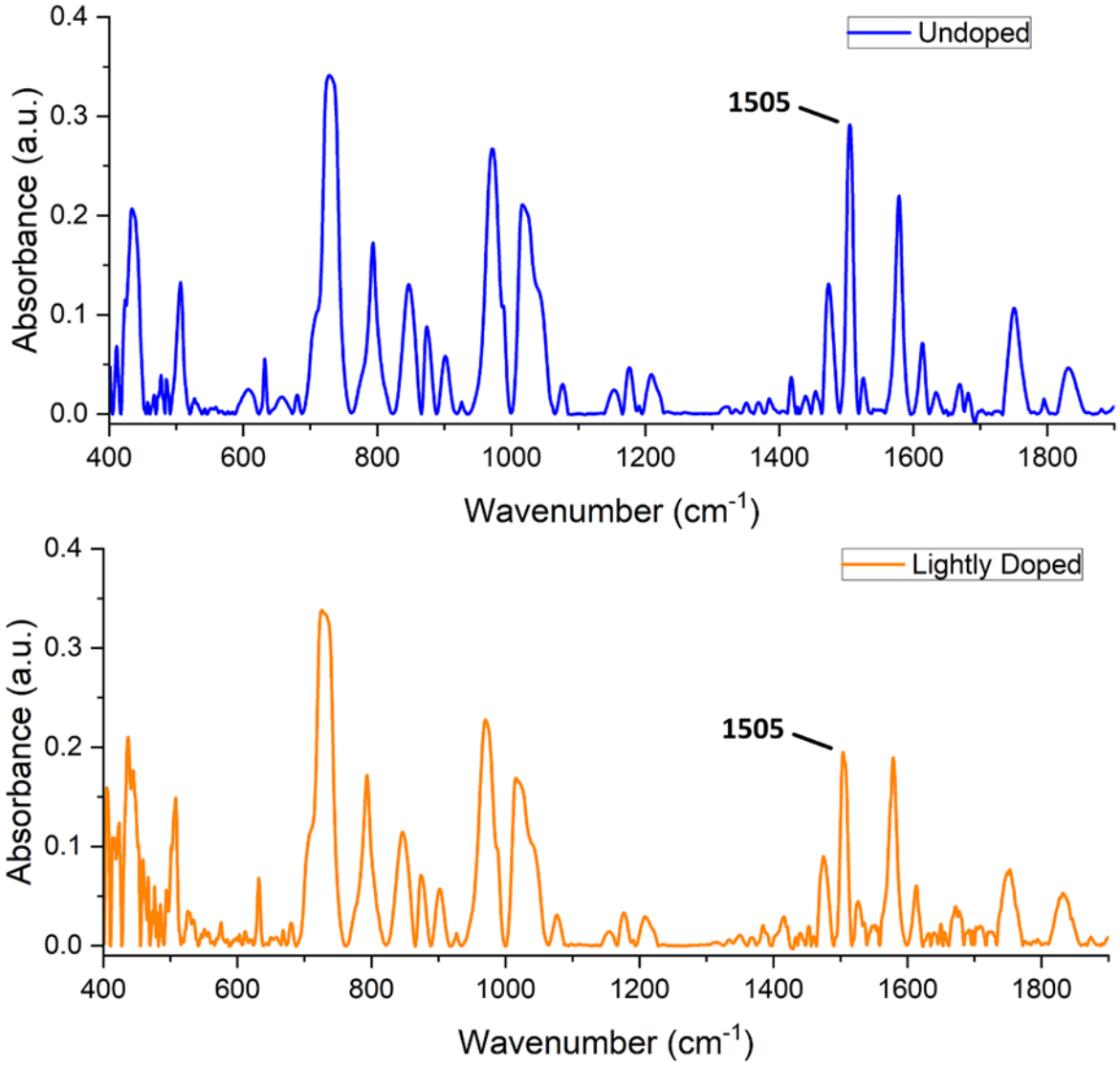

Figure 0.3: FTIR spectra for undoped and lightly doped polyethylene terephthalate.

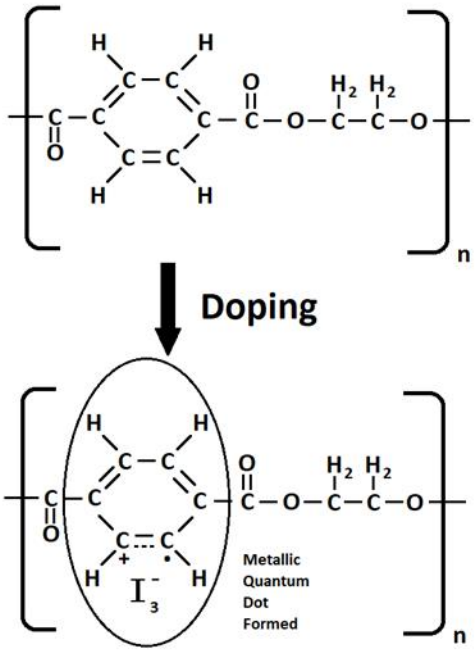

Figure 0.4: Schematic of the effect of Iodine doping on the molecular structure of polyethylene terephthalate.

Quadratic electro-optic effects measurements were made on the Iodine-doped polyethylene terephthalate samples using the field-induced birefringence method discussed earlier. These measurements were made at 633 nm with the laser passing through the thickness of the sample which was about 50 microns. The results of the quadratic electro-optic effect experiments are shown for a lightly doped sample in figure 7.5 and for a more heavily doped sample in figure 7.6[104]. These results show a clear quadratic relationship between the applied electric field and modulation. The more heavily doped sample shows some saturation in the modulation at higher electric field magnitudes. For the medium doping sample, with a molar concentration of iodine of about 0.28, the Kerr coefficient was calculated to be about $1.5 \times 10^{-11}\, m/V^2$. For the heavily doped sample, with a molar concentration of iodine of about 0.83, the Kerr coefficient was calculated to be about $5 \times 10^{-11}\, m/V^2$. These results are

similar in magnitude to those found for other nonconjugated conductive polymers [60, 63, 88, 93].

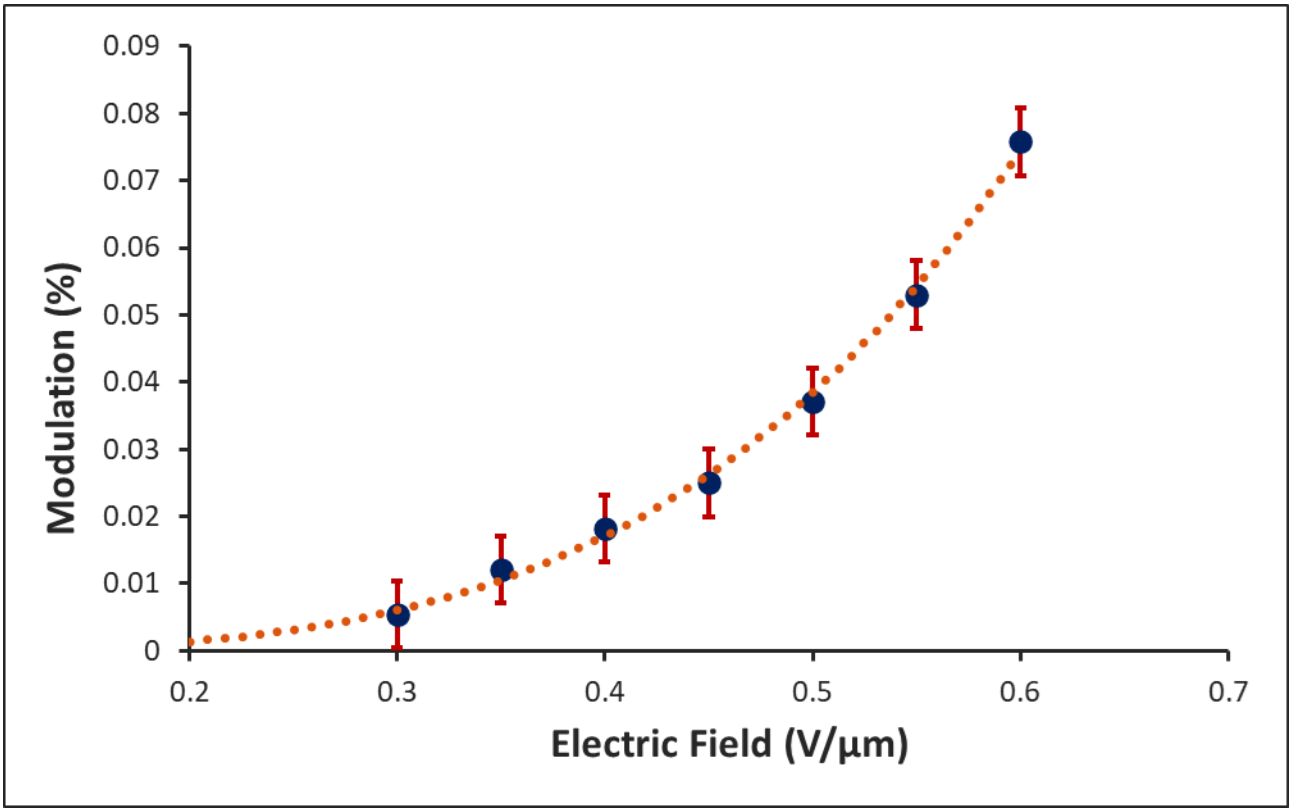

Figure 0.5: Quadratic electro-optic effect measurements for medium doping (molar concentration ~ 0.28) polyethylene terephthalate at 633 nm.

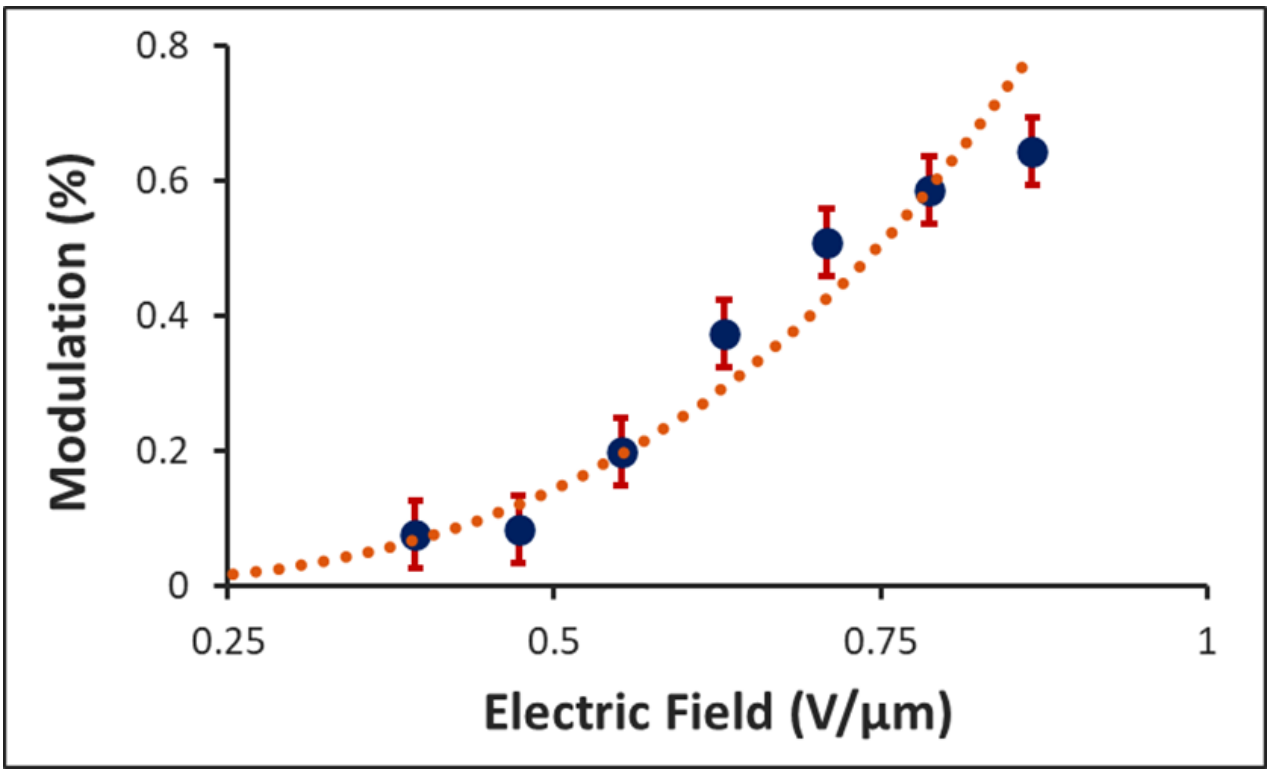

Figure 0.6: Quadratic electro-optic effect measurements for heavily doped (molar concentration ~ 0.83) polyethylene terephthalate at 633 nm.

7.5 Conclusions

Polyethylene terephthalate films, about 50 microns thick, have been obtained and studied. The films were doped with Iodine in the vapor phase using the standard procedure. The effect of Iodine doping on the material was investigated through UV/Vis and IR spectroscopy. The UV/Vis absorption showed an increase in the absorption peak at about 300 nm and a new absorption peak at 375 nm after doping. The FTIR spectroscopy showed a reduction in the peak at about 1505 wavenumber after doping. These results show that the Iodine is interacting with isolated carbon bonds in the molecular structure of the polyethylene terephthalate. Specifically, bonds in the polymer ring are most heavily influenced. The Iodine

doping results in charge transfer from the polymer ring to the Iodine. This forms a metallic quantum dot, with a charge that is confined to a subnanometer sized charge system.

The nonlinear optical properties of the Iodine-doped polyethylene terephthalate films were invested using the field-induced birefringence method to measure the quadratic electro-optic effect at 633 nm in the material. These results showed a clear quadratic correlation between the magnitude of the applied electric field and the optical modulation through the samples. This effect corresponded to a Kerr coefficient of about $1.5 \times 10^{-11}\, m/V^2$ for a sample with a molar concentration of iodine of about 0.28. For a sample with a molar concentration of about 0.83, the Kerr coefficient was calculated to be about $5 \times 10^{-11}\, m/V^2$. This is a similar magnitude if Kerr coefficient as those found in other nonconjugated conductive polymers [60, 63, 88, 93]. Nonconjugated conductive polymers have metallic domains of subnanometer dimensions, also known as quantum dots, which lead to the largest known Kerr coefficients of any studied materials. The results here imply various applications of these systems in ultrafast switching, modulation, and other applications in laser-optics and optoelectronics.

Chapter 8

Quadratic Electro-Optic Effect in Metal Nanoparticles in a Transparent Dielectric Medium

8.1 Introduction

Nonlinear optical properties of metal nanoparticles in transparent dielectric media have been extensively studied [13, 43-46, 48, 49, 87, 89, 93, 106, 107]. In particular, third-order nonlinear optical effects in metal nanoparticles using ultrashort laser pulses have been widely studied and reported. Metallic nanoparticles with diameters under about 10 nm can also be referred to as quantum dots, because they can be modeled as a charged particle experiencing quantum confinement. Therefore, many of the properties of these systems can be understood through the confinement of electrons within nanometer dimensions. Measurements of third-order susceptibilities ($\chi^{(3)}$) and response times have been made for various sizes of nanoparticles. Prior to this report, no measurements of the quadratic electro-optic effect for metal nanoparticles in dielectric media were found in the literature, and no experimental correlation between the third-order susceptibility and particle size had been established. Second-order nonlinear optical effects in these systems have been measured using ultrashort, high intensity pulses by taking advantage of the asymmetry in the particles and interfaces [89]. These second-order effects have no relevance to the quadratic electro-optic effect being discussed in this report. Quadratic electro-optic effects have applications in ultrafast electro-optic modulation, switching, Kerr cells, Kerr gates for mode-locking, Q-switching, and other applications in optoelectronics.

The quadratic electro-optic effect, also known as the Kerr effect, has been measured for gold nanoparticles contained within a dielectric medium with the objective of further elucidating the mechanisms of nonlinear optics in these important systems. Particles of varying size from about 15nm to about 50nm within a glass medium were investigated. Kerr coefficients have been determined for these particles. This is the first time that the Kerr effect has been measured for gold nanoparticles in a dielectric medium.

The quadratic electro-optic effect is given by: $\Delta n = K\lambda E^2$, where Δn is the change in the refractive index, K is the Kerr coefficient, λ is the wavelength of light used in the experiment, and E is the applied electric field. This equation describes a change in the refractive index in a material due to an applied electric field. This change in the refractive index leads to electro-optic switching or modulation and any related device application. A larger Kerr coefficient leads to a larger change in the refractive index for any given electric field, wavelength of light, and optical path length through the sample. Since the magnitude of K is typically small in these samples, a long path length of up to 4 cm was used in order to obtain a detectable electro-optic modulation signal. The difficulty in obtaining suitable samples, and in making the measurements, may be part of the reason such measurements have not been previously reported. One of the advantages of these measurements over four-wave mixing or optical Kerr effect measurement made with ultrashort optical pulses is that the thermal contribution in the quadratic electro-optic effect is expected to be small. This is a result of the metal nanoparticles in glass samples acting as insulators that allow only an extremely small amount of electric current. This very small current flowing through the samples, and the relatively low-power lasers used in the experiments, leads to minimal thermal effects.

Therefore, these experiments may provide evidence of a correlation between the particle diameter and the optical nonlinearity that was possibly obscured by thermal effects in other nonlinear optical measurements that utilized intense laser pulses.

8.2 Experimental

The glass samples used in these experiments were purchased from a commercial glass supply company. The samples used in the experiments were about 4 cm square and 3 mm thick. The samples were characterized using optical absorption spectroscopy and the wavelength of the surface plasmon resonances were determined. The size of the gold particles within the glass was estimated using the optical absorption spectroscopy results. This size estimation used both the wavelength at which the absorption peak occurred (the surface plasmon resonance), and relative peak intensity. This correlation has been widely investigated and estimates were made specifically using the work of Link et al and Haiss et al [43, 107]. The relative peak intensity compared the optical density at the surface plasmon resonance to the optical density at a wavelength of about 400 nm. A surface plasmon resonance peak at a lower wavelength and closer relative peak intensity corresponds to a smaller particle size. The optical absorption spectra of the samples were measured using a CRAIC spectrometer in the transmission mode.

The gold nanoparticle in glass samples were fitted with copper electrodes. An ac field at 4 kHz was applied to the samples through the electrodes using a variable power supply. The quadratic electro-optic effect was measured using the field-induced birefringence method shown in figure 8.1 [57, 61-63, 86, 88, 90]. A Uniphase 1508-1 helium-neon laser with a

wavelength of 633 nm was used in these experiments. This was chosen because the wavelength of the laser is close to the onset of the optical absorption due to the surface plasmon resonance in the samples. This wavelength exhibits enhanced magnitude of the Kerr coefficient due to resonance effects. The laser beam was passed through a polarizer oriented 45 degrees relative to the direction of the applied electric field. The beam then passed through the sample and then through an analyzer that was cross-polarized with respect to the polarizer. The beam was then detected by a photodiode. A Stanford Research Systems SR530 lock-in amplifier, using 2f synchronization, and a Hewlett Packard 5416B oscilloscope were used to measure the modulation signals. The modulation signal was recorded for varying strengths of applied electric field and was found to depend quadratically on the applied electric field strength. The Kerr coefficients were then determined from the observed modulation signals, applied electric field strength, and interaction path length within the sample, for a given wavelength.

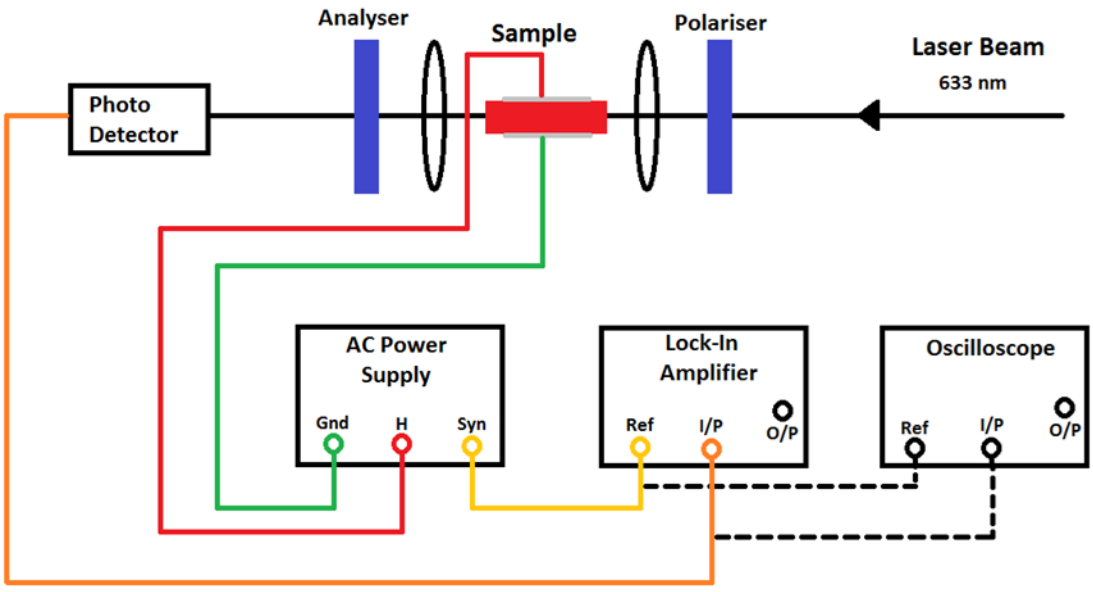

Figure 8.1: Experimental set-up for the measurement of the quadratic electro-optic effect/Kerr coefficient.

8.3 Results and Discussion

Three glass samples containing gold nanoparticles of three different average diameters were studied and are discussed in the following. These samples were purchased from a commercial glass supplier. The optical absorption spectra were recorded for light traveling through the thickness of the samples. The size of the gold nanoparticles was estimated from the wavelength of the absorption peak, which is due to the surface plasmon resonance of the metal nanoparticles in the samples, and the relative peak intensity using the results published in literature [43, 107]. The absorption peak appears at shorter wavelengths and the relative intensity of the peak decreases for smaller nanoparticles. For sample 1, shown in figure 8.2, the peak occurred at a wavelength of about 534 nm, which corresponded to a particle diameter of about 50 nm. For sample 2, the peak occurred at a wavelength of about 527 nm, which corresponded to a particle diameter of about 25 nm. For sample 3, shown in figure 8.3, the peak occurred at a wavelength of about 520 nm, which corresponded to a particle diameter of about 15 nm. The relative peak intensity was determined by dividing the absorbance at the surface plasmon resonance by the absorbance at 400 nm, and was also used in determining the nanoparticle sizes [107].

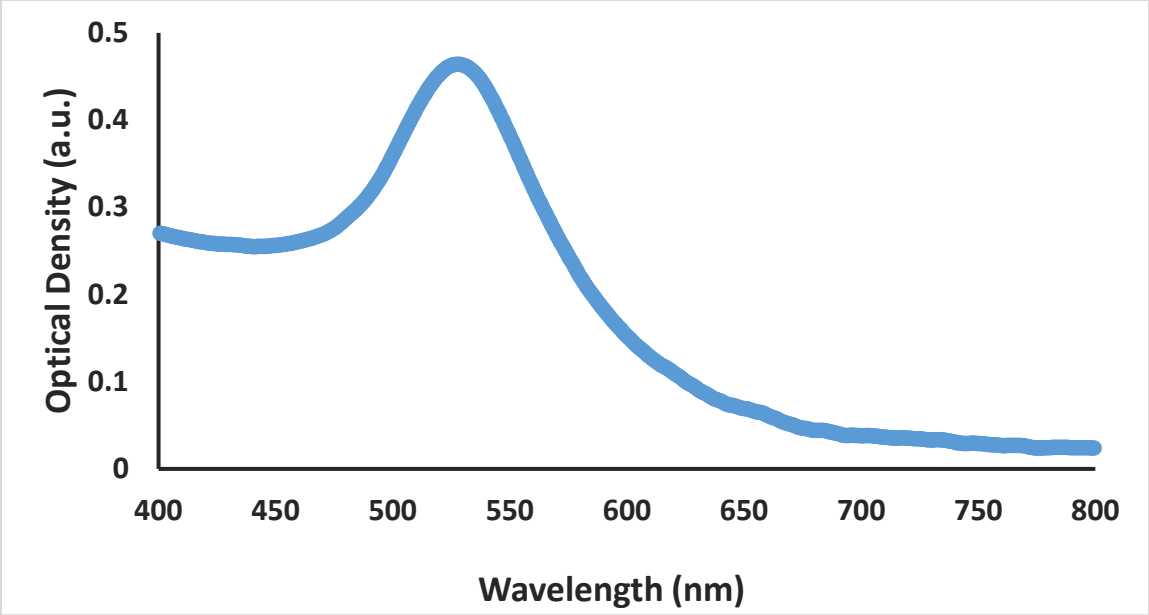

Figure 8.2: Surface plasmon resonance spectrum of gold nanoparticles in glass (sample 1). Peak at 534 nm with a particle diameter of about 50 nm.

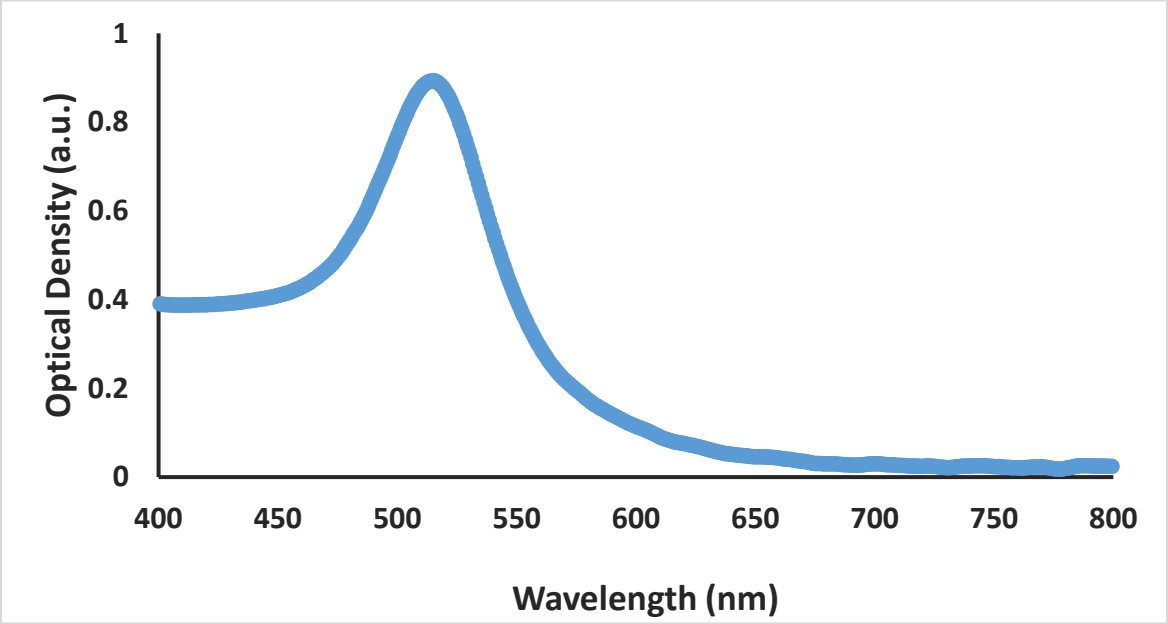

Figure 8.3: Surface plasmon resonance spectrum of gold nanoparticles in glass (sample 3). Peak at 520 nm with a particle diameter of about 15 nm.

Quadratic electro-optic measurements were made in these samples using the field-induced birefringence method discussed earlier. The beam at 633 nm was passed through the long dimension (about 4 cm) of the samples. The results of the quadratic electro-optic effect

experiments are shown in figures 8.4, 8.5, and 8.6 for samples 1, 2, and 3 with particle diameters of about 50 nm, 25 nm, and 15 nm respectively. The Kerr coefficients, as determined from the observed modulation signals, were about $2.5 \times 10^{-15}\ m/V^2$, $2.0 \times 10^{-14}\, m/V^2$, and $7.5 \times 10^{-14}\, m/V^2$, for the 50 nm, 25 nm, and 15 nm samples respectively. Under the same experimental conditions, no detectible modulation was observed for glass samples containing no metal nanoparticles. Considering previous reports, subnanometer size metallic-like particles were obtained in nonconjugated conductive polymers doped with iodine [57, 61-63, 86, 88, 90]. In these materials, charge-transfer from an isolated carbon-carbon double bond to the dopant creates highly confined metallic domains, also known as quantum dots. These metallic-like particles exhibit a surface plasmon resonance at a wavelength of about 400 nm and a radical cation peak at a wavelength of about 300 nm in their optical absorption spectra. These peaks relate to subnanometer size particles, and these materials have shown the largest known Kerr coefficients and two-photon absorption coefficients of any material. The Kerr coefficient for iodine-doped trans-polyisoprene at 633 nm is about $3.5 \times 10^{-10}\, m/V^2$ [63, 90]. All of the magnitudes of the Kerr coefficient reported here, the three samples of gold nanoparticles and the nonconjugated conductive polymer, are for the same optical density of about 0.05 at 633 nm. The Kerr coefficients for the three glass samples and the nonconjugated conductive polymer are shown in table 8.1.

Table 8.1: Calculated Kerr Coefficients for different sizes of gold nanoparticles and a nonconjugated conductive polymer.

MATERIAL	KERR COEFFICIENT (m/V^2)
SAMPLE 1 (50 nm)	2.5×10^{-15}
SAMPLE 2 (25 nm)	2.0×10^{-14}
SAMPLE 3 (15 nm)	7.5×10^{-14}
TRANS-POLYISOPRENE (subnanometer)	3.5×10^{-10}

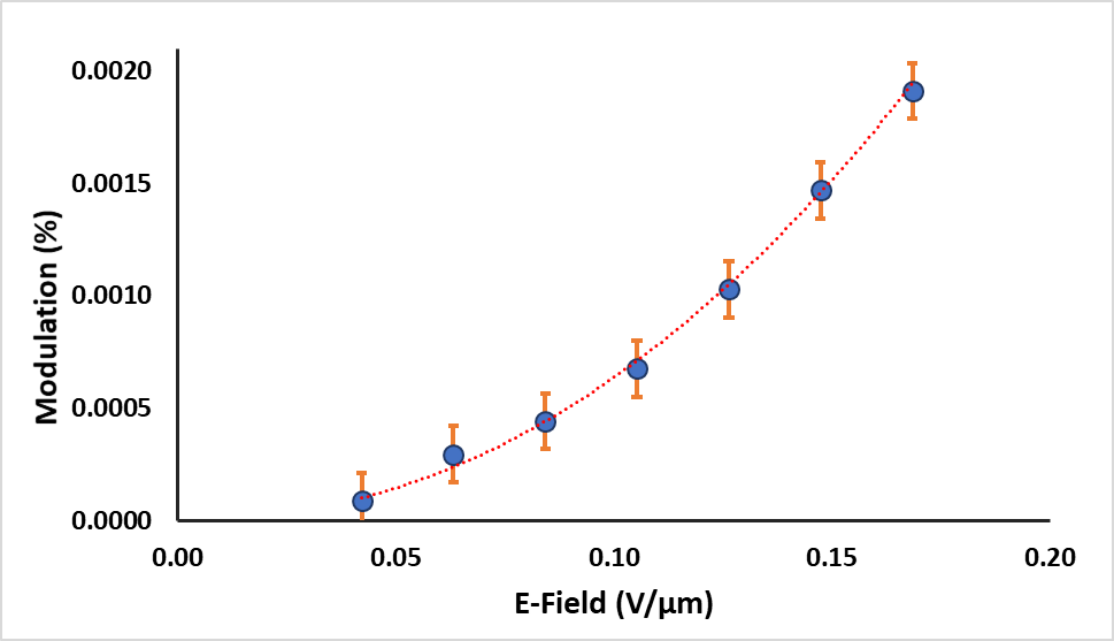

Figure 8.4: Quadratic electro-optic effect measurements at 633 nm for gold nanoparticles with a diameter of about 50 nm.

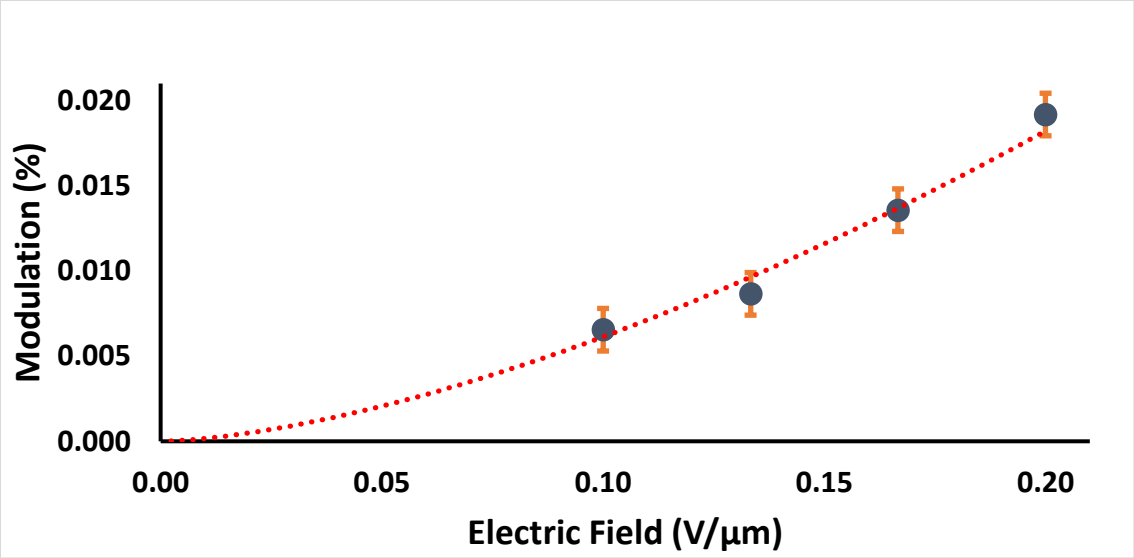

Figure 8.5: Quadratic electro-optic effect measurements at 633 nm for gold nanoparticles with a diameter of about 25 nm.

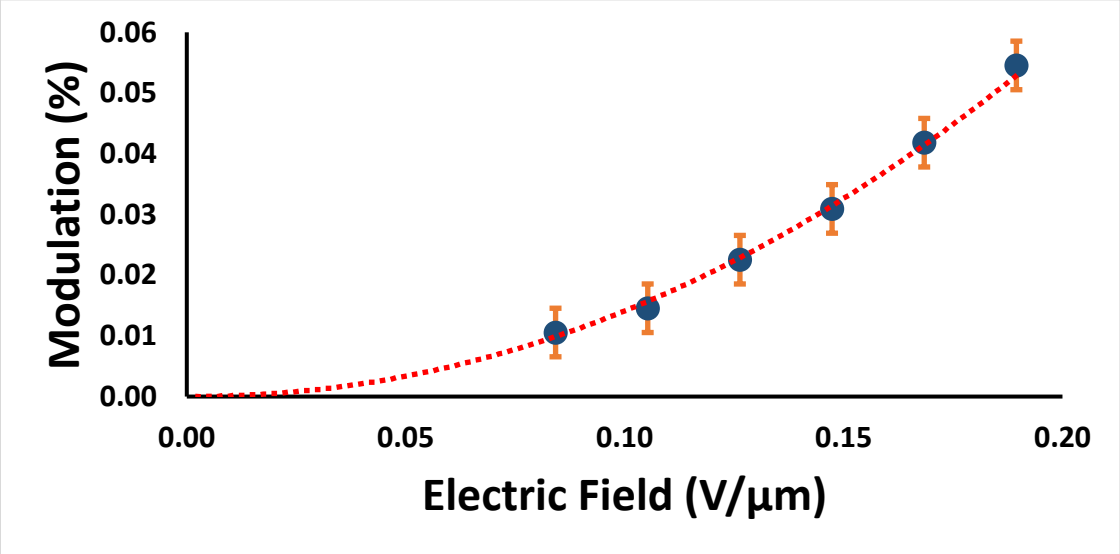

Figure 8.6: Quadratic electro-optic effect measurements at 633 nm for gold nanoparticles with a diameter of about 15 nm.

These results demonstrate that the Kerr coefficient (K) increases rapidly as the particle size decreases. This increase follows a roughly d^{-3} relationship, where d is the diameter of the nanoparticle. From this, the follow equation may be developed: $K = K_0 d^{-3}$, where K_0 is the Kerr coefficient for a nanoparticle with a diameter of 1 nm. A plot of log$K$ against log$d$ is shown

in figure 8.7. This plot shows a slope of about -3 implying a d^{-3} dependence of the Kerr coefficient.

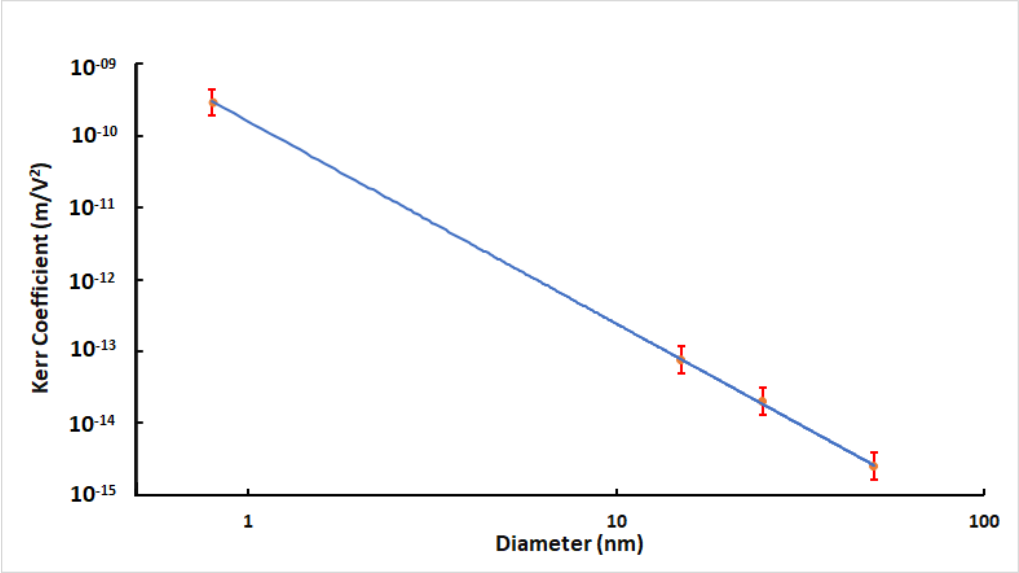

Figure 8.7: Kerr coefficient correlated with the diameter of a metallic nanoparticle.

This correlation between optical nonlinearity and particle diameter (d) can be explained using an earlier theoretical treatment of metal nanoparticles in dielectric media that was outline in subsection 2.7 of chapter 2 [13]. According to this theory, third-order susceptibility ($\chi^{(3)}$) increases as d^{-3}. The Kerr coefficient (K) is proportional to $\chi^{(3)}\ (\omega;\ \omega, 0,0)$. In particular, the Kerr coefficient is proportional to the real part of the third-order susceptibility. The measurements reported here were made at 633 nm, which is near the onset of the surface plasmon resonance. Because of this, the third-order susceptibility at this wavelength is complex, with both real and imaginary parts. The theoretical treatment by Hache et al predicts the maximum value of the third-order susceptibility to be proportional to $T_1T_2(1\text{-}d/d_0)/d^3$, where T_1 is the excited state lifetime, T_2 is the dephasing time, d0 is a characteristic threshold diameter of the system, and d is the diameter of the nanoparticle [13]. Therefore, for $d < d_0$,

$\chi^{(3)}$ increases as d^{-3}. Although the particle concentration was not known for our samples, the optical density (αl) was similar for all of the samples investigated with a value of about 0.05 at 633 nm. The particle concentration would affect the absorption coefficient (α) in the same way it affects the Kerr coefficient (K). Therefore, as long as the optical density is comparable, the Kerr coefficients can be compared at a fundamental level. As the results show, the Kerr coefficient follows the theory and increases as d^{-3}. An alternative interpretation of the d^{-3} dependence of the Kerr coefficient can be obtained through the phase space filling model. In this model, for any given excitation, the fraction of electrons in a smaller nanoparticle is higher for a smaller particle because the overall number of electrons is smaller. Therefore, a larger optical nonlinearity is expected in a smaller nanoparticle [18].

This report provides the first experimental demonstration of the fundamental correlation between third-order optical nonlinearity and the size of metal nanoparticles. It was not possible to demonstrate this correlation earlier, presumably because of thermal effects, which could be significant in other nonlinear optical measurements that utilized ultrashort intense optical pulses. These measurements include time-resolved four-wave mixing and optical Kerr effects using femtosecond pulses. Those measurements have produced a wealth of information, including excited-state lifetimes, dephasing time, multiphoton processes, and many others. They have not been able to clearly delineate the effect of particle size. Use of intense optical pulses may excite interband transitions in gold nanoparticles and, according to theory, does not lead to any particle size dependence. Only intraband transitions involving surface plasmons are expected to show a particle size dependence of third-order susceptibility, as observed here.

These materials involving metal nanoparticles within glass are expected to have various applications in ultrafast electro-optic switching, modulation, Kerr cells, and other applications in optoelectronics. Although the present results are only for metal nanoparticles in glass, the results can be extended to metal nanoparticles in other transparent dielectric media.

8.4 Conclusions

Quadratic electro-optic effects, specifically Kerr coefficients, were measured for the first time for metal nanoparticles within a transparent dielectric medium. In particular, gold nanoparticles of various average particle diameters were studied. The measurements were made using the field-induced birefringence method. The magnitudes of the Kerr coefficients for the different sizes of gold nanoparticles in glass were measured and compared to the Kerr coefficient obtained for subnanometer size metallic particles in a nonconjugated conductive polymer. The magnitude of the Kerr coefficient was found to rapidly increase as the particle diameter (d) decreased, following a roughly d^{-3} relationship. The results are consistent with existing theories and understandings of nonlinear optics in metal nanoparticles. This size dependence was not previously observed in experiments, presumably because of thermal effects. In the present measurements, the thermal effect was insignificant. These results imply a broad range of applications for metal nanoparticles in ultrafast, electro-optic, modulation, switching, low-cost Kerr cells, and other crucial functions in lasers and optoelectronics.

Chapter 9

Electroabsorption in Metallic Nanoparticles within Transparent Dielectric Media

9.1 Introduction

Nonlinear optics in metal nanoparticles within a transparent dielectric media has been extensively studied [13, 43-46, 48, 49, 87, 96, 106-109]. Third-order nonlinear optics in particular have been widely studied and reported using ultrashort (femtosecond) laser pulses for metal nanoparticle systems. The third-order susceptibilities and response times of various metallic nanoparticles in dielectric media have been measured for different diameters of nanoparticles. Saturation of absorption and two-photon absorption in specific nanometallic systems have also been studied [13, 43-46, 48, 49, 87, 96, 106-108]. More recently Thakur et al reported on the quadratic electro-optic effect in metallic nanoparticles within a transparent dielectric media [96]. Second order optical effects have also been shown for specific nanoparticles utilizing the asymmetry involved in shapers/interfaces using high intensity short pulses [89]. Second-order optics are not relevant to the electroabsorption presented in this report. As of this report, no other measurement of electroabsorption in metal nanoparticles has been published or known in the prior art. In the recent article by Thakur et al, the quadratic electro-optic effect in metal nanoparticles, specifically gold, in glass was compared with that of subnanometer-size metallic domains within doped nonconjugated conductive polymers [96]. Both the quadratic electro-optic effect and electroabsorption have applications in ultrafast electro-optic modulation, switching, and other applications in lasers and optoelectronics.

The focus of this report is on the measurement of electroabsorption in gold nanoparticles of various sizes to further elucidate the mechanisms of nonlinear optics in these important systems. Metallic nanoparticles with diameters of less than around 10 nm can also be called quantum dots. This is because many of their properties can be understood through consideration of the quantum confinement of the electrons within the nanometer dimensions of the nanoparticle. The measurements in this study have been compared to those for iodine-doped nonconjugated conductive polymers, such as polyisoprene, which have the smallest known metallic particles which are in the subnanometer domain. While electroabsorption in iodine-doped nonconjugated conductive polymers has been mentioned in previous reports [57, 61-63, 86, 88, 90], in this report more details are discussed and a comparison with gold nanoparticles in a dielectric medium is made.

The quadratic electro-optic effect is given by equation (9.1).

$$\Delta n = K\lambda E^2 \tag{9.1}$$

Where Δn is the change in the refractive index (induced birefringence), K is the Kerr coefficient, λ is the wavelength, and E is the applied electric field. Due to the small magnitude of the Kerr coefficient found for metal nanoparticles in glass, a long path length of about 3 cm was used to obtain a detectable modulation. Nonconjugated conductive polymers, in comparison, have the largest known electro-optic effect and were therefore used samples that provided path lengths on the order of microns. In the previous report by Thakur et al, quadratic electro-optic measurements were successfully made and a clear correlation between the real portion of the Kerr coefficient and the diameter of the metal nanoparticles was established down to the

subnanometer domain [96]. The magnitude of the real portion of the Kerr coefficient was shown to have a roughly $1/d^3$dependence, where d represents the diameter of the metallic nanoparticle.

In this report, electroabsorption will be discussed as given by equation (9.2).

$$\Delta\alpha = 4\pi K' E^2 \tag{9.2}$$

Where $\Delta\alpha$ is the change in the absorption coefficient and K' is the imaginary portion of the Kerr coefficient. The magnitude of K' is related to saturation of absorption and the two-photon absorption coefficient (α_2), where two photon absorption is given by $\Delta\alpha = \alpha_2 I$, and I is the optical intensity. The magnitude of α_2 is proportional to the imaginary part of the third-order susceptibility ($\chi^{(3)}$). As stated earlier, while saturation of absorption and two-photon absorption in gold nanoparticles have been previously reported, no measurements of electroabsorption had been previously reported. This report will discuss results of electroabsorption measurements in gold nanoparticles as well as in specific doped nonconjugated conductive polymers which have subnanometer-size metallic domains (quantum dots).

9.2 Experimental

Samples of glass with dimensions of about 4 cm X 4 cm X 3 mm containing specific diameters of gold nanoparticles were obtained from a commercial vendor. These samples were characterized using optical absorption spectroscopy and from this the wavelengths of the surface-plasmon-resonances (SPR) were determined. Using the surface-plasmon-resonances and relative peak intensities, the gold nanoparticle sizes of each sample were determined

utilizing established procedures [43, 107, 109]. The electroabsorption characteristics of these samples was then measured at a specific wavelength. The optical absorption spectra of the samples were measured using a CRAIC spectrometer in the transmission mode.

Metal electrodes were applied to the samples of gold nanoparticles in glass such that the optical interaction length for modulation was about 3 cm. An AC electric field at 4 kHz was applied to the electrodes using an AC power supply. The electroabsorption measurements were made using the set-up described in figure 9.1 [57, 61-63, 86, 88, 90]. A helium neon laser with a wavelength of 633 nm was used since this is near the onset of absorption due to the surface-plasmon-resonance. An example of the surface-plasmon-resonance for the sample containing gold nanoparticles of about 15 nm is shown in figure 9.2. This wavelength was expected to show enhanced magnitudes of the Kerr coefficient due to this proximity to the surface-plasmon-resonance. The laser beam was passed through a polarizer, then the sample, and then through an analyzer before being detected by a photo-detector. The polarizer and analyzer were set parallel to provide the orientation of polarization for the laser to be along the applied electric field. A lock-in amplifier, operating in 2f synchronization, and an oscilloscope were used to record the modulations. The modulation signal due to electroabsorption was recorded for varying applied electric field strengths and was found to depend quadratically on the strength of the applied electric field. The imaginary portion of the Kerr coefficient (K') was determined from the observed electroabsorption modulation, applied electric field, and interaction path-length within the samples, at 633 nm.

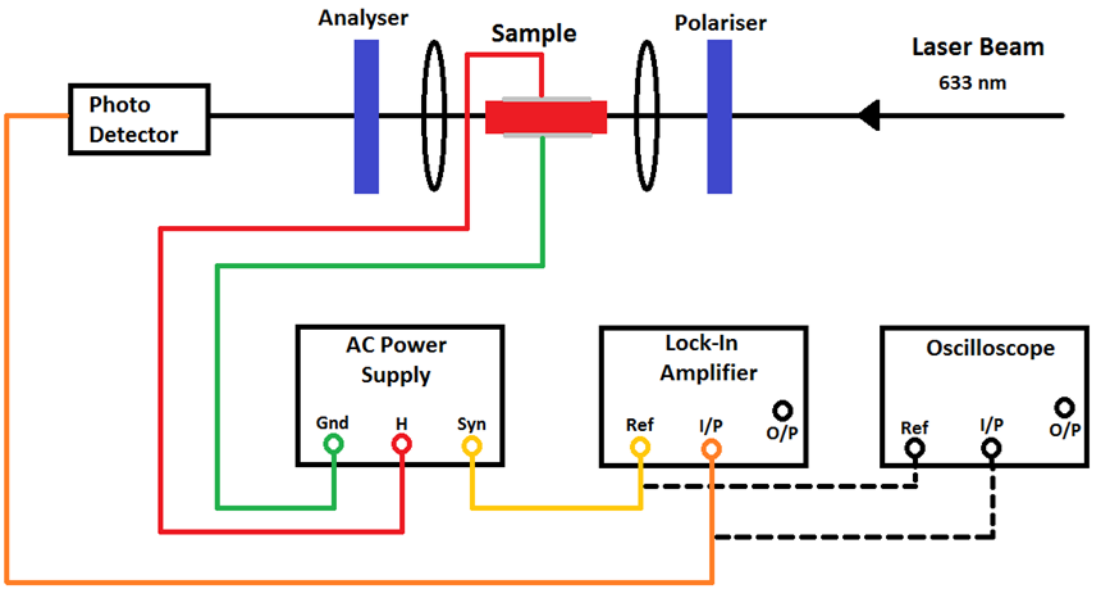

Figure 9.1: Experimental set-up for measurement of electroabsorption.

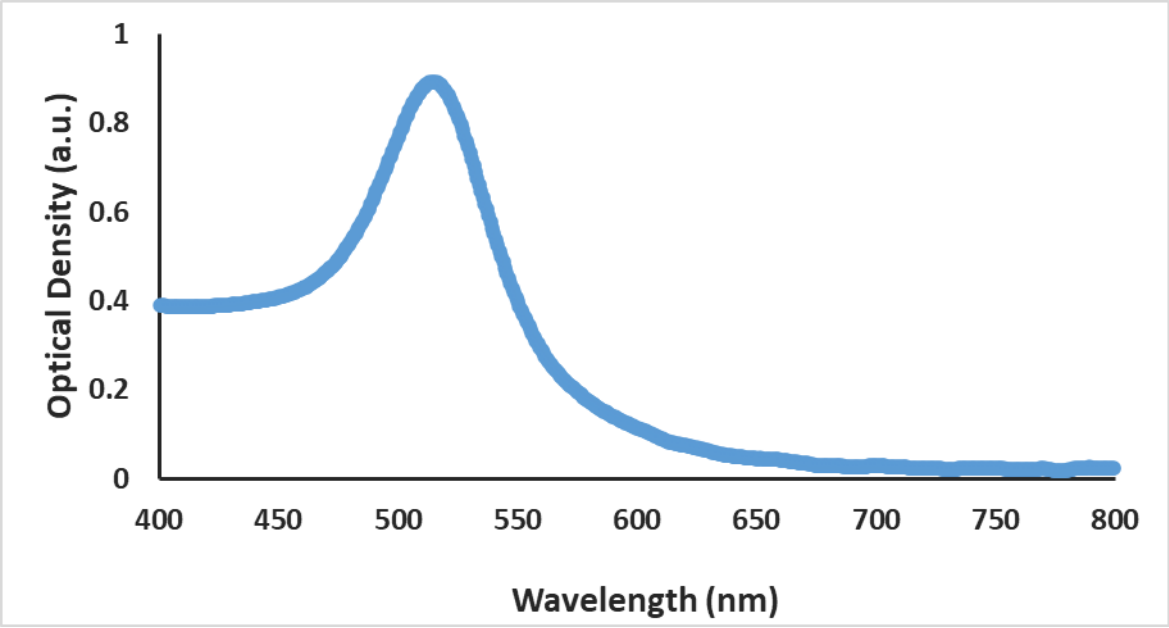

Figure 9.2: Surface plasmon resonance spectrum of gold nanoparticles in glass. Peak at 520 nm with a particle diameter of about 15 nm.

9.3 Results and Discussion

Three samples of gold nanoparticles in glass with three different average particle-diameters were studied. The optical absorption spectrum was recorded for light traveling through the thickness of the sample. For samples with smaller nanoparticles, the absorption peak occurs at shorter wavelengths and the relative intensity of the peak decreases [43, 107, 109]. These were all discussed in the Chapter 8 covering the 2019 article by Thakur et al [96]. For sample 1, the absorption peak occurred at about 534 nm which corresponds to a particle diameter of about 50 nm. For sample 2, the absorption peak occurred at about 527 nm which corresponds to a particle diameter of about 25 nm. For sample 3, with the absorption spectrum shown in figure 9.2, the absorption peak occurred at about 520 nm which corresponds to a particle diameter of about 15 nm. The absorption coefficient as given was found to be about 5.3 cm^{-1} at 520 nm which is consistent with a low concentration of gold nanoparticles of about 10^{-9} M [43, 107].

Electroabsorption measurements were made in these samples at different applied AC fields as discussed in section 9.2 of this chapter. The beam at 633 nm from a He:Ne laser was passed through the long dimension of the sample with an interaction length of about 3 cm. For samples 1 and 2 having particle diameters of about 50 nm and 25 nm respectively, the modulation due to electroabsorption was too weak to measure. The results of the measurements for sample 3, having a particle diameter of about 15 nm, are shown in figure 9.3. The imaginary portion if the Kerr coefficient (K') as determined from the observed modulation signals is about 4×10^{-15} m/V^2 at 633 nm [97].

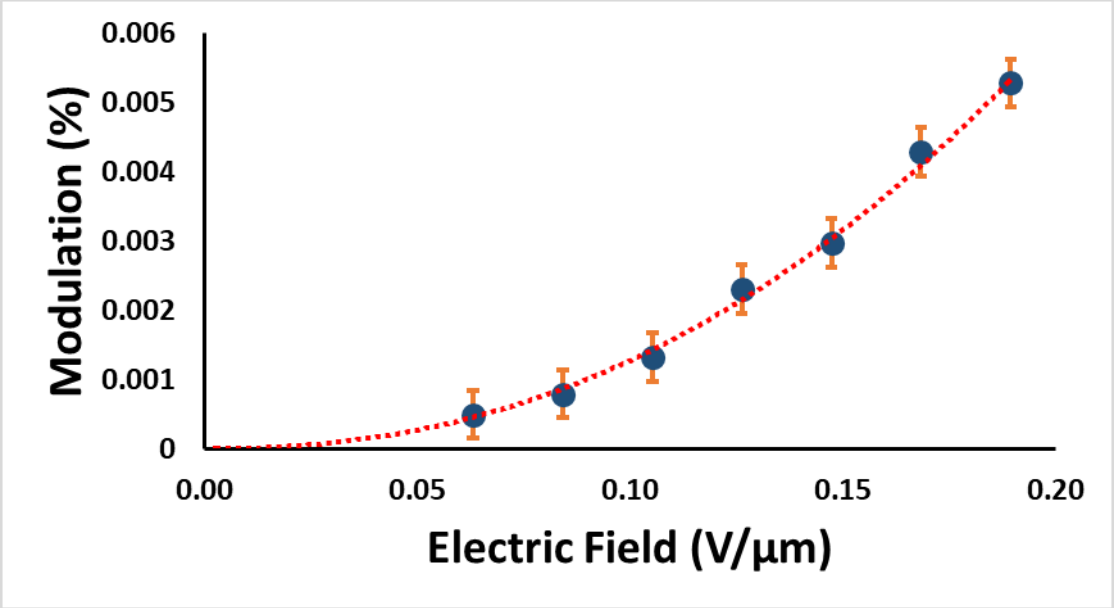

Figure 9.3: Electroabsorption modulation in gold nanoparticles within glass for different applied electric fileds. Particle diameter about 15 nm. Interaction length about 3 cm.

Results of measurements following identical experimental procedures but using films of the iodine doped nonconjugated conductive polymer polyisoprene with a thickness of about 1 micron are shown in figure 9.4. As previously reported, subnanometer-size metallic domains are formed in nonconjugated conductive polymers upon doping with iodine [57, 61-63, 86, 88, 90]. Charge-transfer from an isolated carbon-carbon double bond to the dopant creates the highly confined metallic domains or quantum dots. These materials exhibit a surface-plasmon-resonance peak at about 400 nm and a radical cation peak at about 300 nm. The electrical conductivity, optical absorption, spectral line-width, EPR, magnetic susceptibility vibration spectroscopic and thermal characteristics of doped nonconjugated polymers are all consistent with metallic particles of subnanometer sizes [57, 61-63, 86, 88, 90]. The optical absorption peak of the nonconjugated conductive polymer used in this experiment is at about 400 nm. This is much smaller than the that of the smallest metal nanoparticles reported so far (about 2 nm in

diameter). These are all as would be expected considering the subnanometer particle size [43]. In addition, due to the subnanometer-sizes, these metallic particles have shown the largest known Kerr coefficient and two-photon absorption coefficient foe any material [57, 61, 86, 89, 109]. In this study electroabsorption has been measured which is the imaginary portion of the Kerr coefficient (K'). The imaginary part of the Kerr coefficient (K') as measured is about 3.2×10^{-11} m/V^2 at 633 nm for iodine-doped polyisoprene [97]. All of the magnitudes of the Kerr coefficient stated here are for about the same magnitude of optical density at 633 nm.

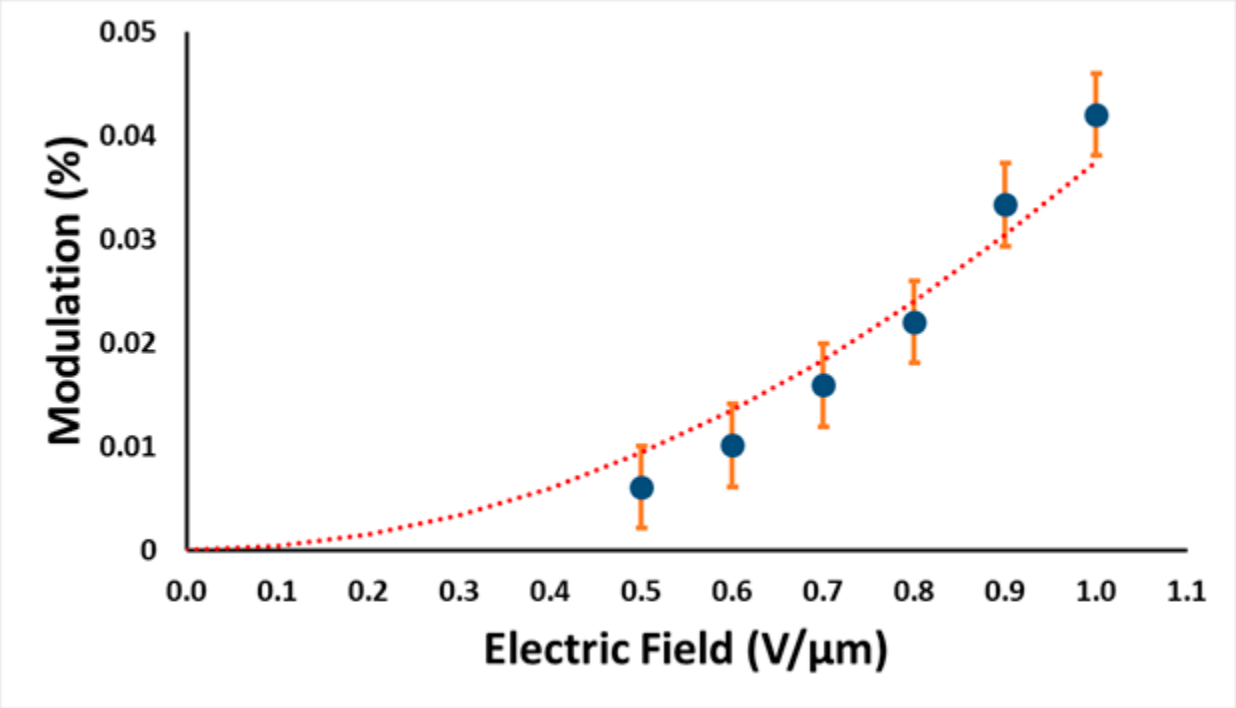

Figure 9.4: Electroabsorption modulation in a nonconjugated conductive polymer (iodine-doped polyisoprene) for different applied electric fields. Film thickness about 1 µm.

As these results show, the electroabsorption, or the imaginary part of the Kerr coefficient (K'), increases rapidly as particle size is decreased. For particles with diameters of about 25 nm and 50 nm, the magnitudes of K' were too small to measure. Comparing these results with those from a doped nonconjugated conductive polymer, the increase goes roughly

as d^{-3}, where d is the nanoparticle diameter. This is identical to the dependence of the real part of the Kerr coefficient (K) on particle diameter as reported in Chapter 8 and in the paper by Thakur et al [96]. For quadratic electro-optic measurements, the magnitudes of the modulation was strong enough to measure for all three samples of gold nanoparticles in glass [96].

As in the case of the quadratic electro-optic effect, this correlation between electroabsorption and particle diameter can be explained using earlier theoretical treatment as well as more recent theory on dimensionally confined electronic systems [13, 15, 17, 18, 101, 108]. According to these theories, $\chi^{(3)}$ should increase as the inverse cube of the particle diameter. The Kerr coefficient is proportional to $\chi^{(3)}$ $(\omega;\ \omega, 0,0)$. In particular, K is proportional to the real part of $\chi^{(3)}$ and K' is proportional to the imaginary part. The measurements reported here were made at 633 nm which is near the onset of the surface-plasmon-resonance. Therefore, $\chi^{(3)}$ at this wavelength is complex and contains both real and imaginary parts. The theoretical treatment mentioned above predicts that the maximum value of $\chi^{(3)}$ is proportional to $T_1T_2(1\text{-}d/d_0)/d^3$, where T_1 is the excited state lifetime, T_2 is the dephasing time, d_0 is a characteristic threshold diameter of the system, and d is the diameter of the nanoparticle. Therefore, for $d < d_0$, $\chi^{(3)}$ increases as d^{-3}. This model was further explained in section 2.7 of chapter 2 in this report. The particle concentration would alter the absorption coefficient and the Kerr coefficient in the same way. Since the optical density at 633 nm is about the same for all of the samples tested, we can compare the magnitudes of Kerr coefficients at the fundamental level. AS the results show, the Kerr coefficient follows the theory and increases roughly as d^{-3}. An alternative interpretation of the d^{-3} dependence is that for any given excitation the fraction of electrons excited in a nanoparticle is higher in a smaller

particle since the total number of electrons in a smaller particle is less. Therefore, a larger optical nonlinearity is expected. This is essentially a result predicted by the phase-space filling model [15, 17, 18, 101] which states that $\delta f/f = -(N/N_s)$, where δf represents the change in the oscillator strength (f), N represents the number of electrons excited, and N_s represents the total number of electrons participating in the excitation process. The value of N_s is proportional to the volume of the particle that confines the electrons which is roughly equal to $\pi\, d^3/6$. Therefore, the change in absorption coefficient $\Delta\alpha$ which is proportional to the change in oscillator strength δf, should have a d^{-3} dependence. As a result, K' also has a d^{-3} dependence. This model was further explained in section 2.8 of chapter 2.

Metallic nanoparticles within transparent dielectric media are expected to have various applications in ultrafast electro-optic switching, modulation, Kerr cells, and other areas of photonics. As the absorption coefficient is small, about 0.2 cm^{-1} at 633 nm, the figure of merit for applications is high for these materials. Although this report involves metal nanoparticles in glass, the results can be extended to metal nanoparticles in other transparent dielectric media.

9.4 Conclusions

Electroabsorption has been measured for the first time for metallic nanoparticles in transparent dielectric media. In particular, gold nanoparticles in glass and subnanometer-size metallic domains in an iodine-doped nonconjugated conductive polymer have been studied. The measurements have been made using an AC field at 4 kHz. Electroabsorption has a quadratic dependence on the strength of the applied electric field. The imaginary part of the Kerr coefficient (K') has been determined for different sizes of metallic nanoparticles. The

magnitude of K' has been found to increase rapidly for smaller diameters (d) of nanoparticles, following a roughly d^{-3} dependence. The magnitudes of K' were measured as about 4×10^{-15} m/V^2 for 15 nm gold particles and about 3.2×10^{-11} m/V^2 for subnanometer metallic domains in an iodine-doped nonconjugated conductive polymer respectively at 633 nm [97]. These results are similar to the results obtained in the quadratic electro-optic measurements, the real part of the Kerr coefficient, in the report by Thakur et al outlined in Chapter 8 [96]. Nonconjugated conductive polymers have metallic domains of subnanometer dimensions, also known as quantum dots, which lead to the largest known Kerr coefficients of any studied materials. The results here imply various applications of these systems in ultrafast switching, modulation, and other applications in laser-optics and optoelectronics.

Chapter 10

Quadratic Electrooptic Effect in Other Nonconjugated Conductive Polymers

10.1 Introduction

Nonlinear optics is an important field to a variety of industries including telecommunications and sensing. Studying the nonlinear optical properties of materials is important to developing improved optical modulators, switches, and other photonic devices. Nonconjugated conductive polymers provide a promising area of research due to their low cost, ease of processing, and exceptionally large nonlinear properties [86, 102]. A variety of nonconjugated conductive polymers have been previously investigated and their third-order nonlinear optical properties reported [55-63, 102]. In this report, new samples have been fabricated and additional measurements made for several of these nonconjugated conductive polymers reported earlier. The nonconjugated polymers that have been investigated include cis-1,4-polyisoprene, trans-1,4-polyisoprene, styrene-butadiene rubber. These polymers were used in experiments designed to measure the quadratic electro-optic effect in the materials. The results of these experiments were then used to calculate the magnitude of the Kerr coefficient of the nonconjugated conductive polymers.

The quadratic electro-optic effect, also known as the Kerr effect, is given by equation (10.1).

$$\Delta n = K\lambda E^2 \tag{10.1}$$

Where Δn is the change in the refractive index (induced birefringence), K is the Kerr coefficient, λ is the wavelength, and E is the applied electric field. This equation describes a change in the refractive index of a material when an electric field is applied. This change in the refractive index leads to electro-optic switching or modulation. The larger the Kerr coefficient is, the larger the change in the refractive index for any given electric field, wavelength, and optical path length through the sample.

10.2 Experimental

The samples fabricated consisted of thin, typically 1 to 10 microns thick, portions of the nonconjugated polymer deposited from a solution onto a glass slide. Toluene was used to dissolve the polymer source material into a solution. This solution was then deposited onto a glass slide using a pipette and then placed under a hood vent to allow the toluene to evaporate leaving a film of the nonconjugated polymer behind.

The polymer samples were then exposed to iodine by placing them in a container along with solid Iodine. These samples were left under a fume hood for several hours to allow for heavy doping. Doping the nonconjugated polymers with Iodine results in significant changes to both the optical absorption spectra of the material as well as its electrical conductivity [54, 56, 86, 100, 102]. After the samples were fully doped, copper strips were used as electrodes and attached to the doped polymer samples with about 1mm spacing between them. These

electrodes were used to provide the applied voltage in the quadratic electro-optic and electro-absorption experiments.

Both the quadratic electro-optic and electro-absorption experiments utilized the same basic equipment. A laser, two linear polarizers, a detector, a chopper wheel with a Stanford Research Systems SR540 chopper controller, and several small lenses were used to produce, manipulate, and measure the intensity of light used in the experiment. A Powertron 250S AC power supply with adjustable frequency and output voltage was used to apply the electric field to the polymer samples. A Stanford Research Systems SR530 lock-in amplifier and a Hewlett Packard 5416B oscilloscope were used to measure the output from the detector at the desired frequency.

For all polymer samples quadratic electro-optic measurements were performed at a wavelength of 633 nm. For these experiments, a Uniphase 1508-1 helium-neon laser was used to produce the incident beam. Two Newport 10GL08 polarizers were used as the analyzer and polarizer, and a Thor Labs DET210 photodetector was used to measure the output beam.

The quadratic electro-optic effect was measured using the field-induced birefringence method as shown in figure 10.1. An AC power supply was connected to the electrodes on the sample and an electric field at 4 kHz was applied to the sample. The laser beam was polarized at 45° with respect to the applied electric field and passed through the sample. The transmitted laser beam was then passed through an analyzer that was cross polarized with respect to the polarizer. The laser beam was then incident onto a photodetector that was used to capture the output of the experiment. The signal from the photodetector was then sent to the lock-in

amplifier which was setup with 2f synchronization in relation to the frequency of the applied electric field. The lock-in amplifier and oscilloscope were used to measure the output signals for varying levels of applied electric field. To determine the modulation from the applied field a base line measurement was needed. This was made using a chopper wheel and no applied field. The lock-in amplifier was synchronized with the chopper wheel and the output was measured. The modulation was recorded as a percent related to this base line measurement.

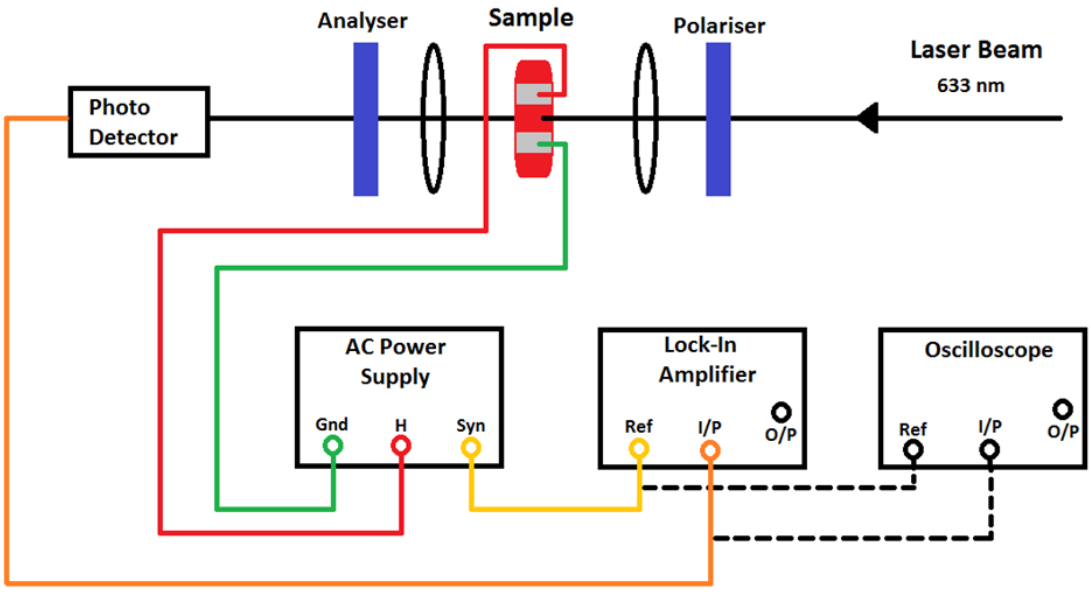

Figure 10.1: Experimental set-up for the measurement of the quadratic electro-optic effect.

In order to calculate the Kerr coefficient, the path length of light through the sample must first be determined. Since the experiment was performed with the laser applied normally to the nonconjugated conductive polymer samples, the path length through the sample was the same as the sample thickness at the point of incidence. Thickness measurements were made using a Tencor alpha-step 200 stylus profilometer. An example of the profilometer measurements is shown in figure 10.2. This figure shows a relatively large peak on the left side

of the graph of about 14 microns. This peak represents a lip that formed around the edge of the sample as the toluene solution evaporated. All electro-optic measurements were performed in the central area of the sample, away from this lip, where the thickness of the samples were generally around 1-2 microns.

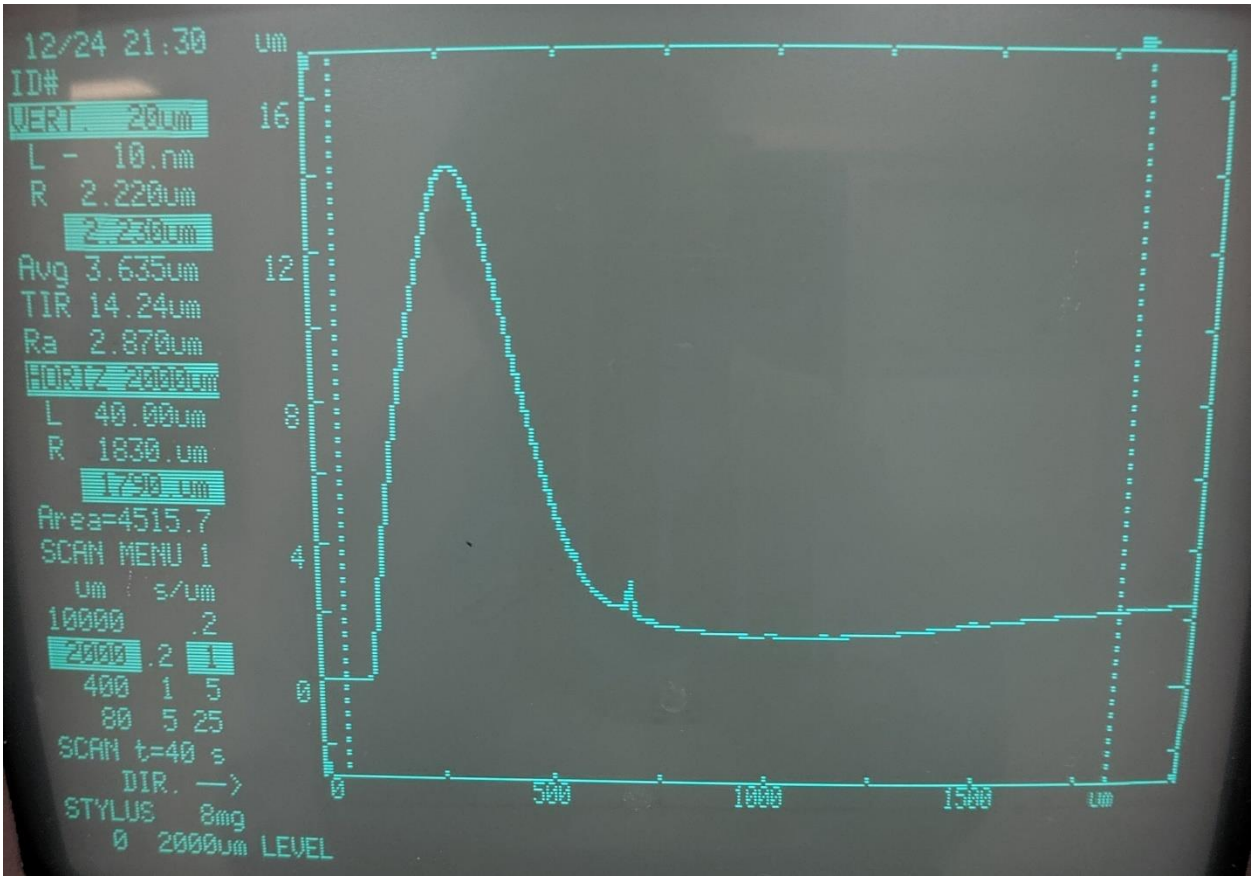

Figure 10.2: Profilometer measurement for a nonconjugated polymer film on a glass slide. This sample has a thickness of about 2 microns in the center of the sample.

10.3 Determination of the Kerr Coefficient

The quadratic electro-optic effect, shown in equation (10.1), is given by: $\Delta n = K\lambda E^2$, where Δn is the change in the refractive index of the material, K is the Kerr coefficient, λ is the wavelength of the applied light, and E is the applied electric field. The phase change in the

electro-magnetic wave passing through the material as a function of the change in refractive index is given by equation (10.2).

$$\Delta\varphi = \frac{2\pi l}{\lambda} \Delta n \tag{10.2}$$

where $\Delta\varphi$ is the phase change, and l is the path length through the material. Substituting equation (10.1) into equation (10.2) gives the relationship between the Kerr coefficient and the phase change as shown in equation (10.3).

$$\Delta\varphi = 2\pi l K E^2 \tag{10.3}$$

The phase change is obtained from the lock-in and/or oscilloscope data which allows the Kerr coefficient to be determined.

10.4 Results and Discussion

Three different nonconjugated polymers, cis-1,4-polyisoprene, trans-1,4-polyisoprene, and styrene butadiene rubber, have been investigated. Each polymer was made into a solution by dissolving them in toluene. These solutions were then deposited on glass slides and allowed to evaporate leaving behind a film with a thickness of about 1 to 2 microns. These films were then doped with Iodine in the vapor phase following the standard procedure. The quadratic electro-optic effect was measured in these samples using the field induced birefringence method at 633 nm.

Modulation was plotted as a percentage as a function of applied electric field strength in volts per micron. For all the nonconjugated conductive polymers tested the modulation was found to depend quadratically on the magnitude of the applied electric field. The experimental

results for CPI, TPI, and SBR are shown in figures 10.3 through 10.5. From the experimental results the Kerr coefficient for the materials was determined using the process outlined in section 10.3. For cis-1,4-polyisoprene, shown in figure 10.3, the Kerr coefficient was determined to be about $2 \times 10^{-11}\, m/V^2$. For trans-1,4-polyisoprene, shown in figure 10.4, the Kerr coefficient was calculated to be about $1.9 \times 10^{-11}\, m/V^2$. For styrene butadiene rubber, shown in figure 10.5, the Kerr coefficient was calculated to be about $2.5 \times 10^{-11}\, m/V^2$. The Kerr coefficients reported here are smaller than some previous reports due to lower overall doping levels in these samples [60, 63].

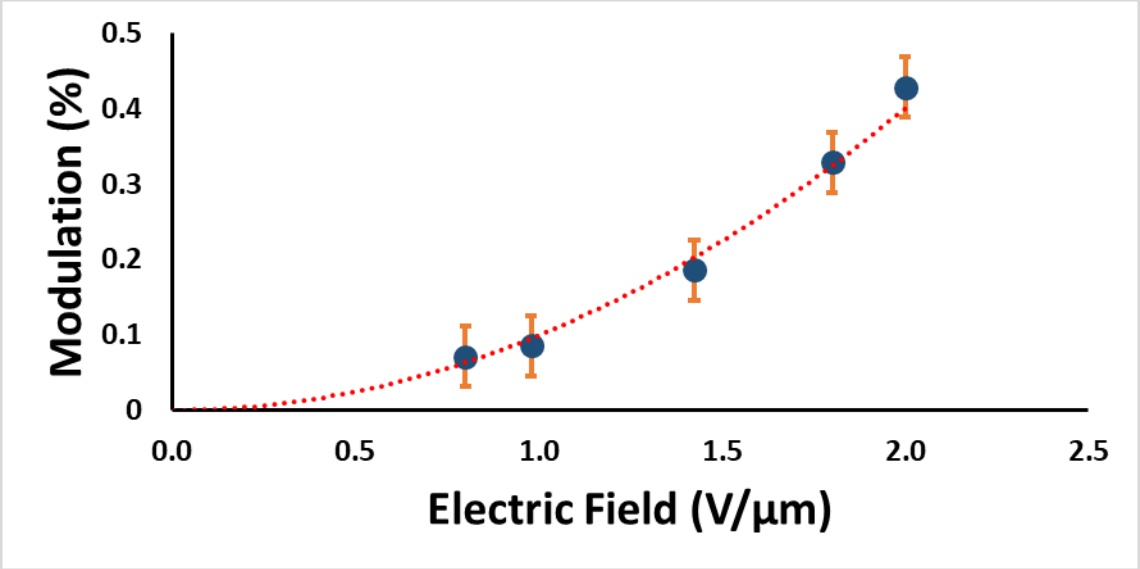

Figure 10.3: Quadratic electro-optic effect measurements for cis-1,4-polyisoprene at 633 nm.

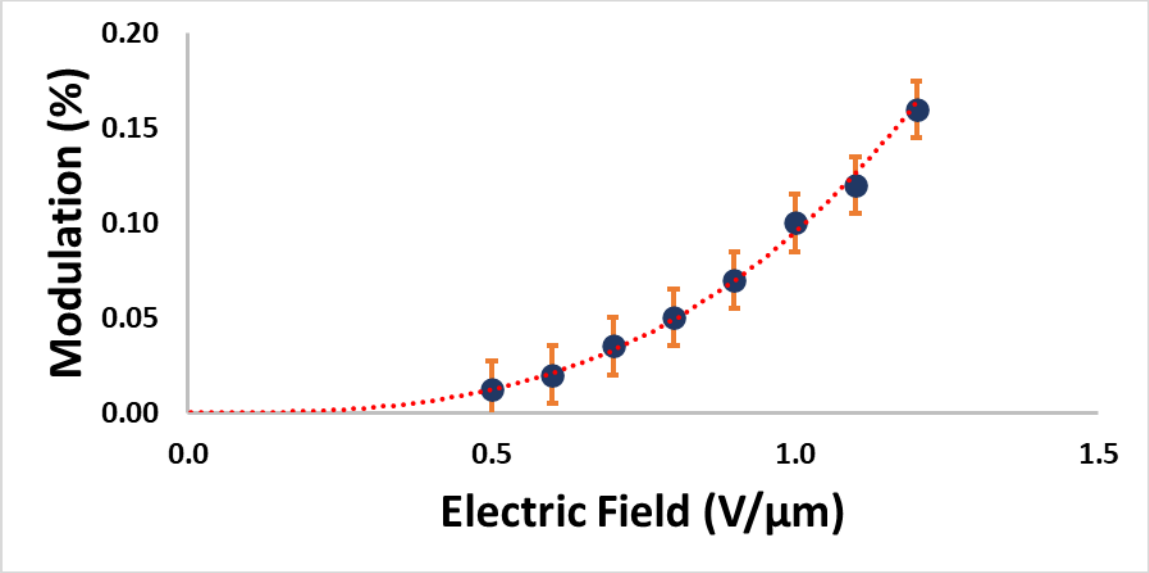

Figure 10.4: Quadratic electro-optic effect measurements for trans-1,4-polyisoprene at 633nm.

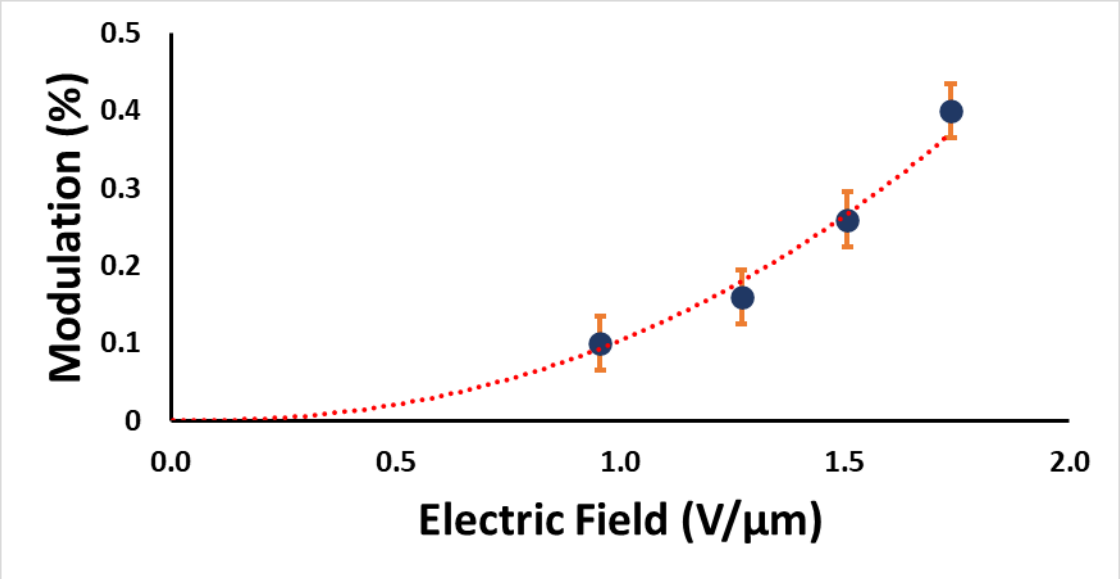

Figure 10.5: Quadratic electro-optic effect measurements for styrene-butadiene rubber at 633 nm.

The magnitudes of the Kerr coefficients found in these experiments are expected given the subnanometer size charge system found in the doped polymers. The third-order susceptibility is related to the size of the nanoparticle/charge system, increasing with d^{-3}, where

d is the diameter [13, 96, 97]. Therefore, doping of the nonconjugated polymers with Iodine results in a metallic quantum dot within the doped polymer and is responsible for the large nonlinear properties found in the materials.

10.5 Conclusions

The quadratic electro-optic effect, also known as the Kerr effect, has been measured for several nonconjugated conductive polymers, specifically cis-1,4-polyisoprene, trans-1,4-polyisoprene, and styrene butadiene rubber. All of these polymers featured subnanometer sized metallic domains that resulted from doping with Iodine. These measurements were made using the field-induced birefringence method at 633 nm with an AC field applied at 4 kHz. The Kerr coefficient has a quadratic relationship to the applied field. The magnitude of the Kerr coefficient has been calculated for these materials based on the results of the quadratic electro-optic measurements. For cis-1,4-polyisoprene the Kerr coefficient was found to be about $2 \times 10^{-11}\, m/V^2$. For trans-1,4-polyisoprene the Kerr coefficient was found to be about $1.9 \times 10^{-11}\, m/V^2$. For styrene butadiene rubber the Kerr coefficient was found to be about $2.5 \times 10^{-11}\, m/V^2$. While the Kerr coefficients reported here are smaller than previous reports due to lower overall doping levels in the samples, these materials have shown some of the largest known Kerr coefficients for any previously studied materials [56-58, 60, 63, 86, 88, 93, 97, 100, 102, 110-112]. These exceptionally large nonlinear optical properties are the result of the metallic quantum dots that are formed when the polymers are doped with Iodine. The results here imply various applications of these systems in ultrafast switching, modulation, and other applications in laser-optics and optoelectronics.

Chapter 11

Conclusions

The nonlinear optical properties of gold nanoparticles and specific nonconjugated conductive polymers, and photovoltaic devices based on nonconjugated conductive polymers have been investigated. The quadratic electro-optic effect has been measured for gold nanoparticles in a dielectric medium for several samples with different average particle diameters. The Kerr coefficients for these samples were measured and compared to previous results for nonconjugated conductive polymers. A correlation between the size of the nanoparticle or charge system and the magnitude of the Kerr coefficient was developed. Electroabsorption was also measured for various particle sizes of gold nanoparticles in glass and the results were compared to those of nonconjugated conductive polymers. The effect of Iodine doping on the nonconjugated conductive polymer polyethylene terephthalate was investigated through UV/Vis and IR spectroscopy and the quadratic electro-optic effect and electroabsorption effect for the material were measured. The quadratic electro-optic effect for several other nonconjugated conductive polymers has also been measured. Photovoltaic devices were fabricated using nonconjugated conductive polymers. The photovoltages and photocurrents for varying incident light intensities were measured. The performance lifetime of these cells was also evaluated. These fabricated devices are similar to a dye-sensitized or Grätzel type solar cell.

Samples of glass containing varying average sizes of gold nanoparticles have been obtained. The average particle sizes in these samples were determined using UV/Vis spectroscopy and the surface plasmon resonance frequency of the samples. The samples tested had average particle diameters of about 50 nm, 25 nm, and 15 nm. The quadratic electro-optic effect was then measured for these samples using the field-induced birefringence method. These measurements were performed at 633 nm using an applied AC field at 4 kHz. The results of the quadratic electro-optic measurements were used to determine the Kerr coefficient for the samples. The Kerr coefficients were compared between the different samples and to a nonconjugated conductive polymer that features a metallic quantum dot with a subnanometer size. For samples with an average particle size of 50 nm the Kerr coefficient was calculated to be about $2.5 \times 10^{-15}\ m/V^2$. For samples with an average particle size of about 25 nm the Kerr coefficient was calculated to be about $2.0 \times 10^{-14}\, m/V^2$. For samples with an average particle size of about 15 nm the Kerr coefficient was calculated to be about $7.5 \times 10^{-14}\, m/V^2$. These were compared to a nonconjugated conductive polymer with a subnanometer size quantum dot that had a Kerr coefficient of about $3.5 \times 10^{-10}\, m/V^2$ [96]. These results showed that there was an increase in the magnitude of the Kerr coefficients as the size of the particles (quantum dots) decreased. Specifically, the magnitude of the Kerr coefficient increased as d^{-3} where d was the particle diameter. This result corresponded to the relationship predicted for the third-order nonlinear susceptibility of a spherical nanoparticle in a mathematical model developed by Hache et al. The observed size dependence of nonlinearity has now been explained using phase-space-filling model as well. This was the first time the relationship

between the Kerr coefficient and the size of a metallic quantum dot was experimentally established.

Electroabsorption was also measured in a gold glass sample. This effect is much weaker than the quadratic electro-optic effect and was not able to be measured for the 50 nm or 25 nm samples. The electroabsorption was measured at 633 nm for varying magnitudes of applied electric field. These results showed an electroabsorption coefficient for the 15 nm gold nanoparticles in glass sample to be 4×10^{-15} m/V^2. This was compared to previous results from a nonconjugated conductive polymer where the electroabsorption coefficient was measured to be 3.2×10^{-11} m/V^2 [97]. These results showed that electroabsorption also increases as the size of the particle decreases. The quadratic electro-optic effect is related to the real portion of the Ker coefficient and the electroabsorption is related to the imaginary part. This research showed that both the real and imaginary parts of the Kerr coefficient are related to the size of the particle with smaller particles giving stronger effects. These results followed predictions from the Hache et al model and the phase space filling model, which both predict that the magnitudes of these effects will increase proportionally to d^{-3}, where d is the diameter of the nanoparticle (quantum dot).

Photovoltaic devices utilizing nonconjugated conductive polymers, specifically cis-1,4-polyisoprene and styrene butadiene rubber, have been fabricated. These cells are similar to a dye-sensitized or Grätzel type solar cell. These devices were constructed using indium tin oxide coated PET substrates. Carbon was used as the counter electrode and titanium dioxide was used as the top electrode. The Iodine-doped nonconjugated conductive polymer acted as the light absorbing layer and was between the two electrodes. A liquid electrolyte was introduced

to the cells after fabrication to facilitate charge transfer within the cell. The mechanism of the photovoltaic effect in these cells is as follows: (i) incident light on the doped polymer is absorbed and results in excitation, (ii) the excited electron is transferred to the TiO_2 electrode, (ii) the charge is transferred through the load to the carbon counter electrode, (iii) the polymer is restored through a redox couple with the electrolyte.

The photovoltaic effect in these fabricated cells was measured by exposing them to varying incident light intensities and measuring the resulting photovoltages and photocurrents. For cells utilizing cis-1,4-polyisoprene the maximum photovoltage and photocurrent measured were 0.73 V and 0.27 mA/cm^2 respectively with an incident light intensity of about 4 mW/cm^2 [85]. For cells utilizing styrene butadiene rubber the maximum photovoltage and photocurrent measured were 0.74 V and 0.24 mA/cm^2 respectively with an incident light intensity of about 4 mW/cm^2 [84].

The performance lifetime of the fabricated cells was studied. These cells were found to generally have a rapid degradation of their performance characteristics after a couple of days. This was explained to be due to the loss of the liquid electrolyte from the cell. Cells were fabricated and sealed between two glass slides using rubber O-rings. The performance of the sealed cells was monitored over time and compared to cells that were left open to the air. The presence of the electrolyte within the sealed cell was monitored by viewing the cell under a microscope. The sealed cell was found to have a significantly reduced performance loss over time, both in the photovoltage and the photocurrent, compared to a cell that was not sealed. The sealed cell showed little performance degradation after about 2 weeks, while the cell that was not sealed showed an almost complete loss of output after a couple of days. The sealed cell

still had some of the liquid electrolyte present within the cell after the 2-week period. This confirmed that maintaining the liquid electrolyte within the cell is vital to maintain the performance of the cell. A better method for sealing the cells and a longer performance study will be required to determine what other factors affect the lifetime of the fabricated cells.

Polyethylene terephthalate films, about 50 microns thick, have been obtained and studied. The films were doped with Iodine in the vapor phase using the standard procedure. The effect of Iodine doping on the material was investigated through UV/Vis and IR spectroscopy. The UV/Vis absorption showed the formation of a peak at about 312 nm and a broad absorption with a peak at about 375 nm after doping. These peaks increased in intensity with higher iodine doping levels. The undoped polyethylene terephthalate had a single absorption peak at about 310 nm, which was due to the terephthalic ring. The FTIR spectroscopy showed a reduction in the peak at about 1505 wavenumber after doping, which was due to carbon-carbon stretching vibration in the terephthalic ring. These results show that the Iodine is interacting with isolated carbon bonds in the molecular structure of the polyethylene terephthalate. Specifically, bonds in the polymer ring are most heavily influenced. The Iodine doping resulted in charge transfer from the polymer ring to the Iodine. This forms a metallic quantum dot, with a charge that is confined to a subnanometer sized charge system.

The nonlinear optical properties of the Iodine-doped polyethylene terephthalate films were investigated using the field-induced birefringence method to measure the quadratic electro-optic effect at 633 nm in the material. These results showed a clear quadratic correlation between the magnitude of the applied electric field and the optical modulation through the samples. This effect corresponded to a Kerr coefficient of about $5 \times 10^{-11}\, m/V^2$

for samples doped with a molar concentration of Iodine of about 0.83. For samples doped with a molar concentration of Iodine of about 0.28, the Kerr coefficient was calculated to be about $1.5 \times 10^{-11}\, m/V^2$. These results show a similar or slightly smaller magnitude of Kerr coefficient compared to other nonconjugated conductive polymers representing metallic quantum dots of subnanometer dimensions. The electroabsorption effect was also measured in polyethylene terephthalate for varying levels of iodine doping. The modulation due to electroabsorption was observed to increase quadratically with the applied electric field. The modulation was also seen to increase with higher levels of iodine doping. These samples showed comparable results to other nonconjugated conductive polymers that have been investigated with the modulation due to electroabsorption being less than that measured due to the Kerr effect.

These experiments provide valuable information for the development of technologies important in the field of telecommunication, optical switching, sensor design, and solar power conversion. The field of electro-optics is of increasing importance as optical methods for sensing and data transmission become more common. These industries have vital needs for new materials that allow for faster switching, smaller device sizes, and lower power consumption. Nonconjugated conductive polymers have exhibited some of the largest known Kerr coefficients.

Solar power conversion technology continues to be a rising field as the need for power generation with reduced CO_2 emissions, sustainable inputs, and low environmental impact waste products becomes increasingly apparent. Organic photovoltaics is one promising solution

to these problems and determining the efficacy of cells utilizing nonconjugated conductive polymers is important to the advancement of this field.

Chapter 12

References

[1] Banerjee, P. P., 2004, Nonlinear Optics, Marcel Dekker Inc.
[2] New, G., 2011, Introduction to Nonlinear Optics, Cambridge University Press.
[3] Franken, P. A., Hill, A. E., Peters, C. W., and Weinreich, G., 1961, "Generation of Optical Harmonics," *Phys. Rev. Lett.*, 7.
[4] Boyd, R. W., 2008, Nonlinear Optics, Academic Press.
[5] Ekimov, A. I., and Onushchenko, A. A., 1981, *Pis'ma Zh.Eksp.Teor.Fiz*, 34.
[6] Ekimov, A. I., Efros, A. L., and Onushchenko, A. A., 1985, "Quantum size effect in semiconductor microcrystals," *Solid State Comm*, 56, pp. 921-924.
[7] Agrawal, G. P., Cojan, C., and Flytzanis, C., 1978, "Nonlinear Optical Properties of One-Dimensional Semiconductors and Conjugated Polymers," *Phys. Rev. B*, 17.
[8] Chemla, D. S., 1987, Nonlinear Optical Properties of Organic Molecules and Crystals, Academic Press.
[9] Prasad, P. N., and Williams, D. J., 1991, Introduction to nonlinear optical effects in molecules and polymers, Wiley, New York.
[10] Jackson, J. D., 1998, Classical Electrodynamics, John Wiley & Sons.
[11] Garnett, J. C. M., 1904, "Colours in Metal Glasses and in Metallic Films," *Phil. Trans. A*, 203, pp. 385-420.
[12] Mie, G., 1908, "Beiträge zur Optik trüber Medien, speziell kolloidaler Metallösungen," *Ann. Phys*, 25, pp. 377-445.
[13] Hache, F., Ricard, D., and Flytzanis, C., 1986, "Optical nonlinearities of small metal particles: surface-mediated resonance and quantum size effects," *J. Opt. Soc. Am. B*, 3, pp. 1647-1655.
[14] Schmitt-Rink, S., Chemla, D. S., and Miller, D. A. B., 1985, "Theory of transient excitonic optical nonlinearities in semiconductor quantum-well structures," *Phys. Rev. B*, 32.
[15] Greene, B. I., Orenstein, J., Millard, R. R., and Williams, L. R., 1987, "Nonlinear Optical Response of Excitons Confined to One Dimension," *Phys. Rev. Lett.*, 58.
[16] Greene, B. I., Orenstein, J., Thakur, M., and Rapkine, D. H., 1987, "Nonlinear Optical Response of Excitons Confined to one Dimension," *MRS Online Proceedings Library*, 109.
[17] Greene, B. I., Mueller, J. F., Orenstein, J., Rapkine, D. H., Schmitt-Rink, S., and Thakur, M., 1988, "Phonon-Mediated Optical Nonlinearity in Polydiacetylene," *Phys. Rev. Lett.*, 61.
[18] Thakur, M., 2016, "Correlation between Nonlinear Optics in Polydiacetylene and Line-width in Super-resolved Fluorescence Microscopy," *J. Macromol. Sci. Part A*, 53.
[19] Fehrenbach, G. W., Schäfer, W., Treusch, J., and Ulbrich, R. G., 1982, "Transient Optical Spectra of a Dense Exciton Gas in a Direct-Gap Semiconductor," *Phys. Rev. Lett.*, 49.
[20] Knox, W. H., Fork, R. L., Downer, M. C., Miller, D. A. B., Chemla, D. S., Shank, C. V., Gossard, A. C., and Wiegmann, W., 1985, "Femtosecond Dynamics of Resonantly Excited Excitons in Room Temperature GaAs Quantum Wells," *Phys. Rev. Lett*, 54.
[21] Schafer, F., and Schmidt, W., 1966, "Geometrical Model and Experimental Verification of Two-Photon Absorption in Organic Dye Solutions," *Journal of Quantum Electronics*, 2.
[22] Hermann, J. P., and Ducuing, J., 1972, "Dispersion of the Two-Photon Cross Section in Rhodamine Dyes," *Opt. Comm.*, 6.

[23] Hermann, J. P., and Ducuing, J., 1972, "Absolute Measurement of Two-Photon Cross Sections," *Phys. Rev. A*, 5.
[24] Foucault, B., and Hermann, J. P., 1975, "Two-Photon Absorption in Organic Dyes – Relation with the Symmetry of the Levels," *Opt. Comm.*, 15.
[25] Ducuing, J., Foucault, B., and Hermann, J. P., 1976, "Two-Photon Absorption in Organic Dyes – Reply to a Comment," *Opt. Comm.*, 10.
[26] Rustagi, K. C., and Ducuing, J., 1974, "Third-Order Optical Polarizability of Conjugated Organic Molecules," *Opt. Comm.*, 10.
[27] Sauteret, C., Hermann, J. P., Frey, R., Padère, F., Ducuing, J., Baughman, R. H., and Chance, R. R., 1976, "Optical Nonlinearities in One-Dimensional-Conjugated Polymer Crystals," *Phys. Rev. Lett.*, 36.
[28] Lequime, M., and Hermann, J. P., 1977, "Reversible Creation of Defect by Light in One Dimensional Conjugated Polymers," *Chem. Phys.*, 26.
[29] Carter, G. M., Chen, Y. J., and Tripathy, S. K., 1983, "Intensity-Dependent Index of Refraction in Multilayers of Polydiacetylene," *App. Phys. Lett.*, 43.
[30] Bubeck, C., Kaltbeitzel, A., Lenz, R. W., Neher, D., Stenger-Smith, J. D., and Wegner, G., 1989, "Nonlinear Optical Properties of Poly(P-Phenylene Vinylene) Thin Films," Nonlinear Optical Effects in Organic Polymers, K. F. Messier J., Prasad P., Ulrich D. , ed., Springer, Dordrecht.
[31] Bolger, J., Harvey, T. G., Ji, W., Kar, A. K., Molyneux, S., and Wherrett, B. S., 1992, "Near-Resonant Third-Roder Optical Nonlinearities in p-toluene Sulfonate Polydiacetylene," *J. Opt. Soc. Am. B*, 9.
[32] Mathy, A., Ueberhofen, K., Schenk, R., Gregorious, H., Garay, R., Müllen, K., and Bubeck, C., 1996, "Third-harmonic-generation spectroscopy of poly(p-phenylenevinylene): A comparison with oligomers and scaling laws for conjugated polymers," *Phys. Rev. B*, 53.
[33] Bader, M. A., Marowsky, G., Bahtiar, A., Koynov, K., Bubeck, C., Tillman, H., Hörhold, H., and Pereira, S., 2002, "Poly(p-phenylenevinylene) derivatives: New Promising Materials for Nonlinear All-Optical Waveguide Switching," *J. Opt. Soc. Am. B*, 19.
[34] Carter, G. M., Thakur, M. K., Chen, Y. J., and Hryniewicz, J. V., 1985, "Time and wavelength resolved nonlinear optical spectroscopy of a polydiacetylene in the solid state using picosecond dye laser pulses," *Appl. Phys. Lett.*, 47.
[35] Arivuoli, D., 2001, "Fundamentals of nonlinear optical materials," *J. Phys.*, 57, pp. 871-883.
[36] Boyd, G. D., Buehler, E., and Storz, F. G., 1971, "Linear and Nonlinear Optical Properties of ZnGeP2 and CdSe," *Appl. Phys. Lett.*, 18.
[37] Hilinski, E., Lucas, P. A., and Wang, Y., 1988, "A picosecond bleaching study of quantumconfined cadmium sulfide microcrystallites in a polymer film," *J. Chem. Phys.*, 89, pp. 3435-3441.
[38] Murray, C. B., Kagan, C. R., and Bawendi, M. G., 2000, "Synthesis and Characterization of Monodisperse Nanocrystals and Close-Packed Nanocrystal Assemblies," *Annu. Rev. Mater. Sci.*, 30, pp. 545-610.
[39] Burda, C., Chen, X., Narayanan, R., and El-Sayed, M. A., 2005, "Chemistry and Properties of Nanocrystals of Different Shapes," *Chem. Rev.*, 105, pp. 1025-1102.
[40] Kumar, H., Barman, P. B., and Singh, R. R., 2015, "Effect of size and shell: Enhanced optical and surface properties of CdS, ZnS and CdS/ZnS quantum dots," *Physica E*, 67, pp. 168-177.
[41] Eustis, S., and El-Sayed, M. A., 2006, "Why Gold Nanoparticles Are More Precious Than Pretty Gold: Noble Metal Surface Plasmon Resonance and Its Enhancement of the Radiative and Nonradiative Properties of Nanocrystals of Different Shapes," *Chem. Soc. Rev.*, 35, pp. 209-217.
[42] Ricard, D., Roussignol, P., and Flytzanis, C., 1985, "Surface-mediated enhancement of optical phase conjugation in metal colloids," *Opt. Lett.*, 10, pp. 511-513.
[43] Link, S., and El-Sayed, M., 1999, "Spectral properties and relaxation dynamics of surface plasmon electronic oscillations in gold and silver nanodots and nanorods," *J. Phys. Chem. B*, 103, pp. 8410-8426.

[44] Zhang, Y., and Wang, Y., 2017, "Nonlinear optical properties of metal nanoparticles: a review," *RSC Adv.*, 7.
[45] Magruder, R. H., Yang, L., Haglund, R. F., White, C. W., Yang, L., Dorsinville, R., and Alfano, R. R., 1993, "Optical Properties of Gold Nanocluster Composites," *Appl. Phys. Lett.*, 62, pp. 1730-1732.
[46] Tanahashi, I., Yoshida, M., Manabe, Y., Tohada, T., Sasaki, S., Tokizaki, T., and Nakamura, A., 1994, "Preparation and Nonlinear Optical Properties of AG/SiO2 Glass Composite Thin Films," *Jpn. J. Appl. Phys.*, 33, pp. L1410-L1412.
[47] Uchida, K., Kaneko, S., Omi, S., Hata, C., Tanji, H., Asahara, Y., Ikushima, A. J., Tokizaki, T., and Nakamura, A., 1994, "Optical nonlinearities of a high concentration of small metal particles dispersed in glass: copper and silver particles," *J. Opt. Soc. Am. B*, 11, pp. 1236-1243.
[48] Inouye, H., Tanaka, K., Tanahashi, I., and Hirao, K., 1998, "Femtosecond optical Kerr effect in the gold nanoparticle system," *Jpn. J. Appl. Phys.*, 37.
[49] Pinçon-Roetzinger, N., Prot, D., Palpant, B., Charron, E., and Debrus, S., 2002, "Large optical effect in matrix-embedded metal nanoparticles," *Mater. Sci. Eng. C*, 19.
[50] Ghosh, B., Chakraborty, P., Mohapatra, S., Kurian, P. A., Vijayan, C., Deshmukh, P. C., and Mazzoldi, P., 2007, "Linear and nonlinear optical absorption in copper nanocluster-glass composites," *Mater. Lett.*, 61(24), pp. 4512-4515.
[51] Garcia, H., Kalyanaraman, R., and Sureshkumar, R., 2009, "Nonlinear optical properties of multi-metal nanocomposites in a glass matrix," *J. Phys. B: At. Mol. Opt. Phys.*, 42.
[52] Wang, Y. H., Wang, Y. M., Lu, J. D., Ji, L. L., Zang, R. G., and Wang, R. W., 2010, "Nonlinear optical properties of Cu nanoclusters by ion implantation in silicate glass," *Opt. Commun.*, 283, pp. 486-489.
[53] Shirakawa, H., Louis, E. J., MacDiarmid, A. G., Chiang, C. K., and Heeger, A. J., 1977, "Synthesis of electrically conducting organic polymers: halogen derivatives of polyacetylene, (CH)x," *J. Chem. Soc., Chem. Commun.*, pp. 578-580.
[54] Thakur, M., 1988, "A Class of Conducting Polymers Having Nonconjugated Backbones," *Macromolecules*, 21, pp. 661-664.
[55] Lin, Y., and Yuzhong, L., 1997, "Electrical conductivity in iodine-doped nonconjugated polyanilinefurfural," *Polymer Bulletin*, 38, pp. 573-577.
[56] Thakur, M., Khatavkar, S., and Parish, E. J., 2003, "Polyalloocimene, a Novel Nonconjugated Conductive Polymer: The Correct Fundamental Basis for Conductive Polymers," *J. Macromol. Sci. Part A*, 40, pp. 1397-1406.
[57] Rajagopalan, H., Vippa, P., and Thakur, M., 2006, "Quadratic electro-optic effect in a nanooptical material based on the nonconjugated conductive polymer, poly(β-pinene)," *Appl. Phys. Lett.*, 033109.
[58] Swamy, R., Rajagopalan, H., Vippa, P., Thakur, M., and Sen, A., 2007, "Quadratic electro-optic effect in a nano-optical material based on the nonconjugated conductive polymer, poly(ethylenepyrrolediyl) derivative," *Solid State Comm.*, 143, pp. 519-521.
[59] Narayanan, A., Palthi, A., and Thakur, M., 2009, "Electrical and Optical Properties of a Novel Nonconjugated Conductive Polymer, Polynorbornene," *J. Macromol. Sci. Part A*, 46, pp. 455-460.
[60] Telang, G., and Thakur, M., 2012, "Quadratic Electro-optic Effect in the Nonconjugated Conductive Copolymer Iodine-doped Styrene-butadiene-rubber Measured at 633 nm and 1550 nm," *Journal of Solids and Structures*, 6, pp. 1-9.
[61] Thakur, M., Swamy, R., and Titus, J., 2004, "Quadratic Electrooptic Effect in a Nonconjugated Conductive Polymer," *Macromolecules*, 34, pp. 2677-2678.
[62] Titus, J., and Thakur, M., 2007, "Two-photon absorption in quantum dots based on a nonconjugated conductive polymer," *Appl. Phys. Lett.*, 90.
[63] Shrivastava, S., and Thakur, M., 2011, "Quadratic electro-optic effect in the nonconjugated conductive polymer iodine-doped trans-polyisoprene, an organic nanometallic system," *Solid State Communications*, 151, pp. 775-777.

[64] Gerischer, H., Michel-Beyerle, M. E., Rebentrost, F., and Tributsch, H., 1968, "Sensitization of charge injection into semiconductors with large band gap," *Electrochimica Acta*, pp. 1509-1515.
[65] Tributsch, H., and Calvin, M., 1971, "Electrochemistry of excited molecules: photo-electrochemical reactions of chlorophylls," *Photochemistry and Photobiology*, 14, pp. 95-112.
[66] Tributsch, H., 1972, "Reaction of excited chlorophyll molecules at electrodes and in photosynthesis," *Photochemistry and Photobiology*, 16, pp. 261-269.
[67] O'Regan, B., and Grätzel, M., 1991, "A low-cost, high-efficiency solar cell based on dye-sensitized colloidal TiO2 films," *Nature*, 353, pp. 737-740.
[68] Kalyanasundaram, K., and Grätzel, M., 1997, "Photovoltaic performance of injection solar cells and other applications of nanocrystalline oxide layers," *Journal of Chemical Sciences*, 109, pp. 447-469.
[69] Hara, K., and Arakawa, H., 2003, "Dye-Sensitized Solar Cells," Handbook of Photovoltaic Science and Engineering, Wiley.
[70] Tian, H., Gardner, J., Edvinsson, T., Pati, P. B., Cong, J., Xu, B., Abrahamsson, M., Cappel, U. B., and Barea, E. M., 2019, "Dye-sensitized Solar Cells," Solar Energy Capture Materials, Royal Society of Chemistry, pp. 89-152.
[71] Smestad, G., 1994, "Testing of dye sensitized TiO2 solar cells II: Theoretical voltage output and photoluminescence efficiencies," *Solar Energy Materials and Solar Cells*, 32, pp. 273-288.
[72] Ferber, J., Stangl, R., and Luther, J., 1998, "An electrical model of the dye-sensitized solar cell," *Solar Energy Materials and Solar Cells*, 53, pp. 29-54.
[73] Yanagida, S., Senadeera, G. K. R., Nakamura, K., Kitamura, T., and Wada, Y., 2004, "Polythiophene-sensitized Ti02 solar cells," *J. Photochem. and Photobio. A: Chem.*, 166, pp. 75-80.
[74] Qiao, Q., and Mcleskey, J. T., 2005, "Water-soluble polythiophene/nanocrystalline TiO2 solar cells," *Appl. Phys. Lett.*, 86, p. 153501.
[75] Sharma, S. N., 2006, "Photophysics nd photochemistry of colloidal poly(p-phenylinevinylene) (PPV) polymer," *Materials Chemistry and Physics*, 100, pp. 345-350.
[76] Glenis, S., Horowitz, G., Tourillon, G., and Garnier, F., 1984, "Electrochemically Grown Polythiophene and Poly(3-methylthiophene) Organic Photovoltaic Cells," *Thin Solid Films*, 111, pp. 93-103.
[77] Spanggaard, H., and Krebs, F. C., 2004, "A brief history of the development of organic and polymeric photovoltaics," *Solar Energy Materials and Solar Cells*, 83, pp. 125-146.
[78] Sun, S. S., and Sariciftci, N. S., 2005, Organic Photovoltaics, Mechanisms, Materials, and Devices, CRC Press.
[79] Yamanari, T., Taima, T., Hara, K., and Saito, K., 2006, "Investigation of optimum conditions for high-efficiency organic thin-film solar cells based on polymer blends," *J. Photochem. and Photobio. A: Chem.*, 182, pp. 269-272.
[80] Vippa, P., Rajagopalan, H., and Thakur, M., 2005, "Electrical and optical properties of a novel nonconjugated conductive polymer, poly(B-pinene)," *J. Poly. Sci. Part B: Poly. Phys.*, 43, p. 3695.
[81] Palthi, A., Narayanan, A., and Thakur, M., 2010, "Photo-induced Charge-transfer and Photovoltaic effect in a Composite Involving a Nonconjugated Conductive Polymer and C60," *J. Macromol. Sci. PAC*, 47.
[82] Sangal, M., Jaju, S., Telang, G., and Thakur, M., 2014, "Photovoltaic Cells Involving the Nonconjugated Polymer, Iodine-Doped Poly(β-pinene)," *J. Macromol. Sci. PAC*, 51, pp. 796-798.
[83] Grätzel, M., 2004, "Conversion of sunlight to electric power by nanocrystalline dye-sensitized solar cells," *J. Photochem. and Photobio. A: Chem.*, 164, pp. 3-14.
[84] Van Cleave, J., and Thakur, M., 2015, "Photovoltaic Cells Involving the Nonconjugated Conductive Polymer Iodine-Doped Styrene-Butadiene-Rubber (SBR)," *J. Macromol. Sci. Part A*, 52(10), pp. 798-800.
[85] Van Cleave, J., Jaju, S., and Thakur, M., 2017, "Photovoltaic cells involcing the nonconjugated conductive polymer, iodine-doped cis-poly(isoprene)," *J. Macromol. Sci., Part A*, 54(8), pp. 543-545.

[86] Thakur, M., 2009, "New Additions to Nonconjugated Conductive Polymers; Nonlinear Optical Effects," *J. Macromol. Sci. Part A Pure Appl. Chem.*, 46, pp. 1185-1190.
[87] Kim, K. H., Husakou, A., and Hermann, J., 2010, "Linear and nonlinear optical characteristics of composites containing metal nanoparticles of different sizes and shapes," *Opt. Exp.*, 18, p. 7488.
[88] Narayanan, A., and Thakur, M., 2010, "Quadratic electro-optic effect in th enonconjugated conductive polymer iodine-doped poly(B-pinene) measured at longer wavelengths including 1.55µm," *Solid State Comm.*, 150, pp. 375-378.
[89] Rocha-Mendoza, I., Rangel-Rojo, R., Rodríguez-Fernández, L., and Oliver, A., 2011, "Second order nonlinear response of composites containing aligned elongated silver nanoparticles," *Opt. Exp.*, 19, p. 21575.
[90] Shrivastava, S., 2011, "Study of Structures, Quadratic Electro-Optic Effect and Rechargeable Battery Characteristics of Specific Nonconjugated Conductive Polymers Including Trans-1,4-Polyisoprene," Master of Science, Auburn University.
[91] Shcherbakov, M. R., Neshev, D. N., Hopkins, B., Shorokhov, A. S., Staude, I., Melik-Gaykazyan, E. V., Decker, M., Ezhov, A. A., Miroshnichenko, A. E., Brener, I., Fedyanin, A. A., and Kivshar, Y. S., 2014, "Enhanced Third-Harmonic Generation in Silicon Nanoparticles Driven by Magnetic Response," *Nano Letters*, 14, pp. 6488-6492.
[92] Carletti, L., Locatelli, A., Stepaneko, O., Leo, G., and De Angelis, C., 2015, "Enhanced second-harmonic generation from magnetic resonance in AlGaAs nanoantennas," *Optics Express*, 23(20).
[93] Van Cleave, J., and Thakur, M., "Quadratic Electro-optic Effect in Nanometallic particles in Glass; Comparison with Iodine-doped Nonconjugated Conductuve Polymers," Proc. Am. Phys. Soc., p. K36.
[94] Ota, Y., Katsumi, K., Watanabe, K., Iwamoto, S., and Arakawa, Y., 2018, "Topological photonic crystal nanocavity laser," *Communications Physics*, 1.
[95] Najer, D., Söllner, I., Sekatski, P., Dolique, V., Löbl, M. C., Riedel, D., Schott, R., Starosielec, S., Valentin, S. R., Wieck, A. D., Sangouard, N., Ludwig, A., and Warburton, R. J., 2019, "A gated quantum fot strongly coupled to an optical microcavity," *Nature*, 575.
[96] Thakur, M., and Van Cleave, J., 2019, "Quadratic Electro-Optic Effect in Metal Nanoparticles in a Transparent Dielectric Medium," *J. Appl. Sci.*, 9.
[97] Thakur, M., and Van Cleave, J., 2020, "Electroabsorption in Metallic Nanoparticles within Transparent Dielectric Media," *J. Appl. Sci.*, 10.
[98] Buono, W. T., and Forbes, A., 2022, "Nonlinear optics with structured light," *Opto-Electron Adv*, 5.
[99] McKenna, T. P., Stokowski, H. S., Ansari, V., Mishra, J., Jankowski, M., Sarabalis, C. J., Hermann, J. F., Langrock, C., Fejer, M. M., and Safavi-Naeini, A. H., 2022, "Ultra-low-power second-order nonlinear optics on a chip," *Nature Communications*, 13, p. 4532.
[100] Thakur, M., and Elman, B. S., 1989, "Optical and magnetic properties of a nonconjugated conducting polymer," *J. Chem. Phys.*, 90, p. 2042.
[101] Thakur, M., 1992, Polymers for Light Wave and Integrated Optics, Marcel Dekker, New York, NY.
[102] Thakur, M., 2001, "Nonconjugated Conductive Polymers," *J. Macromol. Sci. Part A*, 38, pp. 1337-1344.
[103] Cholli, A. L., and Thakur, M., 1989, "Structural investigation of nonconjugated conducting polymer by solid state C13 nuclear magnetic resonance spectroscopy," *J. Chem. Phys.*, 91, p. 7912.
[104] Thakur, M., and Cleave, J. V., 2023, "Quadratic electro-optic effect in the nonconjugated conductive polymer iodine-doped polyethylene terephthalate," *Journal of Macromolecular Science, Part A*.
[105] Sreelatha, K., and Predeep, P., 2013, "Electrically Conducting Plastic Films fromPolyethylene Terephthalate for Optoelectronic Applications," *Polymer Science Series A*, 55, pp. 480-486.

[106] Ballesteros, J. M., Serna, R., Solis, J., Afonso, C. N., Petford-Long, A. K., Osborne, D. H., and Haglund, R. F., Jr., 1997, "Nonlinear Optical Physics and Applications of The Plasmonic Response in Metal Nanoparticles," *App. Phys. Lett.*, 71, p. 2445.
[107] Haiss, W., Thanh, N. T. K., Aveyard, J., and Fernig, D. J., 2007, "Determination of size and concentration of gold nanoparticles from uv-vis spectra," *Anal. Chem.*, 79, pp. 4215-4221.
[108] Flytzanis, C., 2005, "Nonlinear optics in mesoscopic composite materials," *J. Phys. B: At. Mol. Opt. Phys.*, 38, p. s661.
[109] Jacak, W. A., 2015, "Size-dependence of the Lorentz friction for surface plasmons in metallic nanospheres," *Opt. Express*, 23, pp. 4472-4481.
[110] Greene, B. I., Thakur, M., and Orenstein, J., 1989, "Quadratic electro-optic effect in polydiacetylene single crystals," *App. Phys. Lett.*, 54, p. 2065.
[111] Park, S. Y., Cho, H., and Kim, N., 1994, "Third-order optical nonlinearity of conjugated poly(4,4-disubstituted_1,6-heptadiyne)s," *Apply. Phys. Lett.*, 65, p. 289.
[112] Gubler, U., Concilio, S., Bosshard, C., Biaggio, I., and Günter, P., 2002, "Third-order nonlinear optical properties of in-backbone substituted conjugated polymers," *Appl. Phys. Lett.*, 81, p. 2322.